Master's Degree in Energy and Nuclear Engineering

Techno-Economic Study of a RES Plant with Green Hydrogen Electrolyzers and Storage Systems using a Object-Oriented Programming approach in Coding

October 16, 2025

Author: Emanuele Carello

Supervisor: Marta Gandiglio, Eduardo Prieto-Araujo

Cosupervisor: Massimo Santarelli, Paolo Marocco

Lorenzo Bruno, Esteban Gonzalez Iakl





Abstract

This thesis presents a techno-economic analysis of a renewable energy system (RES) integrated with electrolyzers and green hydrogen storage. The research aims to identify the most efficient and cost-effective configurations by comparing different electrolyzer technologies and hydrogen storage options.

The work is structured into three main phases.

The first phase, Data Collection and Laboratory Review, includes a comprehensive state-of-the-art survey of electrolyzer technologies and hydrogen storage systems, covering both physical and material-based storage solutions, as well as the collection of relevant data for subsequent analyses.

The second phase, Computational Framework Development, focuses on the application of object-oriented programming (OOP) methods to design a modular, adaptable, and transparent simulation environment. This framework allows the definition of multiple scenarios, optimization of the computational structure, and improved usability of the code.

The third phase, Plant Simulation and Economic Analysis, implements the developed models to simulate RES plants coupled with electrolyzers and hydrogen storage systems. The simulation results are then assessed through a detailed economic evaluation.

Two computational models were developed, both based on fixed-point iteration with temporal discretization. The second model was simplified with respect to the thermal analysis to facilitate broader scenario exploration and reduce computational costs.

The results of this research provide a scalable and adaptable framework for optimizing hydrogenbased RES systems, thereby contributing to the development of sustainable and economically viable energy solutions. This thesis has been conducted within the broader context of the European H2Glass project, in collaboration with the CITCEA research group at the Universitat Politècnica de Catalunya, where the internship work was carried out.





3 Contents

Contents

1	Pre	eface	7
2	Intr	roduction	8
	2.1	Hydrogen: Benefits and Challenges	8
	2.2	Objectives	10
	2.3		11
	2.4		13
	Q1 - I		10
3		· · · · · · · · · · · · · · · · · · ·	16
	3.1		16
	3.2	1	26
	3.3	Comparison Between the Different Types of Electrolyzers	30
4	Stat		48
	4.1	σ	48
		4.1.1 Gaseous hydrogen	48
		4.1.2 Liquid Hydrogen	48
		4.1.3 Cryo-Compressed Hydrogen	49
	4.2		49
		4.2.1 Physisorption	49
			50
	4.3		51
	4.4	Focus on Metal Hydrides and Solid Storage	53
	1.1		53
		1	56
			60
			62
		4.4.4 Economic and environmental factors	02
5	Cas	se study and Methodology	65
	5.1	Design of the PtX Plant	65
		5.1.1 Power-to-X Overview	65
		5.1.2 Software Environment	65
			66
	5.2	Object-Oriented Programming Approach	71
	5.3	Model of the PtX	72
	0.0	5.3.1 Photovoltaic System	74
		5.3.2 Electrolyzer	75
		5.3.3 Hydrogen Storage	78
6			81
	6.1		81
			81
			82
			83
	6.2	1 0	84
	6.3	Economic Analysis: LCOE, LCOH, NPC and Payback Period	85
7	Res	sults	88



Contents 4

	7.2 7.3 7.4	Daily Simulation	95 96 98
8	Con	clusion	106
9	Ack	nowledgments	107
10	Pyt	hon code	112



5 List of Figures

List of Figures

1	H2GLASS
2	H2GLASS goal
3	Power to X
4	Various Hydrogen Production Method [1]
5	Thermochemical water splitting processes [2]
6	Schematic of PC-WS for hydrogen production [3]
7	PEC-WS for hydrogen production [3]
8	Schematic for DBP [3]
9	Schematic for IBP [3]
10	Schematic of PV-electrolysis [3]
11	STH efficiency conversion 1 [3]
12	STH efficiency conversion 2 [3]
13	LCOH [3]
14	STH method comparison [3]
15	PV + ELY cost analysis [3]
16	lifetime ELY [3]
17	Technical characteristic of typical water electrolysis technologies [4]
18	Advantages and disadvantages of typical water electrolysis technologies [4]
19	Alkaline Electrolysis [1]
20	Solid Oxide Electrolysis [1]
21	Future Develope CAPEX [5]
$\frac{21}{22}$	Future Develope LCOH [5]
23	TRL Electrolyzer [6]
$\frac{23}{24}$	PEM [1]
$\frac{24}{25}$	AEM [4]
26	Commercial AEM and PEM [4]
$\frac{20}{27}$	Publication AEM [7]
28	Ion Exchange Capacity [7]
29	Area Specific Resistance [7]
30	Ion Conductivity [7]
31	ion conductivity
	Tensile Strength [7]
	Tensile Strength [7]
32	Voltage - Current Density [7]
32 33	Voltage - Current Density [7] 42 AEM Multicore Stack [8] 42
32 33 34	Voltage - Current Density [7] 42 AEM Multicore Stack [8] 42 AEM Multicore [8] 43
32 33 34 35	Voltage - Current Density [7] 42 AEM Multicore Stack [8] 42 AEM Multicore [8] 43 AEM Multicore structure [8] 43
32 33 34 35 36	Voltage - Current Density [7] 42 AEM Multicore Stack [8] 42 AEM Multicore [8] 43 AEM Multicore structure [8] 43 AEM Multicore Theorical specification [8] 44
32 33 34 35 36 37	Voltage - Current Density [7] 42 AEM Multicore Stack [8] 42 AEM Multicore [8] 43 AEM Multicore structure [8] 43 AEM Multicore Theorical specification [8] 44 Nominal Current Density 45
32 33 34 35 36 37 38	Voltage - Current Density [7] 42 AEM Multicore Stack [8] 42 AEM Multicore [8] 43 AEM Multicore structure [8] 43 AEM Multicore Theorical specification [8] 44 Nominal Current Density 45 Lifetime 45
32 33 34 35 36 37 38 39	Voltage - Current Density [7] 42 AEM Multicore Stack [8] 42 AEM Multicore [8] 43 AEM Multicore structure [8] 43 AEM Multicore Theorical specification [8] 44 Nominal Current Density 45 Lifetime 45 Voltage 46
32 33 34 35 36 37 38 39 40	Voltage - Current Density [7] 42 AEM Multicore Stack [8] 42 AEM Multicore [8] 43 AEM Multicore structure [8] 43 AEM Multicore Theorical specification [8] 44 Nominal Current Density 45 Lifetime 45 Voltage 46 Capital cost (stack) min 1 MW 46
32 33 34 35 36 37 38 39 40 41	Voltage - Current Density [7] 42 AEM Multicore Stack [8] 42 AEM Multicore [8] 43 AEM Multicore structure [8] 43 AEM Multicore Theorical specification [8] 44 Nominal Current Density 45 Lifetime 45 Voltage 46 Capital cost (stack) min 1 MW 46 Degradation Rate 47
32 33 34 35 36 37 38 39 40 41 42	Voltage - Current Density [7] 42 AEM Multicore Stack [8] 42 AEM Multicore [8] 43 AEM Multicore structure [8] 43 AEM Multicore Theorical specification [8] 44 Nominal Current Density 45 Lifetime 45 Voltage 46 Capital cost (stack) min 1 MW 46 Degradation Rate 47 Hydrogen content in different storage technologies (weight %) 52
32 33 34 35 36 37 38 39 40 41 42 43	Voltage - Current Density [7] 42 AEM Multicore Stack [8] 42 AEM Multicore [8] 43 AEM Multicore structure [8] 43 AEM Multicore Theorical specification [8] 44 Nominal Current Density 45 Lifetime 45 Voltage 46 Capital cost (stack) min 1 MW 46 Degradation Rate 47 Hydrogen content in different storage technologies (weight %) 52 Volumetric energy density of hydrogen storage technologies (MJ/L) 52
32 33 34 35 36 37 38 39 40 41 42 43 44	Voltage - Current Density [7]
32 33 34 35 36 37 38 39 40 41 42 43	Voltage - Current Density [7] 42 AEM Multicore Stack [8] 42 AEM Multicore [8] 43 AEM Multicore structure [8] 43 AEM Multicore Theorical specification [8] 44 Nominal Current Density 45 Lifetime 45 Voltage 46 Capital cost (stack) min 1 MW 46 Degradation Rate 47 Hydrogen content in different storage technologies (weight %) 52 Volumetric energy density of hydrogen storage technologies (MJ/L) 52



List of Figures 6

48	Transient temperature profile of the electrolyzer stack
49	HyLYZER-500
50	Photovoltaic Power over time
51	Electric Current
52	Instantaneous H2 production
53	Comulative H2 production
54	Polarization Curve
55	PEM Cell Voltage
56	Electrolyzer Efficiency
57	Cumulative Energy Comparison
58	H2 Storage State of the Charge
59	H2 Stored
60	Tank Temperature
61	Monthly Hydrogen production
62	CO2 emissione avoided annually
63	Annual reduction in methane consumption
64	Levelized Cost of Electricity (LCOE)
65	Levelized Cost of Hydrogen (LCOH)
66	Discounted Cash Flow 0.4€/m3 of CH4
67	Discounted Cash Flow $0.8 \ \ \ \ \ \ \ \ \ \ \ \ \ \ \ \ \ \ \$
68	Discounted Cash Flow 1.2 $\mbox{\em C}/\mbox{m3}$ of CH4
69	Discounted Cash Flow 2 $\mbox{\em C}/\mbox{m3}$ of CH4
70	Discounted Cash Flow 8 $\P/m3$ of H2
71	Discounted Cash Flow 6 $\mbox{\em C}/\mbox{m3}$ of H2
72	Discounted Cash Flow 4 €/m3 of H2



1 Preface

This thesis marks the conclusion of an important and formative stage in both my academic and personal journey. The fact that it coincided with my Erasmus experience is a source of great pride, as it further emphasizes the international dimension of this path and the global relevance of the Renewable Energy Engineering program.

I am deeply convinced that the study of hydrogen in the energy sector can represent one of the key solutions for a more sustainable and greener future for our continent, improving both quality of life and the health of the planet. The urgency of decarbonizing hard to abate sectors and the role of hydrogen as an energy vector, supporting grid stability with a high share of renewable sources and enabling large scale energy storage, were at the heart of my motivation to undertake this work.

Equally significant was the opportunity to carry out my research at CITCEA, within a stimulating and international environment, in the dynamic and multicultural city of Barcelona. This setting offered the ideal context to develop a research project aligned with the challenges of the energy transition and the vision of a sustainable future.

Ultimately, the deeper meaning of this work is to remind us that a different future is not only necessary but also possible. Research in hydrogen technologies is progressing in promising ways, bringing us closer to Europe's goals of clean and accessible energy for all, and to the ambition of making our continent a better place for present and future generations.



2 Introduction 8

2 Introduction

2.1 Hydrogen: Benefits and Challenges

The energy problem represents one of the greatest challenges for contemporary human society. Only a few decades ago, it was believed to be an issue that would primarily concern future generations in the distant future. However, it has emerged much earlier than expected, or at least sooner than many had hoped. Humanity is now confronted with the urgent necessity of identifying alternative solutions to the use of fossil fuels as an energy source, mainly for two reasons:

The imminent depletion of fossil fuel reserves.

The high environmental and pollutant impact of combustion products.

Given that the structure of our electricity production system, as well as the vast majority of engines used for transportation, relies on the combustion of gases or fossil fuels, the most immediate and straightforward solution to the energy problem may lie in the identification of a superior fuel compared to those currently in use. This would make it possible to avoid the radical transformation of the entire industrial and energy infrastructure.

By analyzing the two main issues related to current fuels, it is possible to state that a "good" fuel should meet two fundamental requirements:

High quantitative availability.

Low environmental impact and minimal pollutant emissions from combustion products.

At present, hydrogen appears to be the most promising candidate to satisfy both of these conditions, both from a technological and economic standpoint. In its elemental state, hydrogen is a colorless, odorless, and highly flammable gas, while in the universe it predominantly exists in plasma form (the state that constitutes stars). In fact, hydrogen accounts for 73.9

The primary challenge, however, lies in the chemical form in which hydrogen is found. Due to its molecular structure, hydrogen is highly unstable in isolation and tends to form bonds with electronegative atoms such as those in Group VI (oxygen, forming HO) and Group VII (fluorine and chlorine, forming HF and HCl). As a result, molecular hydrogen (H) is almost absent in nature. It is generally found bound to other elements, for instance in water (a molecule of hydrogen and oxygen) or hydrocarbons (hydrogen and carbon). To isolate hydrogen on Earth, it is necessary to "extract" it by supplying energy to drive separation processes, thus incurring both economic and, often, environmental costs.

Since hydrogen does not exist freely in nature and its production requires an external energy input, it is considered an energy carrier rather than a primary energy source.

In an oxygen-rich atmosphere such as Earth's, hydrogen burns in a manner similar to methane or natural gas. Among conventional fuels, it possesses the highest energy content per unit mass—three times greater than gasoline. A significant advantage of hydrogen lies in its potential to act as an effective energy storage medium for electricity generated from renewable sources (such as solar or wind power). These energy sources, although clean, suffer from high intermittency both seasonally and daily, and are strongly affected by unpredictable fluctuations in productivity



due to climatic variability.

Another critical advantage of hydrogen as a future fuel is its specific energy density, which is significantly higher than that of fossil fuels: 140 MJ/kg for hydrogen, compared with 55 MJ/kg for methane, 42 MJ/kg for petroleum, and 15 MJ/kg for coal—exceeded only by nuclear fuels. This advantage is partially offset by hydrogen's low volumetric energy density, a consequence of its low physical density, which makes storage and transport relatively challenging.

The first major obstacle to the practical realization of a hydrogen-based society, often referred to as the "Hydrogen Economy," lies in producing hydrogen in its usable molecular form, H. As noted, although hydrogen is abundant on Earth, it is chemically bound to other elements. Its extraction requires specific physico-chemical processes capable of isolating it in pure form.

According to the latest report from the International Energy Agency (IEA), global hydrogen consumption amounts to approximately 75 million tonnes per year. At present, hydrogen is primarily used as a feedstock in industrial processes, such as ammonia production, fertilizer manufacturing, and petroleum refining. Nearly all of this hydrogen is produced from fossil fuels, mainly via coal gasification:

$$C + CO \rightarrow 2 CO$$

$$C + HO \rightarrow CO + H$$

or via natural gas steam reforming:

$$CH + HO \rightarrow CO + 3 H$$

$$CO + HO \rightarrow CO + H$$

Currently, 95% of global hydrogen production (55 Mtpa) originates from fossil fuels, predominantly natural gas. These processes are associated with significant CO emissions, with a carbon footprint estimated at $10-12~\rm kgCO/kgH$ for hydrogen obtained from natural gas reforming (grey hydrogen).

The gasification process involves the conversion of carbon with CO and steam into syngas (CO and H). In steam reforming, the first step decomposes methane into hydrogen and carbon monoxide. In the subsequent step, known as the water-gas shift reaction, carbon monoxide reacts with steam to form carbon dioxide and additional hydrogen.

Such processes are unlikely to be viable in the long term, as they are highly polluting and inconsistent with European directives on reducing climate-altering emissions. It is worth noting that gasification could, in principle, be performed using renewable feedstocks such as biomass or waste. However, these processes also risk generating significant pollutant by-products.

Hydrogen production via steam reforming cannot contribute to decarbonization unless combined with carbon capture and storage/utilization (CCS/U) technologies. When hydrogen from fossil fuels is produced in facilities integrated with CCS/U, it is referred to as blue hydrogen.

The only truly sustainable and commercially viable hydrogen is so-called green hydrogen, produced through water electrolysis in specialized electrochemical cells powered by electricity from renewable sources.



2 Introduction 10

2.2 Objectives

Within such a complex and constantly evolving energy scenario, the purpose of this work takes shape. The central idea is the development of a digital twin of a plant designed for the production of green hydrogen, with the specific goal of evaluating its potential application in a blast furnace for hydrogen-based processes. A digital twin may be defined as a virtual counterpart of a real system, which enables the reproduction of its dynamics in a simulated environment and therefore makes it possible to analyze, predict, and optimize its performance under a wide range of operating conditions.

The project was carried out using Python, following the principles of object-oriented programming. This programming paradigm is based on the definition of objects that bring together both the data that describe them and the functions that govern their behavior. In the present case, a class was created for each component of the plant, while a main function was designed to coordinate and recall all classes in an orderly manner. Such a structure proved to be particularly effective, as it allowed us to maintain a clear and modular organization of the code, thereby facilitating both the implementation of simulations and the future extension of the model.

Thanks to this digital twin it became possible to simulate the operation of the plant, to carry out preliminary sizing activities, and to explore different combinations of parameters that optimize hydrogen production. In particular, the simulations were enriched by the integration of meteorological data, which made it possible to assess the long-term effects of environmental variability on plant performance and lifetime.

Alongside the technical analysis, a cost analysis of the system was also performed. In this respect, hydrogen storage was deliberately excluded from the economic evaluation, since the specific technology considered, although particularly promising for the future development of stationary storage systems, is still at a non-commercial Technology Readiness Level. This condition made it impossible to obtain reliable data for an accurate simulation of its economic implications. For this reason, the economic analysis was conducted instead by exploring different scenarios and future perspectives based on solid and verifiable data. This approach proved to be fruitful, as it allowed us to obtain a number of significant graphs that highlight under what conditions and within what timeframes a project of this kind could become appealing not only from an environmental standpoint, but also, and above all, from an economic and industrial perspective.



11 2.3 H2Glass

2.3 H2Glass



Figure 1: H2GLASS

The H2GLASS project is a Horizon Europe initiative that addresses one of the most pressing challenges for European industry: the decarbonisation of glass production. Glass is a material of growing global demand, widely appreciated for its recyclability and for its central role in the development of sustainable materials. However, glass manufacturing remains highly energy-intensive and responsible for significant carbon emissions. Achieving the European Union's ambitious goal of net zero emissions by 2050 requires immediate innovation, especially considering that the average lifetime of a glass furnace is around twelve to fifteen years. In practical terms, this means that only two generations of furnaces remain before the 2050 deadline, which underlines the urgency of developing breakthrough solutions.

Within this framework, hydrogen emerges as a particularly promising alternative to fossil fuels. The use of green hydrogen can substantially reduce carbon dioxide emissions without increasing other harmful by-products such as nitrogen oxides. Unlike other renewable energy alternatives, hydrogen can improve the energy efficiency of air-fuel combustion and enable higher furnace throughput, all while preserving furnace lifetime. Furthermore, the flexibility offered by different hydrogen concentration mixtures allows for a gradual and adaptable transition between natural gas and hydrogen without compromising product quality.



2 Introduction 12

Safety is a fundamental consideration in this transition. Hydrogen is already employed in a variety of industrial applications and is considered a safe fuel when handled correctly. Nevertheless, scaling up its use and introducing new technologies inevitably introduces risks. For this reason, H2GLASS has placed safety at the heart of its objectives, dedicating a specific focus to risk management. The project includes the design and implementation of detailed safety protocols, fully aligned with the recommendations of the European Hydrogen Safety Panel, to ensure the secure handling, storage and combustion of hydrogen in industrial environments.

Although H2GLASS is centred on the glass industry, its ambition goes further. One of its objectives is to ensure that the developed solutions can be transferred to other energy-intensive industries facing similar challenges. The aluminium industry, which also relies on high-temperature furnaces and energy-intensive processes, has been chosen as a demonstrator to test the scalability and flexibility of the technologies developed. This confirms the potential of hydrogen not only to revolutionise glassmaking but also to provide a pathway for the decarbonisation of other strategic sectors in Europe.

The scope and ambition of H2GLASS are reflected in its scale. The project brings together twenty-three partners from eight European countries, combining industrial leaders, research centres and technology developers. In total, six industrial demonstrators will be implemented, five in the glass industry and one in aluminium, to validate the solutions in real operating conditions. With funding of 23.3 million euros, the project represents one of the most significant investments in hydrogen applications for heavy industry at European level.

Within this context, the project is structured around five key objectives. The first is the development of a technology stack enabling one hundred percent hydrogen combustion in glass furnaces. The second is the validation of the proposed solutions in industrial environments and the demonstration of their economic and environmental viability. The third objective focuses on the creation of an IT architecture and digital twin platform to enable automatic control, smart management and the improvement of industrial processes. The fourth seeks to raise public awareness and understanding of hydrogen technologies as a decarbonisation pathway. The fifth and final objective is the transfer of these solutions to other energy-intensive industries within the European Union.



13 2.4 Why Power-to-X



Figure 2: H2GLASS goal

My contribution to H2GLASS, during my work at CITCEA-UPC in Barcelona, was closely connected to the third objective. I was involved in the development of the digital twin and the related IT architecture, adopting an object-oriented programming approach that made it possible to create a structured and modular tool. Each component of the plant was represented as a class, while a main function coordinated the overall operation of the system. This model enabled the simulation of hydrogen combustion processes, the study of different operational scenarios and the evaluation of the influence of meteorological data on the long-term performance of the plant.

2.4 Why Power-to-X

The concept of Power-to-X has emerged over the past decade as a central element in the transition towards a carbon-neutral energy system. It refers to the conversion of renewable electricity into other forms of energy carriers or chemical products, with the aim of overcoming the inherent variability of renewable energy sources such as solar and wind. The "X" in Power-to-X represents the wide range of possible products that can be generated, the most relevant being hydrogen (Power-to-Hydrogen), methanol (Power-to-Methanol), and ammonia (Power-to-Ammonia).

At the core of Power-to-X lies hydrogen production via electrolysis, where water is split into hydrogen and oxygen using renewable electricity. Hydrogen can then be used directly as a fuel in fuel cells or combustion systems, producing only water as a byproduct. On a mass basis, hydrogen has a high energy density, around 33.3 kWh per kilogram, but its low volumetric density makes storage challenging. For this reason, further conversion into methanol or ammonia can be advantageous, as both of these compounds can be stored and transported more easily in liquid form at moderate conditions.



2 Introduction 14

Methanol synthesis combines hydrogen with captured carbon dioxide, thus creating a liquid fuel while also contributing to carbon recycling. Ammonia, on the other hand, is produced by reacting hydrogen with nitrogen separated from air, and it offers the benefit of being entirely carbon-free when used as an energy vector. These additional pathways provide higher volumetric energy density compared to hydrogen gas and are therefore more attractive for large-scale storage and international energy transport.

The importance of Power-to-X is tied to its ability to balance renewable generation with demand across different time scales. Renewable electricity is intermittent by nature, and conventional battery storage cannot always provide the flexibility needed for seasonal or large-scale energy storage. Power-to-X enables long-term storage and sector coupling, integrating the power sector with transportation, industry, and even agriculture. For instance, ammonia not only serves as a fuel but also as a fertilizer, which allows synergies between the energy and agricultural sectors.

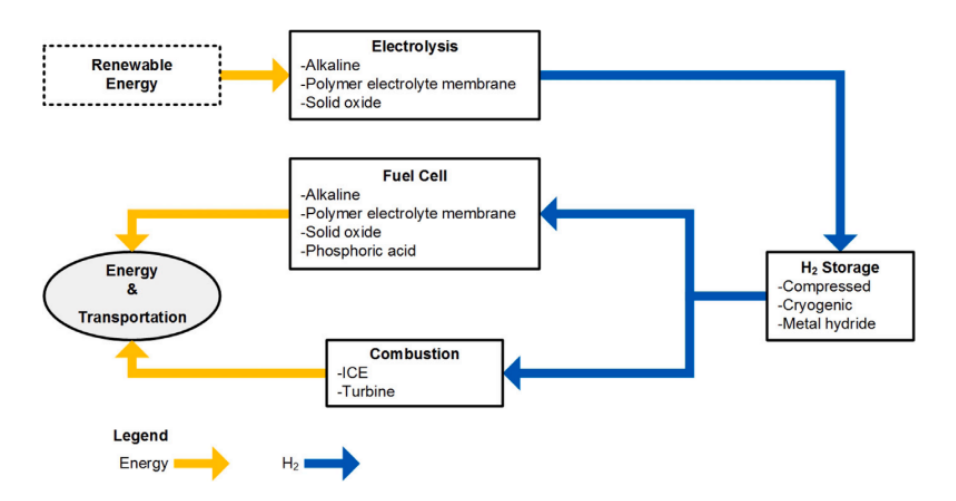


Figure 3: Power to X

From an economic and environmental perspective, Power-to-X technologies are still at an early stage, facing high capital costs and efficiency challenges. Electrolysis technologies such as alkaline, PEM, and solid oxide systems are expected to see cost reductions as production scales up, with projections that by 2030 costs could fall by nearly half compared to current values. Similarly, the development of flexible methanol and ammonia synthesis processes adapted to fluctuating renewable inputs is crucial to improve economic viability.

Despite these challenges, the potential impact of Power-to-X is significant. It offers a pathway to decarbonize sectors that are otherwise difficult to electrify directly, such as heavy transport, shipping, and energy-intensive industries. In addition, by creating liquid or gaseous fuels from renewable electricity, Power-to-X enables the storage, transport, and trade of renewable energy across regions, turning intermittent power into a versatile and globally tradable commodity.

In conclusion, Power-to-X should be seen not only as a technical solution to integrate renewable energy but also as a strategic pillar for the wider decarbonisation of the global economy. While hydrogen remains the backbone of Power-to-X, methanol and ammonia expand its potential by addressing storage, transport, and sectoral integration challenges. Continued research and system-level optimization will be key to reducing costs and achieving large-scale deployment in the coming decades.



The content of this paragraph is presented as a broad synthesis of the referenced paper Powerto-X: A review and perspective (Matthew J. Palys, Prodromos Daoutidis, 2022) [9]



3 State of the Art: Electrolyzer

3.1 Why Electrolyzer

As discussed in the Introduction, we are at a critical turning point in the technological development of renewable energy sources. Technologies like solar photovoltaic and wind power are now technologically mature and economically competitive, with economies of scale approaching stability. However, energy storage remains a fundamental challenge, and hydrogen is currently the most promising solution in terms of environmental impact. In concept, it is now possible to produce energy exclusively from renewable sources and water, significantly minimizing environmental impact, almost to zero, while utilizing natural elements that are abundantly available and evenly distributed across the planet, such as water, wind, and solar energy. In comparison with conventional fuels, hydrogen offers a higher energy density per unit mass. Its higher heating value (HHV) is 141.6 MJ/kg, and its lower heating value (LHV) is 119.9 MJ/kg, while burning with a colorless flame. Key safety considerations, under standard atmospheric pressure (101.3 kPa), include its autoignition temperature of 585°C, a relatively high flame temperature of 2045°C, flame velocity ranging from 265 cm/s to 325 cm/s, detonation limits, and low ignition energy. Today, global energy consumption has been gradually increasing due to population growth and rising living standards. Moreover, as global warming and environmental pollution worsen, the development of renewable energy sources becomes more critical. Hydrogen is one of the most promising clean and sustainable energy carriers, emitting only water as a byproduct with no carbon emissions. Hydrogen has many appealing properties as an energy carrier, including its high energy density (140 MJ/kg), which is more than twice the energy density of typical solid fuels (50 MJ/kg). Hydrogen can be produced from both renewable and non-renewable energy resources. To determine if green hydrogen production processes are viable, several techno-economic analysis frameworks have been developed. One of the most well-known and environmentally friendly methods for hydrogen production is electrolysis. Electrolysis technology, particularly proton exchange membrane (PEM) electrolysis, has advanced significantly. Green hydrogen can be generated using renewable energy sources like wind and solar, with minimal costs ranging from 2.94 to 3.32 USD per kg of H2. Furthermore, biomass gasification technology plays an important role in producing low-emission, sustainable hydrogen, especially for decarbonizing hard-to-abate sectors like industrial and residential heating. As shown in the Fig. 4, which outlines various hydrogen production methods, we can initially exclude fossil fuel-based methods from our analysis, despite their lower economic cost. This leaves us with renewable sources, which can be broadly divided into two categories: those derived from biomass and water splitting technologies. It is logical to focus our research on water splitting technologies, as they are essentially free from CO2 emissions. Therefore, we will provide a brief overview of the three main methods before focusing on electrolysis, and we will discuss the four main types of electrolyzers currently available.



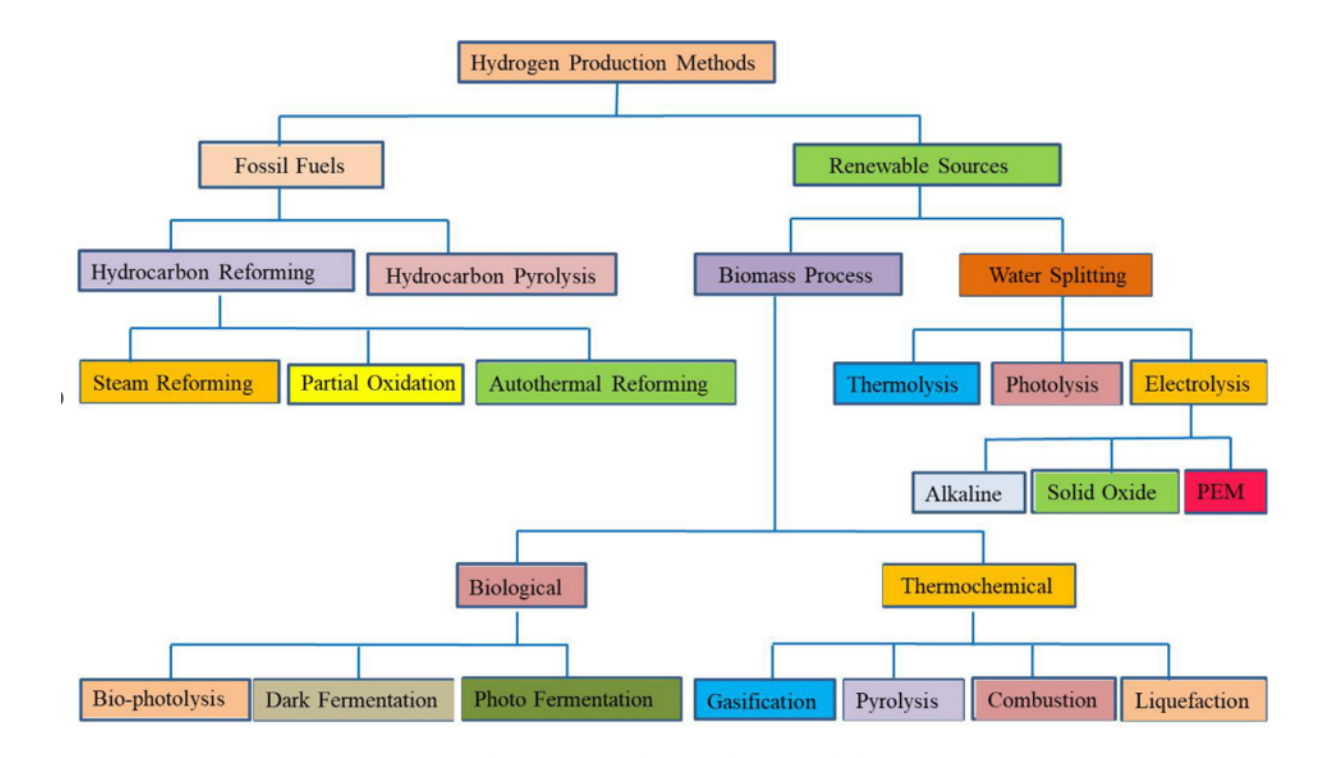


Figure 4: Various Hydrogen Production Method [1]

THERMOCHEMICAL WATER SPLITTING

Thermochemical water splitting processes utilize high-temperature heat (500°–2,000°C) to drive a series of chemical reactions that produce hydrogen. The chemicals used in the process are recycled within each cycle, creating a closed-loop system that consumes only water and produces hydrogen and oxygen. The necessary high temperatures can be generated in the following ways: Concentrating sunlight onto a reactor tower using a field of mirror "heliostats," as illustrated in Fig. 5. Using waste heat from advanced nuclear reactors.

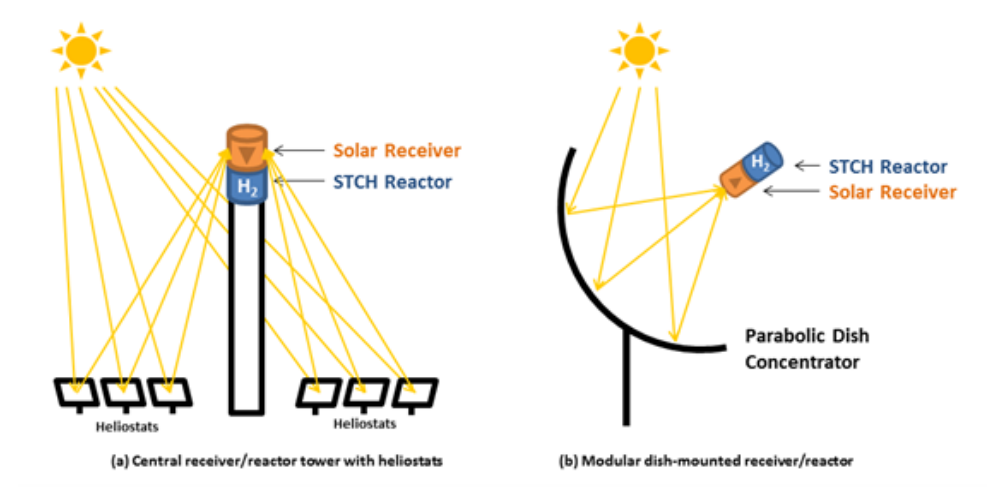


Figure 5: Thermochemical water splitting processes [2]



Several solar thermochemical water-splitting cycles have been investigated for hydrogen production, each with different operating conditions, engineering challenges, and hydrogen production potential. In fact, over 300 water-splitting cycles have been described in the literature. For more details, refer to "Solar Thermochemical Hydrogen Production Research: Thermochemical Cycle Selection and Investment Priority." However, challenges remain in the research, development, and demonstration of commercially viable thermochemical cycles and reactors:

- Efficiency and durability of reactant materials for thermochemical cycling need significant improvement.
- Efficient and robust reactor designs that can withstand high temperatures and thermal cycling need to be developed.
- For solar thermochemical systems, the cost of concentrating mirror systems needs to be reduced.

Exciting progress continues in this field, especially by leveraging synergies with concentrated solar power technologies and emerging solar-fuel production technologies. However, the technology is still not commercially viable due to the high costs and the need for significant power flows to enable thermal electrolysis. Regarding the comparison of hydrogen production from sunlight, there are currently two viable methods: Photolysis and electrolysis powered by renewable energy sources (RES) like photovoltaic solar energy. In the paper "Analysis of photon-driven solar-tohydrogen production methods in the Netherlands," [3] a comprehensive comparison between these technologies is presented. Utilizing energy from other photon-driven solar-to-hydrogen (STH) methods holds promising prospects due to their relatively high theoretical efficiency potential and potentially lower costs compared to indirect hydrogen production methods. While extensive research has been conducted on the theoretical aspects of these direct renewable hydrogen production methods, the actual technologies are not yet commercially adopted. There are two types of photochemical water splitting methods: photoelectrochemical (PEC-WS) and photocatalytic (PC-WS) water splitting. It is worth noting that there is no consensus in the literature regarding this distinction, and the terms "PC" and "PEC" are often used interchangeably. Both methods share many similarities. Essentially, the same processes occur in both, but in PC-WS, all reactions take place within individual particles, whereas in PEC-WS, the components are separated. In some literature, PC-WS is referred to as particulate photocatalytic water splitting. A photoelectrochemical reactor can either be a fixed panel or a reactor that uses a solar concentrator to optimize energy absorption. The most common catalysts used in PEC-WS systems include metal oxides because of their high electrochemical stability, relatively low cost, and wide range of band gaps. A combination of platinum (Pt) and iridium oxide (IrO2), or platinum (Pt) and titanium oxide (TiO2), is frequently used. Additionally, much research is being done on implementing iron oxide (Fe2O3) due to its high solar-to-hydrogen (STH) efficiency potential. A schematic representation of hydrogen production via PEC-WS is shown in Fig 6 and Fig 7.



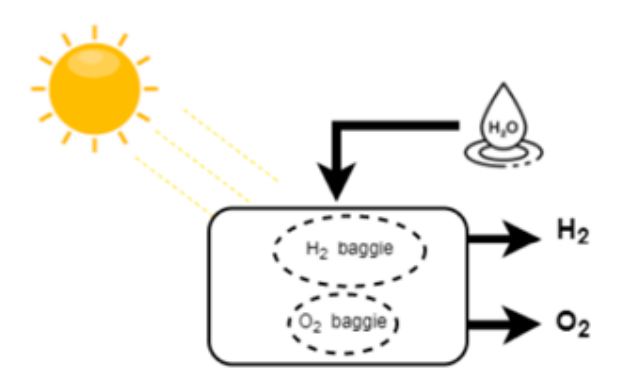


Figure 6: Schematic of PC-WS for hydrogen production [3]

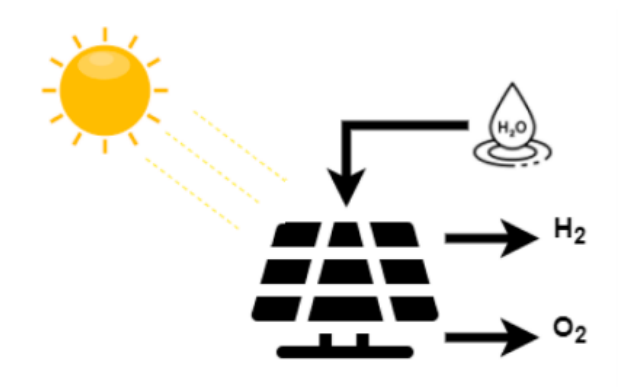


Figure 7: PEC-WS for hydrogen production [3]

BIO-PHOTOLYSIS

Direct bio-photolysis is an aerobic process, while indirect bio-photolysis is an anaerobic process. In the latter, CO2 is temporarily sequestered, and fermentation occurs as part of the anaerobic process. The schematics for both methods are shown in Fig. 8 and in Fig. 9. Bio-photolysis is a light-dependent process where photosynthesis enables the splitting of water molecules to produce hydrogen. Bio-photolysis utilizes incoming solar light for hydrogen production. Both methods commonly use microalgae, such as green algae, specifically the single-celled Chlamy-domonas reinhardtii, as they contain hydrogenase. This is crucial as hydrogenase catalyzes the reduction of CO2 and hydrogen formation. Generally, cyanobacteria or green algae are used for this process, with hydrogenase and nitrogenase enzymes acting as catalysts. Cyanobacteria are typically mutants of Anabaena, and the green algae are Chlamydomonas reinhardtii.



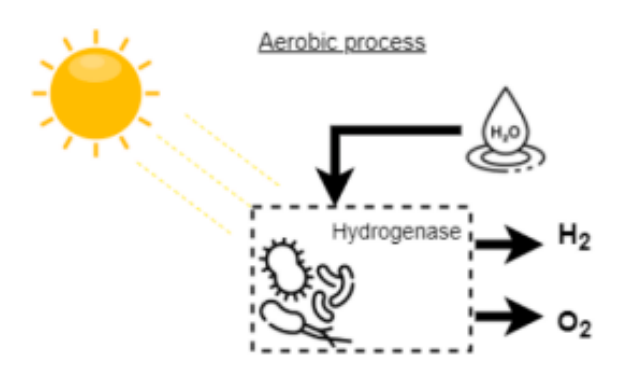


Figure 8: Schematic for DBP [3]

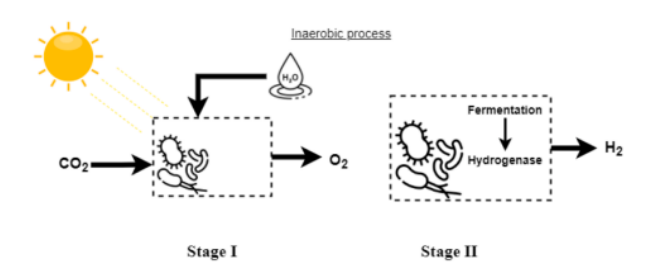


Figure 9: Schematic for IBP [3]

PV-ELECTROLYSIS

With PV-electrolysis, hydrogen is produced through an indirect method using photovoltaic (PV) electricity to power an electrolyzer. A schematic of this process is shown in Fig. 10. Both PV and electrolyzers are mature technologies, but currently, only a small percentage of global hydrogen is produced in this manner. The most common water electrolyzer methods are alkaline electrolyzers and proton exchange membrane (PEM) electrolyzers. Both methods generate hydrogen and oxygen by using a cathode and an anode.



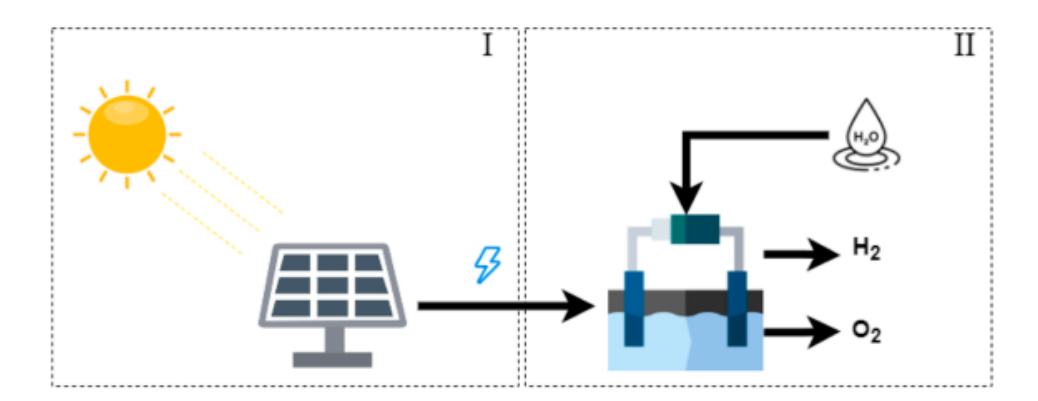


Figure 10: Schematic of PV-electrolysis [3]

As can be seen from tables in Fig. 11 and Fig. 12, the best systems are PV combined with alkaline or PEM electrolyzers, with efficiencies ranging from 8% to 14%. Photoelectrochemical (PECWS) systems have similar efficiencies, but they are still in much earlier stages of technological and commercial development, as can be seen from the hydrogen price graphs. In contrast, photocatalytic (PC-WS) water splitting systems have efficiencies that are about one order of magnitude lower, around 1%.



STH method	Rounded STH Efficiency	Materials	Environment
PC-WS	0.4%	$SrTiO_3$	Outside environment (Japan)
	0.1%	TiO ₂	Laboratory AM1.5
	0.4%	SrTiO ₃ :Al	Laboratory AM1.5
	0.1%	Si and ${\rm TiO_2}$	Laboratory (simulated sunlight)
	1.0%	Not specified	Not specified
	1.1%	SrTiO3:La, Rh/Au/	Laboratory
		BiVO ₄	AM1.5
	1.0%	Not specified	Laboratory AM1.5
	1.0%	SrTiO ₃ :La,Rh/Au/ BiVO ₄ :Mo	Laboratory AM1.5
	1.1%	SrTiO ₃ :La,Rh/Au/ BiVO ₄ :Mo photocatalyst sheet loaded with Ru and Cr ₂ O ₃	Laboratory (simulated sunlight)
	1.1%	SrTiO ₃ :La,Rh/Au/ BiVO ₄ :Mo	Laboratorium (simulated visible sunlight)
PEC-WS	10.0%	c-Si + Electrocatalyst: Pt, IrO_x	Laboratory (simulated sunlight)
	9.8%	c-Si + Electrocatalyst: Pt, IrO _x	Laboratory (simulated sunlight)
	12.7%	Perovskite photovoltaic + Earth- Abundant Electrocatalysts	Laboratory AM1.5
	10.0–16.0%	Not specified, but based on multiple studies	Laboratory AM1.5

Figure 11: STH efficiency conversion 1 [3]



STH	Rounded	Materials	Environment
method	STH		
	efficiency		
DBP	2.0%	Green Algae:	Laboratory
		Chlamydomonas	
		reinhardtii D1 protein	
		mutant	
	2.0%	Green Algae: Sulfur-	Laboratory
		deprived Chlamydomonas	AM1.5
		reinhardtii	
	2.0%	Green Algae:	Laboratory
		Chlamydomonas	AM1.5
		reinhardtii	
IBP	0.5-2.5%	Cyanobacteria: mutant of	Laboratory
		Anabaena	AM1.5
	1.5-2.0%	Cyanobacteria: Anabaena	Laboratory
		variabilis mutant PK84	AM1.5
	1.5-2.0%	Cyanobacteria: Anabaena	Outdoor
		variabilis ATCC 29413	conditions
	0.5%	Green Algae:	Laboratory
		Chlamydomonas	AM1.5
		reinhardtii	
	0.1%	Green Algae:	Laboratory
		Chlamydomonas	AM1.5
		reinhardtii	
	<1.0%	Green Algae:	Laboratory
		Chlamydomonas	AM1.5
		reinhardtii	

Figure 12: STH efficiency conversion 2 [3]

From the graph provided in the study "Analysis of photon-driven solar-to-hydrogen production methods in the Netherlands" [3] by Laurens S.F. Frowijn and Wilfried G.J.H.M. van Sark, it is clear that the most cost-effective choice at present is to focus on PV + Electrolysis systems. However, it is still reasonable for research into direct hydrogen production methods through photocatalysis to continue, as, in theory, it could be one of the best methods since it uses a single element for the reaction, maximizing theoretical efficiency and reducing plant complexity. But for now, this method is still in experimental stages



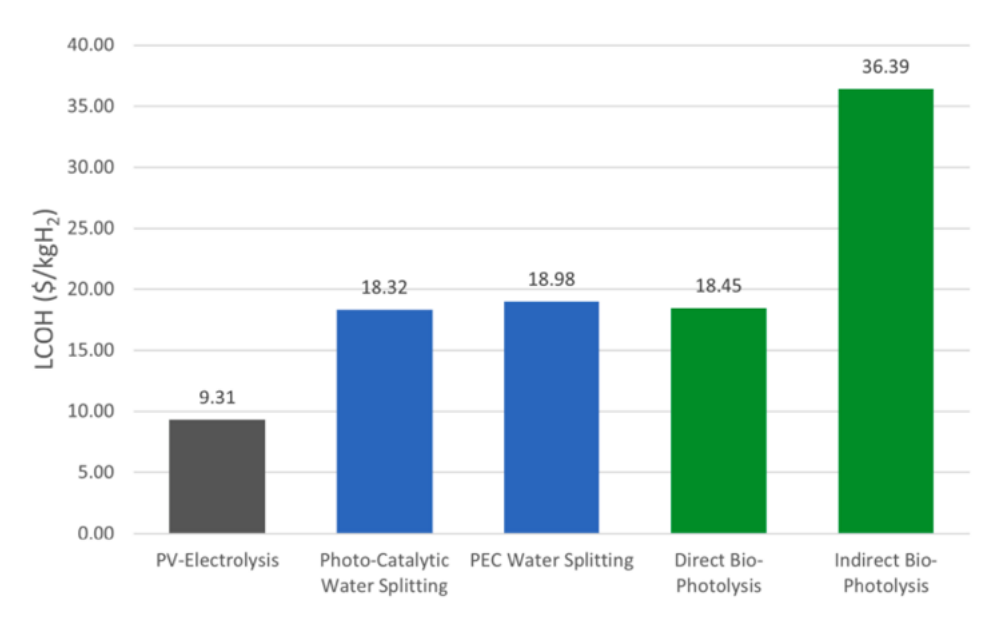


Figure 13: LCOH [3]

Overarching STH method	Sub STH method	Safety risk	Upscaling potential	Relative carbon footprint
PV-electrolysis	PV- alkaline	low	high	emissions
	PV-PEM	low	high	emissions
Photochemical water splitting	PC-WS	medium	very high	zero emissions
	PEC-WS	low	high	emissions
Bio-Photolysis	DBP IBP	low low	low low	uptake uptake

Figure 14: STH method comparison [3]

Having established that the PV + Electrolysis system is the most economically viable and technologically ready for real-world applications, let us now look at how the plant costs are evaluated in this study, as shown in the graph below.



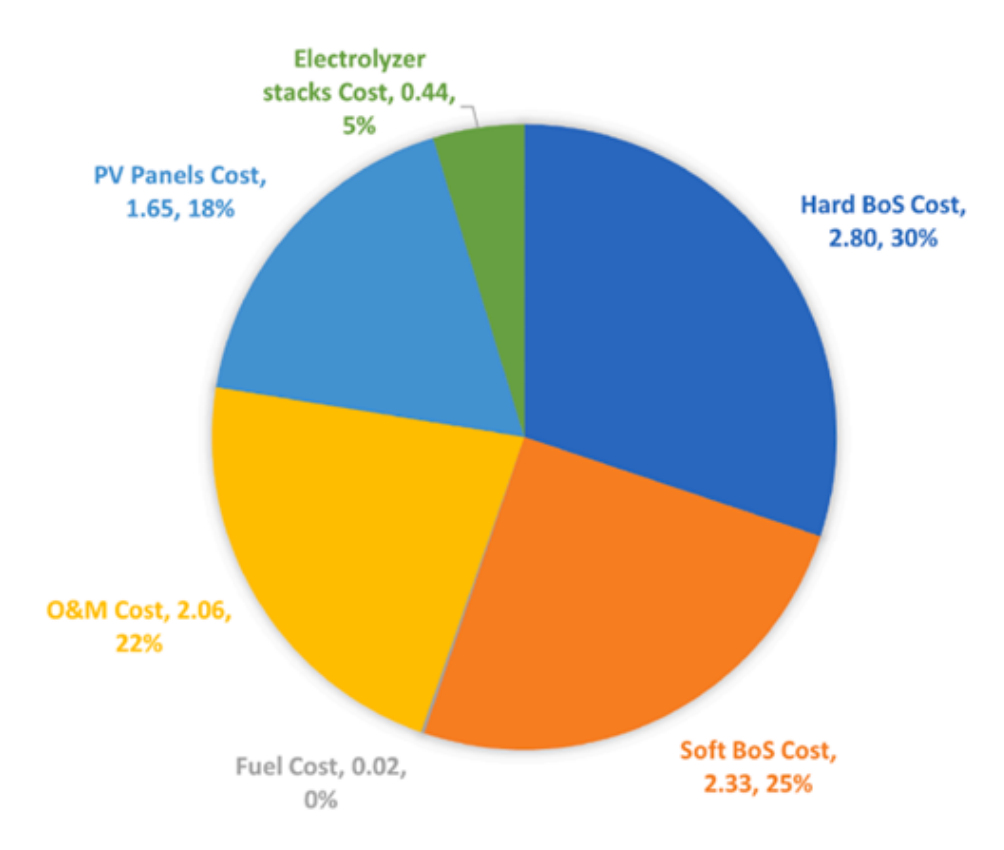


Figure 15: PV + ELY cost analysis [3]

Another important parameter highlighted in this study when choosing the PV + Electrolysis system is the minimum (tested) stable operation time (MTSOT). The MTSOT refers to the stability of the solar-to-hydrogen (STH) methods during a specific operation time. The operation time of a particular technology was assumed to be stable and sufficient for a minimum of 500–1000 hours, without significant efficiency losses or other key performance issues. To perform an accurate comparative analysis of all these solar-to-hydrogen methods, seven key parameters were defined to assess how each one varies individually and to conduct a sensitivity analysis. This led to the determination of an average Levelized Cost of Hydrogen (LCOH) based on all the possible variations of these seven parameters. Below is the graph for the PV + Electrolysis system; for the other systems, reference can be made directly to the aforementioned study. In any case, the numerical results are as shown in the graph.



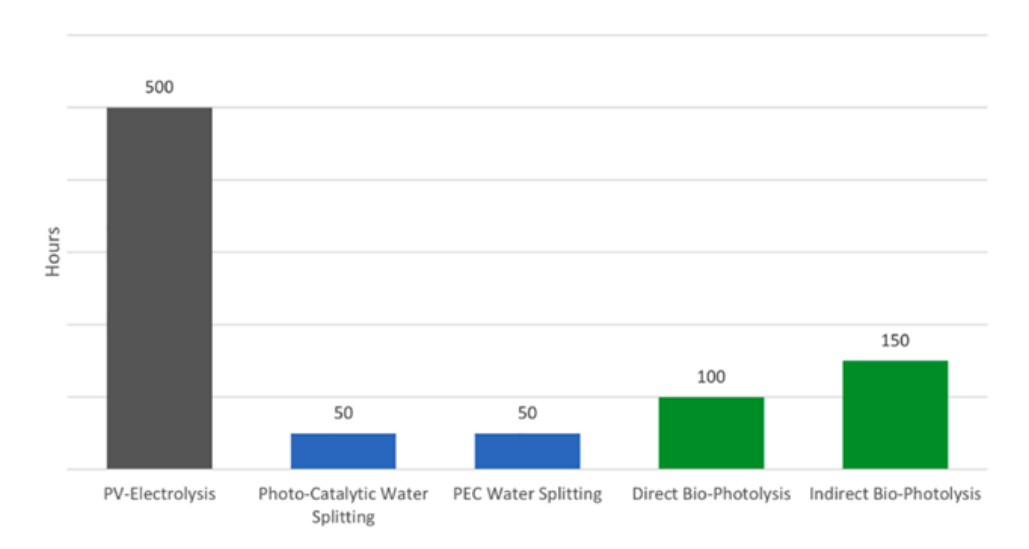


Figure 16: lifetime ELY [3]

To perform an accurate comparative analysis of all these solar-to-hydrogen methods, in this paper [3] seven key parameters were defined to assess how each one varies individually and to conduct a sensitivity analysis. This led to the determination of an average Levelized Cost of Hydrogen (LCOH) based on all the possible variations of these seven parameters. Below is the graph for the PV + Electrolysis system; for the other systems, reference can be made directly to the aforementioned study. In any case, the numerical results are as shown in the graph.

3.2 State of the Art and Technical Specifications

Having justified in the first chapter the need to introduce hydrogen into our energy system and verified that among all possible hydrogen production technologies, the only ones with zero CO2 impact and economically sustainable (although current technologies for hydrogen production from fossil fuels are still the most cost-effective) are electrolyzers, it is now necessary to focus our study on these technologies. This will allow us to conduct a state-of-the-art analysis of both the commercial and technical status of the current electrolyzer technologies in order to determine which ones would make sense to incorporate into a Power-to-X (PtX) plant. Water electrolysis is one of the most promising methods for hydrogen production because it uses renewable water (H2O) as a feedstock and produces only pure oxygen as a by-product. Additionally, the electrolysis process utilizes direct current (DC) power derived from sustainable energy sources, such as solar and wind. Currently, only 4% of hydrogen is produced from renewable sources through electrolysis. However, numerous studies indicate that this percentage is expected to grow, particularly in light of the targets set by the European Union's Energy Directive, which has set a goal to achieve 14% hydrogen production from renewable sources. The advantages of this technology for hydrogen production include high conversion efficiency and excellent hydrogen purity quality. In the electrolysis process, water molecules dissociate into hydrogen and oxygen molecules under the influence of electricity. Water electrolysis can be classified into four types based on their electrolyte, operating conditions, and ionic agents (OH-, H+, O2-). However, the operating principles remain the same across all methods. The four main types of electrolysis are: Alkaline Water Electrolysis (AWE), Solid Oxide Electrolysis (SOE), Proton Exchange Membrane (PEM) Water Electrolysis, and Anion Exchange Membrane (AEM) Electrolysis. In the following sections, we will describe each of these technologies in detail, with a particular



focus on PEM and AEM electrolyzers, as they are commercially more viable and better suited for integration into a Power-to-X plant, such as the one we aim to develop. In the table below, we can see a comparison between the four main types of electrolyzers. This table, taken from the 2020 IRENA report [10], shows the chemical reactions at the anode and cathode, the overall reaction, the different electrolytes and cell construction materials, the voltage range, operating temperature, hydrogen purity, electrode area, and also the capital cost. Some data for AEM are missing in this table, but we will discuss them later on, as AEM is a newer technology and not yet as mature as PEM.

	Alkaline	AEM	PEM	Solid Oxide
Anode reaction	$20H^- \rightarrow H_2O + \frac{1}{2} O_2 + 2e^-$	$2OH^- o H_2O + \frac{1}{2} O_2 + 2e^-$	$H_2O \rightarrow 2H^+ + \frac{1}{2} \ O_2 + 2e^-$	$0^{2-} ightarrow rac{1}{2} \ 0_2 + 2e^-$
Cathode Reaction	$2 \text{ H}_2\text{O} + 2\text{e}^- \rightarrow \text{H}_2 + 2\text{OH}^-$	$2 \text{ H}_2\text{O} + 2\text{e}^- \rightarrow \text{H}_2\text{+} 2\text{OH}^-$	$2 H^+ + 2 e^- \! \rightarrow H_2$	$H_2O+2e^- ightarrowH_2+O^{2-}$
Overall cell	$H_2O \rightarrow H_2 + \frac{1}{2} O_2$	$H_2O \rightarrow H_2 + \frac{1}{2} O_2$	$2H_2O \rightarrow H_2 + \frac{1}{2} O_2$	$H_2O \rightarrow H_2 + \frac{1}{2} O_2$
Electrolyte	KOH/NaOH (5M)	DVB polymer support with 1 M KOH/NaOH	Solid polymer electrolyte (PFSA)	Yttria stabilized Zirconia (YSZ)
Separator	Asbestos/Zirfon/Ni	Fumatech,	Nafion [®]	Solid electrolyte YSZ
Electrode/Catalyst (Hydrogen side)	Nickel coated perforated stainless steel	Nickel	Iridium oxide	Ni/YSZ
Electrode/Catalyst (Oxygen side)	Nickel coated perforated stainless steel	Nickel or NiFeCo alloys	Platinum carbon	Perovskites (LSCF, LSM) (La,Sr,Co,FE) (La,Sr,Mn)
Gas Diffusion layer	Nickel mesh	Nickel foam/carbon cloth	Titanium mesh/carbon cloth	Nickel mesh/foam
Bipolar Plates	Stainless steel/Nickel coated stainless steel	Stainless steel/Nickel coated stainless steel	Platinum/Gold-coated Titanium or Titanium	Cobalt coated stainless steel
Nominal current density	0.2-0.8 A/cm ²	0.2-2 A/cm ²	1–2 A/cm ²	0.3–1 A/cm ²
Voltage range (limits)	1.4–3 V	1.4-2.0 V	1.4-2.5 V	1.0-1.5 V
Operating temperature	70–90 °C	40-60 °C	50-80 °C	700–850 °C
Cell pressure	<30 bar	<35 bar	<70 bar	1 bar
H2 purity	99.5-99.9998%	99.9–99.9999%	99.9-99.9999%	99.9%
Efficiency	50%-78%	57%-59%	50%-83%	89% (laboratory)
Lifetime (stack)	60 000 h	>30 000 h	50 000-80 000 h	20 000 h
Development status	Mature	R & D	Commercialized	R & D
Electrode area	10 000–30 000 cm ²	<300 cm ²	1500 cm ²	200 cm ²
Capital costs (stack) minimum 1 MW	USD 270/kW	Unknown	USD 400/kW	>USD 2000/kW
Capital costs (stack) minimum 10 MW	USD 500-1000/kW	Unknown	USD 700-1400/kW	Unknown

Figure 17: Technical characteristic of typical water electrolysis technologies [4]

This second table provides a summary of the advantages and disadvantages of the different electrolysis technologies.



Advantages and disadvantages o	f typical water electrolysis technologies.	
Flectrolysis technology	Advantages	

Electrolysis technology	Advantages	Disadvantages
Alkaline water electrolysis	 Well established Technology Commercialized for industrial applications Noble metal-free electrocatalysts Relatively low cost Long-term stability 	 Limited current densities Crossover of the gasses High concentrated (5M KOH) liquid electrolyte
AEM water electrolysis	 Noble metal-free electrocatalysts Low concentrated (1M KOH) liquid electrolyte. 	 Limited stability Under development
PEM water electrolysis	 Commercialized technology Operates higher current densities High purity of the gases Compact system design Quick response 	 Cost of the cell components Noble metal electrocatalysts Acidic electrolyte
Solid oxide water electrolysis	High working temperatureHigh efficiency	Limited stabilityUnder development

Figure 18: Advantages and disadvantages of typical water electrolysis technologies [4]

Now, before presenting a comparison between the different technologies using appropriate charts, let's analyze each of the four technologies individually.

1) ALKALINE WATER ELECTROLYSIS

Hydrogen production by alkaline water electrolysis is well established technology up to the megawatt range for commercial level in worldwide. Alkaline water electrolysis process initially at the cathode side two molecules of alkaline solution (KOH/NaOH) were reduced to one molecule of hydrogen (H2) and two hydroxyl ions (OH) are produced. The produced H2 eliminate from the cathode surface to recombine in a gaseous form and the hydroxyl ions (OH) transfer under the influence of the electrical circuit between anode and cathode through the porous diaphragm to the anode, here in discharged to $\frac{1}{2}$ molecule of oxygen (O2) and one molecule of water (H2O). The O2 recombined at the surface of electrode and escapes as hydrogen. In alkaline water electrolysis process, asbestos diaphragm and nickel materials are used as the electrodes. The diaphragm having in the middle of the cell and it separates the cathode, and anode also separates the produced gases from their respective electrodes and avoiding the mixing of produced gases electrolysis process. However, in alkaline electrolysis have negative aspects such as limited current densities (below 400 mA/cm2), low operating pressure and low energy efficiency.



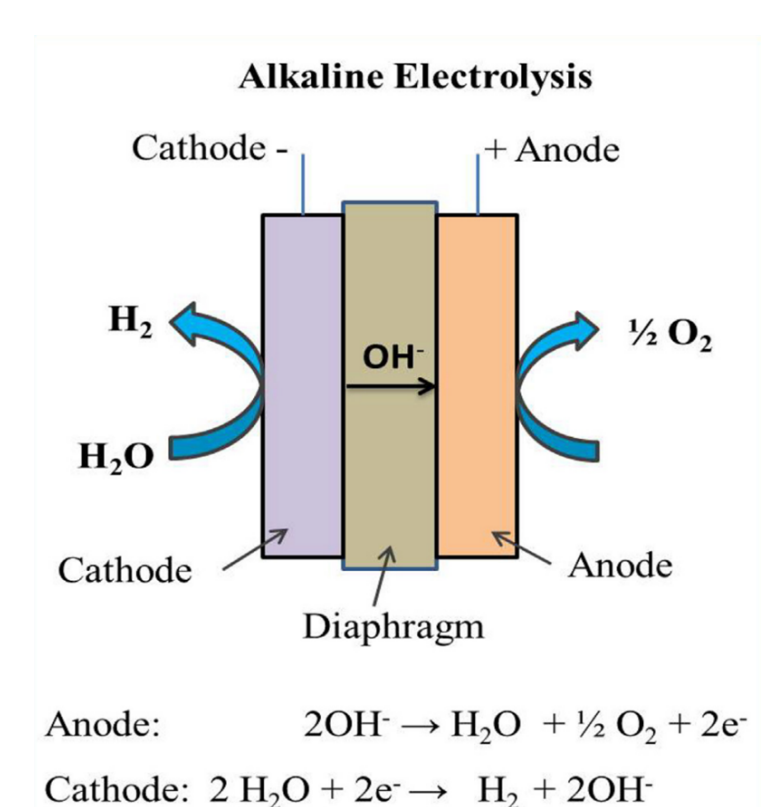


Figure 19: Alkaline Electrolysis [1]

 $H_2O \rightarrow H_2 + \frac{1}{2}O_2$

2) SOLID OXIDE OLECTROLYSIS (SOE)

Overall cell:

Solid oxide electrolysis has attracted an abundant deal of attention due to the electrical energy converts into the chemical energy along with producing the ultra-pure hydrogen with greater efficiency. Solid oxide electrolysis operates at high pressure and high temperatures 500–850 C and utilizes the water in the form of steam. Solid oxide electrolysis process conventionally uses the O2 conductors which are mostly from nickel/yttria stabilized zirconia. Nowadays, some of the ceramic proton conducting materials have been developed and studied in solid oxide fuel cells. However, increasing the much attention towards ceramic proton conducting materials for SOE electrolysis process, due to these materials demonstrates high efficiency and superior ionic conductivity than O2 conductors at an operating temperature of 500–700 C. The main characteristics of solid oxide electrolysis (SOE) technology is higher operating temperature which makes advantageous compared to low temperature electrolysis. Although, the SOE having some issues related to lack of stability and degradation, which have to be solved before going to commercialization on a large scale



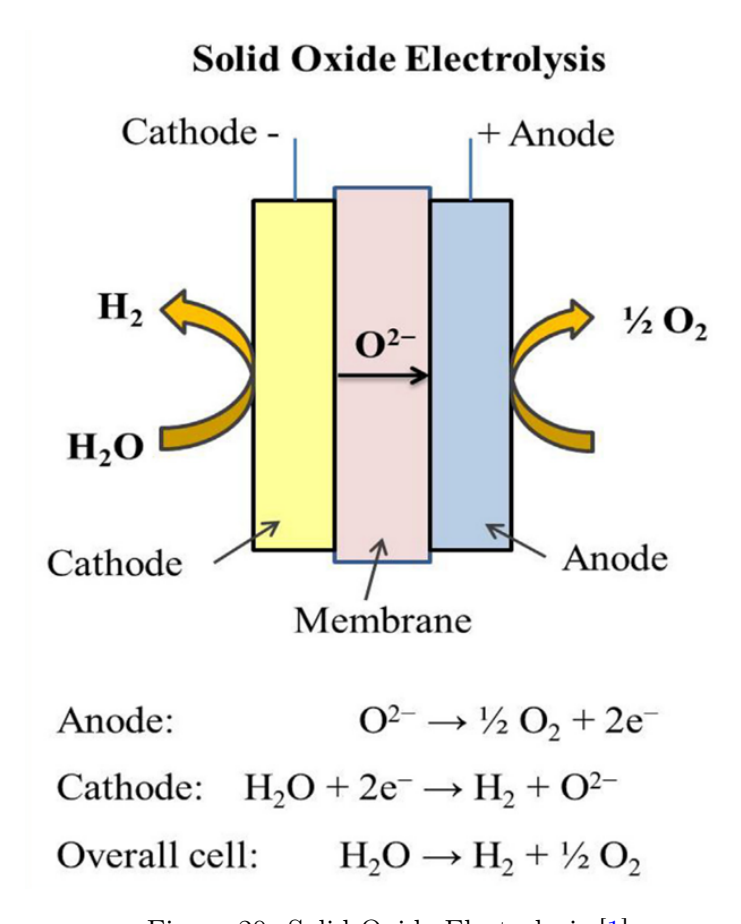


Figure 20: Solid Oxide Electrolysis [1]

I won't go into too much detail about PEM and AEM for now, because once the comparison is completed, it will become clear that these two are the most interesting options for our Power-to-X plant.In PEM water electrolysis, water is electrochemically split into hydrogen and oxygen at their respective electrodes such as hydrogen at the cathode and oxygen at the anode. PEM water electrolysis is accrued by pumping of water to the anode where it is spilt into oxygen (O2), protons (H+) and electrons (e). These protons are travelled via proton conducting membrane to the cathode side. The electrons exit from the anode through the external power circuit, which provides the driving force (cell voltage) for the reaction. At the cathode side the protons and electrons re-combine to produce the hydrogen.

3.3 Comparison Between the Different Types of Electrolyzers

CAPEX and Future Developments

The actual capital expenditures (CAPEX) for the four types of electrolyzers are presented in this table.

Regarding potential future developments in CAPEX for the two most commercially mature technologies, ALK and PEM, a report compares 22 studies conducted worldwide on this topic. As shown in the following charts—though highly uncertain and often inconsistent with each other—both technologies are expected to see a reduction in CAPEX. However, as with most energy-related forecasts, future projections are complex and unreliable, being influenced by numerous geopolitical, social, economic, and technological factors. This is simply to highlight that



Type	Industrial demonstration size (MW)	CAPEX (SoA), Euro/kW
AEL	150	600
PEM	10	900
AEM	1	1.000
SOE	4	2.130

Table 1: CAPEX (State of the Art) and demonstration sizes for various types of electrolyzers [11]

potential future developments should not be overly relied upon when choosing an electrolyzer today. Instead, decisions should be based on solid, current, and concrete data, while keeping in mind that there is no strong reason to believe any alternative technology will clearly outperform the ones we will model in the future. The study also highlights how the region of the world where a specific technology is deployed can significantly impact the CAPEX of the electrolyzer. This is why it will be necessary to localize our plant in order to give more reliability and relevance to the simulation.

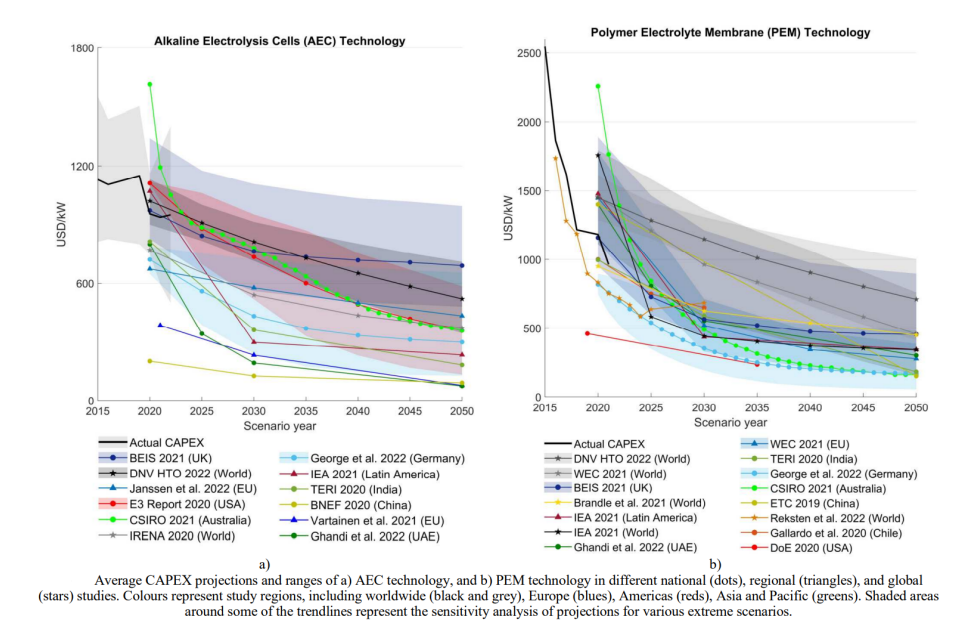


Figure 21: Future Develope CAPEX [5]



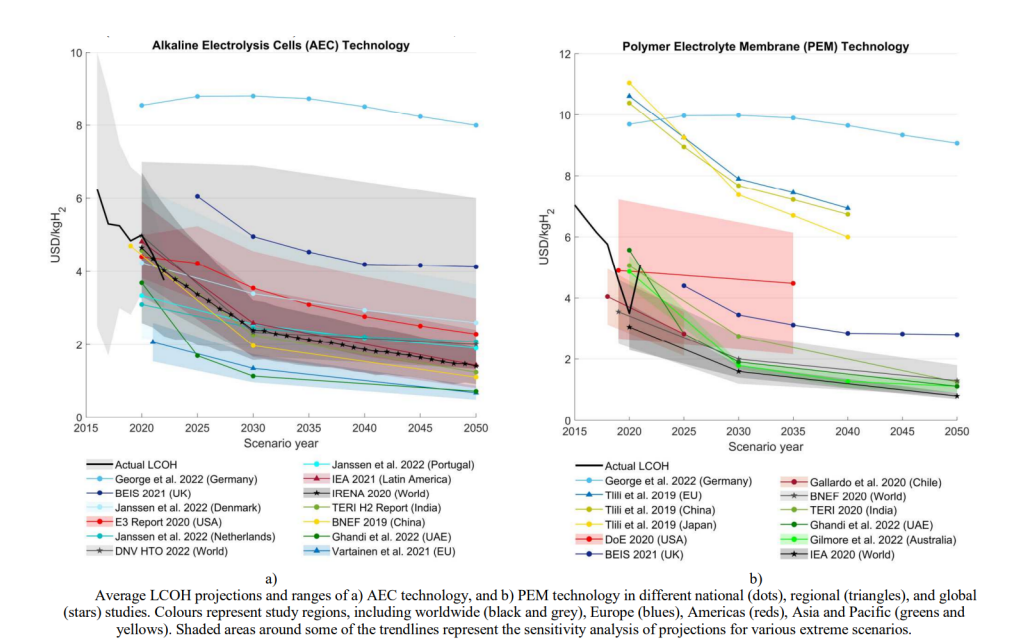


Figure 22: Future Develope LCOH [5]

Some conclusions from this paper are cited to support the previous statements.

- "1) There is a general agreement between the projections of CAPEX for both AEC and PEM technologies as almost all show a declining trend until 2050, though with different magnitudes: 60 and 75
- 2) LCOH projections also show a downward behavior trend throughout the studied timeframe, affirming the agreement on the potential for production cost reductions in future for both AEC and PEM technologies.
- 3) The analyzed projections are aligned with the trendline of actual market costs of CAPEX and LCOH. Even with sudden changes in the pattern of actual costs, as is the case for PEM LCOH between 2020 and 2022, a majority of projections have a value near to the actual market costs.
- 4) In terms of disagreements, on CAPEX for AEC technology, China shows the lowest values by far. Australia is on the other extreme. For PEM, United States is cheapest, and Australia most expensive. On AEC LCOH, Germany and the United Kingdom are most expensive due to high electricity prices, while UAE is cheapest. On PEM LCOH, Japan and again Germany project substantially higher costs. The difference between extremes in CAPEX and LCOH are about a factor of 4 and 8, respectively, underscoring the significance of considering specific country contexts in hydrogen production assessments."

conclusion of: "Electrolyzer cost projections compared to actual market costs: A Critical Analysis" [5].

TRL Level

Another important parameter in choosing the right electrolyzer is the level of technological development, which is summarized in the image below.



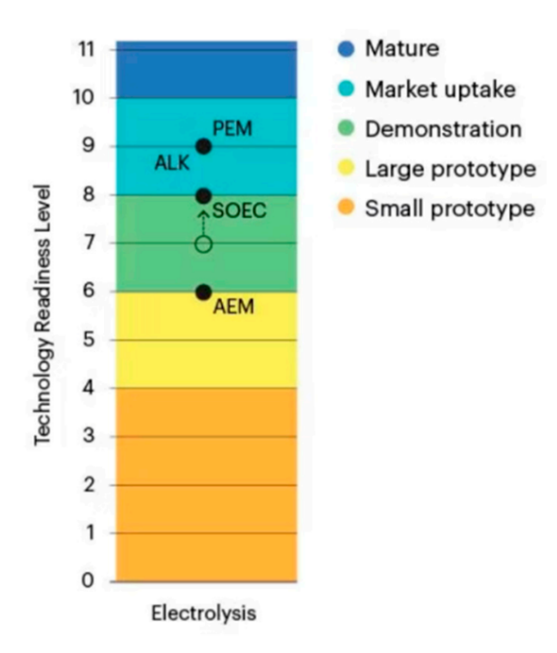


Figure 23: TRL Electrolyzer [6]

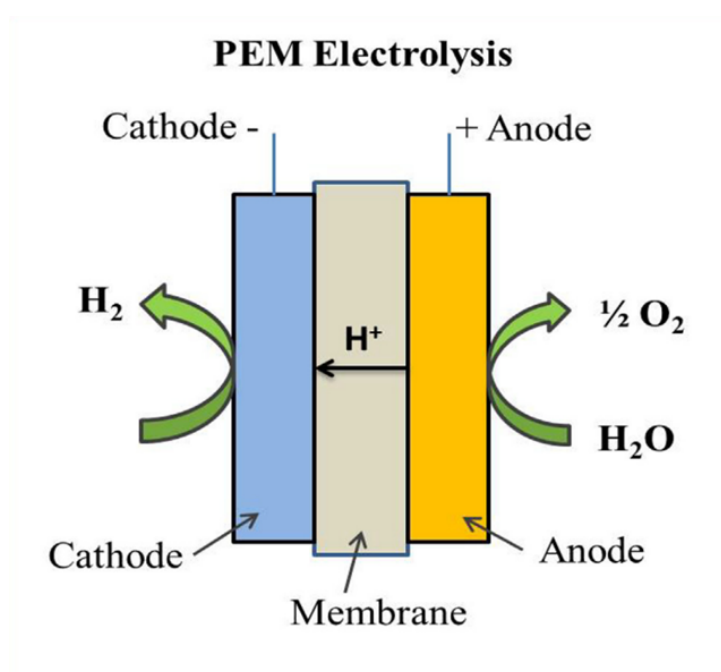
Moreover, the conclusion of the research work on AEM electrolyzers by the research group at the Warsaw University of Technology helps us understand that the purpose of this work—attempting to model a plant with AEM—makes sense in order to explore the potential developments of this technology, including the possible integration with storage systems. "First, no studies were found in the literature that present advanced models for energy-storage applications. Secondly, most research has focused on single-cell experimental tests to explore the chemistry of individual cell components, assess their stability, and evaluate new membranes and electrode compositions. While this research offers a foundational base of knowledge, it highlights the need for further numerical and experimental research to develop models applicable to larger-scale systems" Cit.[6]

PEM and AEM

Now, let's carry out a more detailed analysis of the two technologies that will be simulated in the plant: PEM and AEM. While currently, PEM is the only technology ready to power a Power-to-X plant of this kind, AEM is one of the most promising prospects for further reducing hydrogen production costs, even though, as shown in Fig. 23, it is still not ready for actual industrial use. Following the description of these two technologies, we will examine some graphs created from the data in the previous tables and make considerations to justify the choice of PEM electrolyzers for Power-to-X and AEM as a potential better future option. **PEM** Let's begin by describing PEM technology:

In PEM water electrolysis, water is electrochemically split into hydrogen and oxygen at their respective electrodes such as hydrogen at the cathode and oxygen at the anode. PEM water electrolysis is accrued by pumping of water to the anode where it is split into oxygen (O2), protons (H+) and electrons (e). These protons are travelled via proton conducting membrane to the cathode side. The electrons exit from the anode through the external power circuit, which provides the driving force (cell voltage) for the reaction. At the cathode side the protons and electrons re-combine to produce the hydrogen.





Anode: $H_2O \rightarrow 2H^+ + \frac{1}{2}O_2 + 2e^-$

Cathode: $2H^+ + 2e^- \rightarrow H_2$

Overall cell: $2H_2O \rightarrow H_2 + \frac{1}{2}O_2$

Figure 24: PEM [1]

A PEM consists of:

- Two bipolar plates: These ensure charge transport between cells, manage reactants (water) and produced gases (H, O), and provide mechanical stability. They also facilitate mass transport and heat dissipation through flow channels that allow water to wash over the gas diffusion layer and remove residual gases.
- Gas diffusion layers: Enable the flow of components. In fuel cells, hydrogen enters the anode and oxygen enters the cathode. In electrolyzers, water enters the anode (oxygen exits), while hydrogen exits from the cathode.
- Catalyst-coated membrane: Enhances the reaction. Since the membrane (NAFION) is sensitive to temperature and carbon cracking, an expensive catalyst is used. On the cathode side, platinum (a noble metal) is typically supported by conductive materials to improve conductivity and reduce catalyst loading.
- Solid acidic membrane: Also known as a proton exchange membrane (PEM), it facilitates H proton exchange, separates product gases, and supports both the anode and cathode catalyst layers.

Whether the power comes from a renewable intermittent, variable, or constant source, the component must exhibit dynamic behavior. Temperature fluctuations inside the cell, caused by degradation phenomena and variable power, can lead to changes in current, affecting hydrogen production. Additionally, material degradation may cause malfunctions, hot spots, obstructions, and ultimately, cell failure. PEM electrolyzer have advantages like: Less caustic, can be reversible



device, operate a lower cell voltage, higher current density, higher temperature and pressures lead to higher efficiencies (80-99%).

Soma disadvantages can be high material cost, cross permeation phenomena is neede a dunamic connection between electrolysis system and the intermittent electrical source The production of Idrogen in an electrolyser is related to the currents that flows in it. A cell operates with two types of currents: one from electron transport through the external circuit and another from ion movement across the membrane between electrodes. Since the cell current directly correlates with the number of reacting or produced chemical species, both currents are equivalent in magnitude. This relationship is governed by Faraday's law:

$$n_i = \frac{I}{z * F} \tag{1}$$

Where:

- ni is the molar flow of species i participating to the reaction [mol/s]
- I is the cell current [A]
- F is the faraday constant [c/mol]
- z is the charge number of species i

This way, we can calculate the molar flow of hydrogen produced as a function of the current supplied to the electrolyzer at the specific nominal voltage for each electrolyzer. With the molar flow, we can then calculate the mass flow.

The Nernst voltage represents the ideal voltage required for the electrolyser to operate under perfect conditions, defining the minimum thermodynamic voltage needed for the electrochemical reaction. The Nernst law is derived by modeling the cell/electrolyser as a black box exchanging work, heat, and mass with the surroundings under these assumptions: Neglecting transport mechanisms, thus ignoring entropy generation due to irreversibility. Ideal operating conditions are assumed. Steady-state operation is considered. Applying the first and second laws of thermodynamics under these constraints (derivation omitted here, to be included later) leads to the following expression:

$$E_{\text{cell}} = +\frac{\Delta G(T, p)}{zF} \tag{2}$$

$$E_{cell} = E_{rev}^{0} + \frac{RT}{2F} \left[ln \left(\frac{P_{H_2} P_{O_2}^{1/2}}{P_{H_2} O} \right) \right]$$
 (3)

G0 is the free enthalpy of reaction at temperature T and pressure p of the cell [J mol-1] – E, also known as Nerst Voltage or Reversible cell voltage he Nerst voltage depends on the Temperature and on the pressure of the cell and it decreases linearly while the Temperature increases. To explicit the relationship between the temperature and the pressure and see how it affects the Nerst voltage it is possible to write the voltage of the cell explicating it in the following way:

Erev is the Nerst voltage calculated at standard temperature and pressure (25°C, 1 bar). p refers to the partial pressure of reactant (H2O) and of the products (H2 and O2). Ecell is still under ideal conditions



POLARIZATION CURVE

The real voltage of the cell can be expressed through the polarization law:

$$V_c = E_{cell} + E_{act} + E_{ohm} + E_{conc} \tag{4}$$

- -Eact is the activation overvoltage, which accounts for charge transfer at the electrode and is related to the kinetics of the charge transfer mechanism.
- Eohm is the ohmic overvoltage, considering the charge conduction and migration through the electrolyte and electrodes, reflecting the ohmic resistance and associated losses.
- Econc is the concentration overvoltage, which relates to mass transport and molecular diffusion within the electrodes, accounting for concentration differences between reactants at the bulk and the active sites in the catalyst layer.

Temperature also affects the current-voltage curve of an electrolyzer and, consequently, its efficiency. This is why it is essential to manage the cooling system effectively in order to optimize the plant's operation.

AEM

The AEM water electrolysis technology is similar to conventional alkaline water electrolysis. However, the key difference between alkaline and AEM water electrolysis is the substitution of traditional diaphragms (such as asbestos) with an anion exchange membrane (quaternary ammonium ion exchange membranes) in AEM water electrolysis. AEM water electrolysis offers several advantages, such as the use of cost-effective transition metal catalysts instead of noble metal catalysts. Additionally, it can utilize distilled water or a low-concentration alkaline solution (1M KOH) as the electrolyte, rather than a highly concentrated (5M KOH) solution1. Despite these significant advantages, AEMWE still requires further research and improvements regarding MEA stability and cell efficiency, which are crucial for large-scale or commercial applications. Currently, the reported stability is 2,000 hours with Sustain ion and 1,000 hours with Furnatech (A 201 and FAA3-50), and over 35,000 hours for the Enapter multicore AEM electrolyzer. AEM water electrolysis is one of the electrochemical water splitting techniques with the help of an anion exchange membrane and electricity. The electrochemical reaction consists of two half-cell reactions they are hydrogen evolution reaction (HER) and oxygen evolution reaction (OER). Initially, at the cathode side, the water molecule is reduced to generate hydrogen (H2) and hydroxyl ions (OH) by the addition of two electrons. The hydrogen is released from the surface of cathode and the hydroxyl ions (OH) are diffused through the ion exchange membrane to the anode side by the positive attraction of the anode, while the electrons are transported through the external circuit to the anode. At the anode side, the hydroxyl ions recombine as a water molecules and oxygen by losing electrons. The produced oxygen is released from the anode. The basic principle and half-cell reactions of AEM water electrolysis as shown in Fig. 25



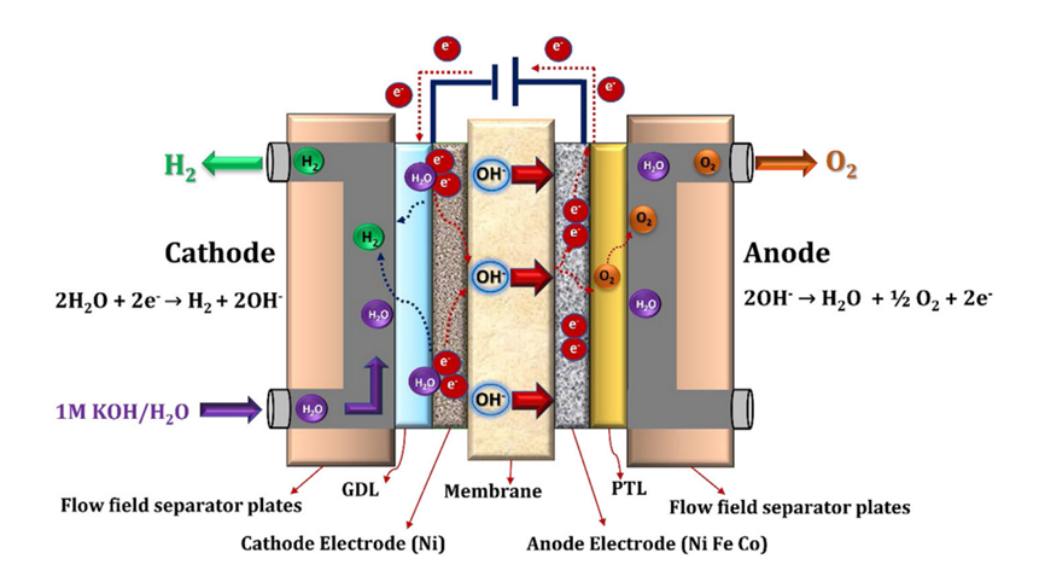


Figure 25: AEM [4]

Generally, AEM water electrolysis cell components are membrane (separator), electrode materials current collectors (gas diffusion layer), separator plates (bipolar plates), and end plates respectively. Typical anion exchange membranes are quaternary ammonium ion exchange membranes i.e., Sustanion®, Fumasep, Fumatech respectively. Commonly used anode and cathode electrode materials are transition metal based electrocatalysts especially Nickel and NiFeCo alloy materials respectively. The nickel foam/porous nickel mesh and carbon cloth are used as anode and cathode gas diffusion layers. Stainless steel and nickel-coatedstainless steel separator plates are used as bipolar and end plates respectively. AEM water electrolysis technology is under the developmental stage up to the kW scale. Globally, several research organizations/institutions are actively working on the development of AEM water electrolyzers, some of the AEM and PEM water electrolyzer manufacturers/developers are listed in table.

Enapter	Germany	AEM Multicore	210	35	4.8
PEM water elect	rolysis				
Nel.	Norway	M5000	5000	30	4.5
Cummins	Canada	HyLYZER® -4.000-30	4000	30	4.3
Siemens	Germany	Silyzer 300	100-2000	35	N/A
Proton onsite	USA	M400	417	30	N/A
ITM Power	UK	HGASXMW	110-1900	20	N/A
Plug Power	USA	GenFuel 5 MW	1000	40	5.2
Elogen	France	ELYTE 260	260	30	4.9

Figure 26: Commercial AEM and PEM [4]

PEM electrolyzers, mostly using IrO2 and Pt as catalyst materials, generate hydrogen with highpurity at lower temperatures. Proton exchange membranes conduct hydrogen ions, and act as a solid electrolyte. One constraint of PEM water electrolysis is its dependence on scarce materials such as platinum and iridium for operation. As said before the AEM electrolyzers are a recent water electrolysis technology that combines the benefits of Alkaline and PEM water electrolyzers. The AEM plays an important role in the transporting of hydroxide ions. At the cathode, both



hydrogen and hydroxyl ions are generated. Furthermore, AEM cells can use non-noble catalyst materials, which reduces the cost of producing hydrogen.

Anode:
$$4OH^- \rightarrow O_2 + 2H_2O + 4e^-$$

Cathode: $4H_2O + 4e^- \rightarrow 2H_2 + 4OH^-$ (5)
Overall reaction: $2H_2O \rightarrow 2H_2 + O_2$

To effectively perform the functions of AEM as the ion conducting path and gas separation barrier, AEM must possess several key characteristics: high ionic conductivity (ideally exceeding 100 mS/cm at the operating temperature), excellent alkaline stability, good thermal and dimensional stability, and robust mechanical properties.

However, achieving these ideal properties simultaneously remains a challenge. The harsh alkaline environment in water electrolyzers can compromise AEM stability, while strategies to enhance ionic conductivity, such as increasing ion exchange capacity (IEC), often lead to excessive water uptake and swelling, impacting the membrane's integrity. The structure of AEM generally consist of polymer backbones and anion exchange functional groups. Some of conductive polymer such as poly (vinyl alcohol), polystyrene, polyphenylenes, poly (arylene ether ketone), and polybenzimidazole was currently intensive in research for high mechanical and chemical stable polymer backbones in AEM. This trend is exemplified by a substantial increase in research publications on AEM water electrolysis, particularly over the past two years, as depicted in the Fig. 27

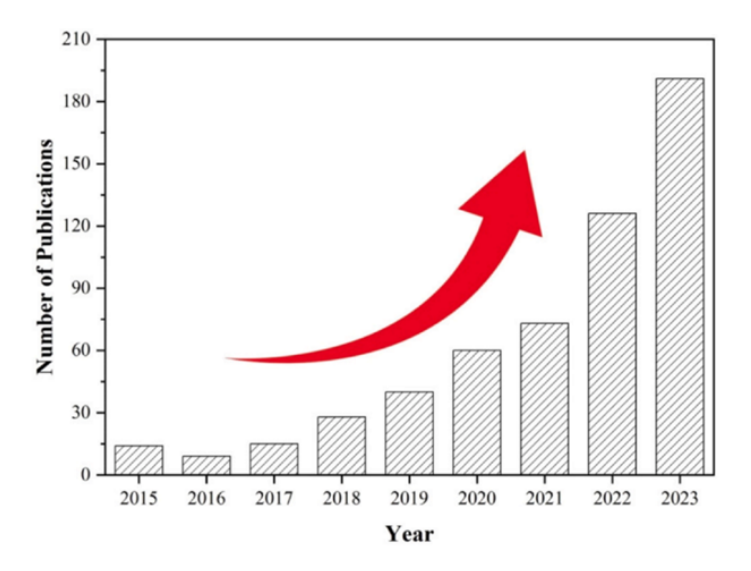


Figure 27: Publication AEM [7]

COMMERCIAL AEM

Several AEM membranes have been developed for commercial use. In the following section, a comparison is made based on key performance parameters.

Fumasep® FAA-3 series: fumatech One of the most affordable and durable AEM polymers offering the best balance between price and performance is the membrane from the Fumatech with their product are Fumasep® FAA-3 series [44]. This membrane is offered in a variety of thicknesses in the range of 20 to 50 μm for unsupported membrane and from 75 to 130 μm for membrane with reinforced with PP or PEEK. The price of the membrane is affordable



among other commercial AEMs in the market. Fumasep® FAA-3-50 is the type of Fumasep® series that is frequently used in the electrochemical system, especially for water electrolysis. It is derived from a polysulfone (PSf) polymer backbone with QA groups in the side chain Sustainion® X37-50: dioxide materials Sustainion® X37-50 is an imidazolium functionalized polystyrene membrane provided by Dioxide Materials

PiperION®: versogen PiperION® is a poly(aryl piperidinium)-based AEM provided by Versogen^{\mathbb{M}} that was first introduced as a hydroxide exchange membrane (HEM) fuel cell. Because of its higher ultimate stress when compared to other AEMs (Sustainion® and Fumasep® FAA-3), the PiperION® membrane also exhibits better wet/dry cycling stability

A201 and A901: tokuyama A201 and A901 types of Tokuyama membranes are hydrocarbonbased membranes with QA groups terminated side chains. Unfortunately, it is also necessary to mention that the chemical formula of A201 and A901 is not disclosed in the public domain

Aemion[™]: ionomr innovation inc Aemion[™] is a membrane fabricated by Ionomr Innovation and was developed based on methylated polybenzimidazoles

TM1: ORION polymer Orion[™] TM1 membrane is based on a terphenyl polymer with quaternary ammonium (QA) groups on alkyl side chains. It was specifically designed to prevent backbone degradation by eliminating aromatic ether groups, making it an all-carbon poly(arylene) structure with medium molecular weight. The National Renewable Energy Laboratory (NREL) tested over 50 AEM membranes from more than 10 partners. Orion[™] TM1 stood out as one of the most durable and stable, showing no signs of degradation. Its alkyl side chains help protect QA groups by reducing electron-withdrawing effects and mitigating cation deterioration.

All the membranes listed above are available in various thicknesses, which affects their structural strength. In the graphs above, we can see a comparison between the different types of membranes in terms of ion exchange capacity, area-specific resistance, ionic conductivity as a function of temperature, and tensile strength.



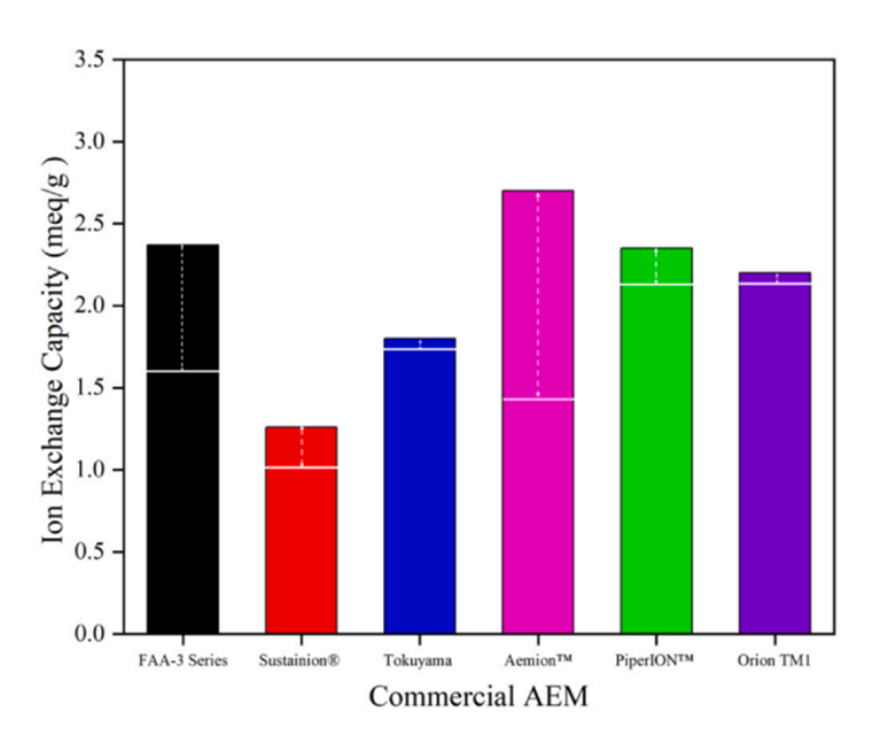


Figure 28: Ion Exchange Capacity [7]

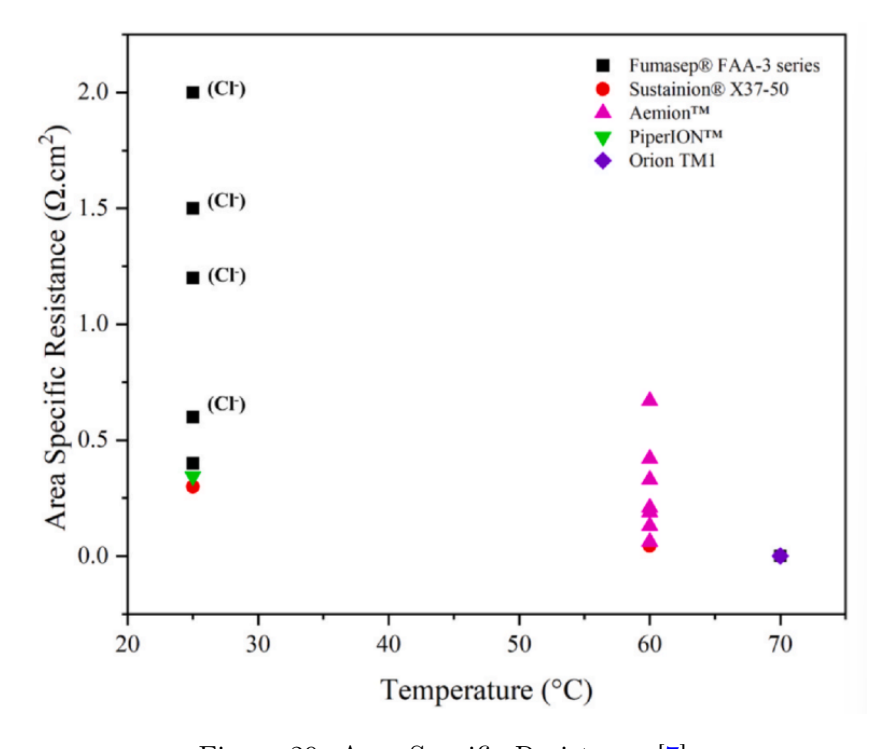


Figure 29: Area Specific Resistance [7]



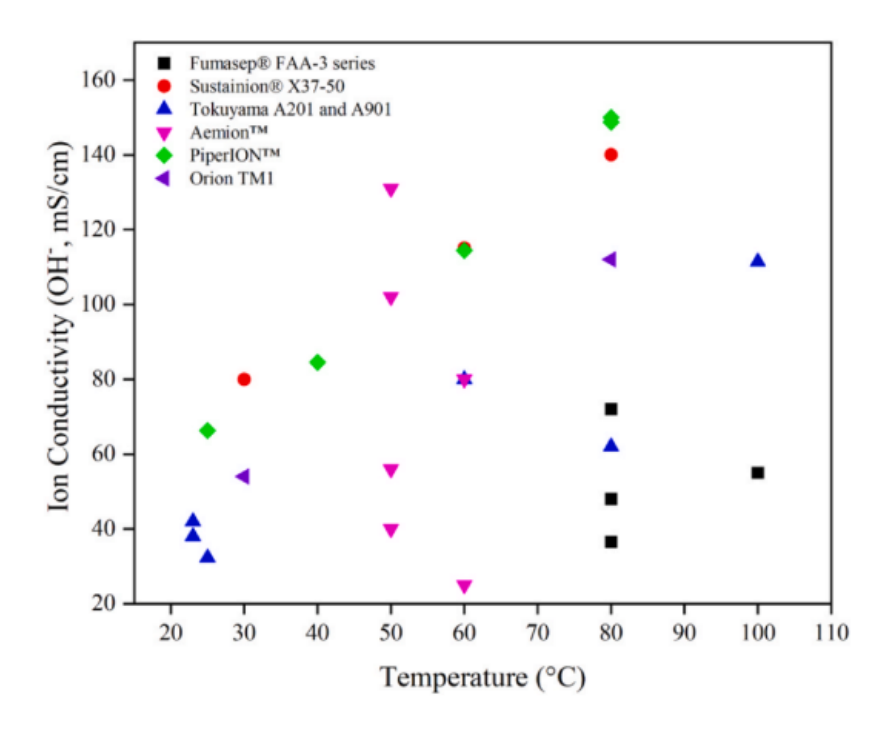


Figure 30: Ion Conductivity [7]

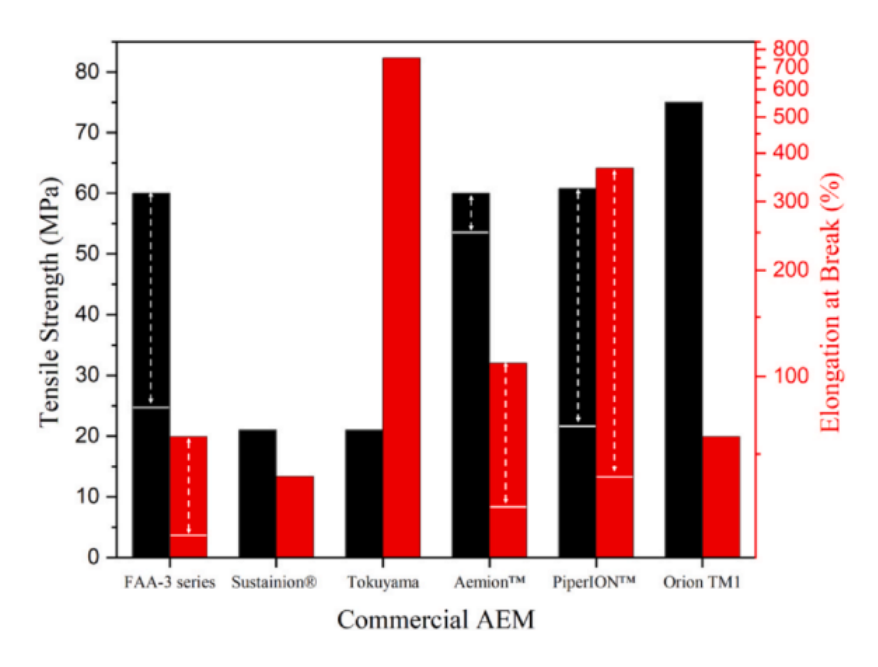


Figure 31: Tensile Strength [7]



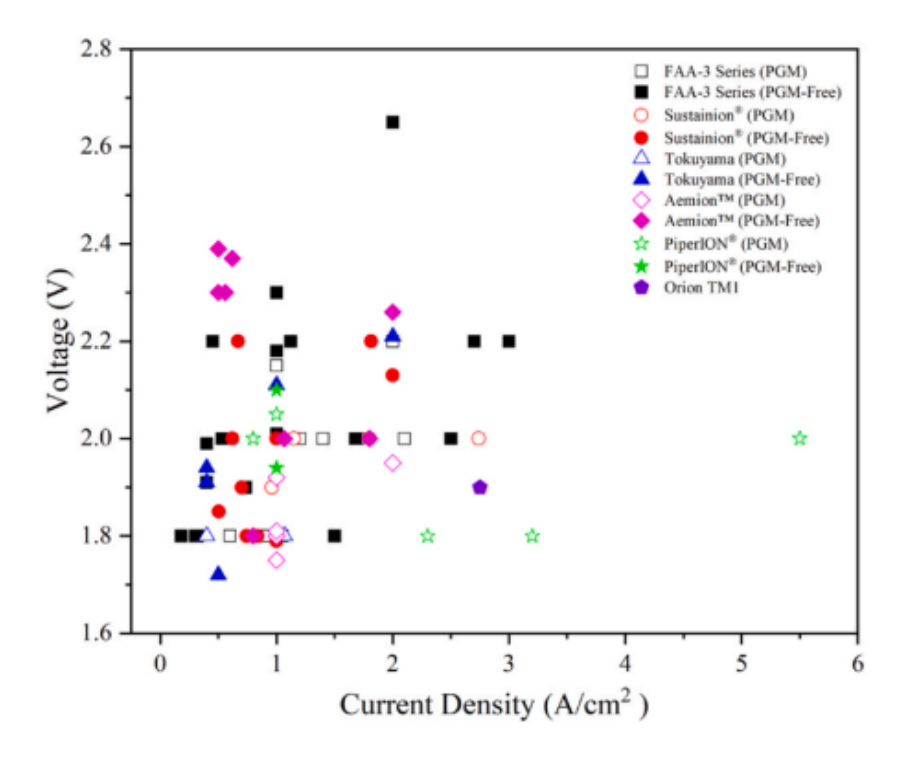


Figure 32: Voltage - Current Density [7]

AEM Multicore At the commercial level, one of the available AEM electrolyzers is the AEM Multicore. The product's commercial brochure provides some key technical specifications. The concept behind it is an electrolyzer designed to reach megawatt-scale power, using a scalable module architecture arranged in stacks.



Figure 33: AEM Multicore Stack [8]





Figure 34: AEM Multicore [8]

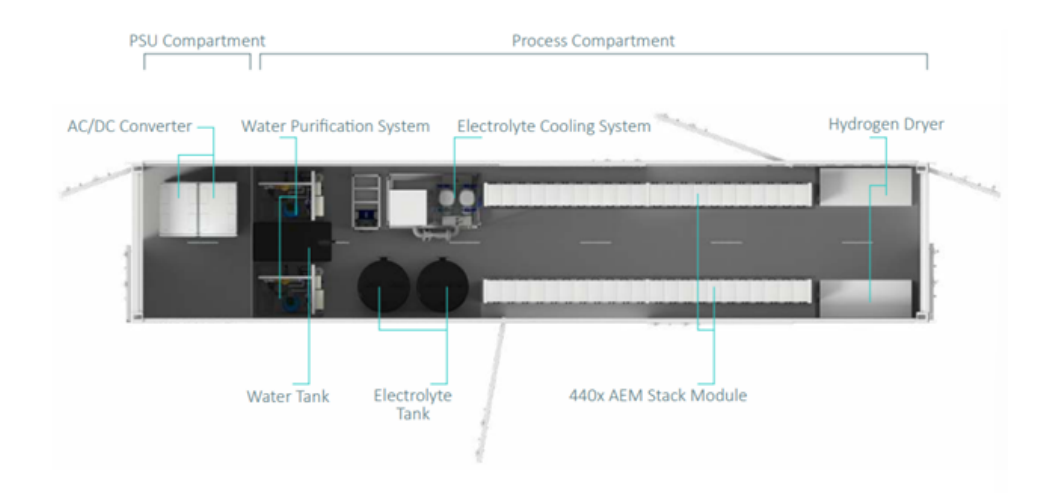


Figure 35: AEM Multicore structure [8]

Multiple stacks avoid a single point of failure. But not only this, a redundant balance of plant fully ensures that the failure of any single component doesn't result in complete shutdown of hydrogen production. Racks are installed on each side of the container, with plenty of working space in between. The entire system can be managed in a simple and intelligent way through an app and a dedicated IT system developed by the company itself. The technical datasheet is provided below.



Technical paramenters AEM Multicore

Nominal H₂ flow	210 Nm³/h	Net volume flow rate
H₂ outlet pressure	Up to 35 bar	
H₂ purity without optional dryer	99.8% in molar fraction	Impurities: $H_2O \approx 1500$ ppm, $O_2 < 5$ ppm
H₂ purity with optional dryer	99.999% in molar fraction	Impurities: H ₂ O < 5 ppm, O ₂ < 5ppn
Flexibility	3% - 105% of nominal production rate	
O ₂ outlet pressure	Atmospheric	
Specific power consumption	4.8 kWh/Nm³	Including all utilities inside the battery limit of module
Nominal electrical power consumption	1,035 kW	
Voltage	3 x 400 Vac three-phase grid	
Frequency	50/60 Hz	
Nominal water flow	0.19 Nm³/h purified water	Consumption of tap water input fo water purification is approximately 2x higher
Inlet water pressure	0.5 bar - 4 bar	
Inlet water temp.	6 °C - 30 °C	
System life	20 years	
Stack life	> 35,000 operating hours	
Hot startup time	0 - 100% within seconds	
Cold startup time	0 - 100% in ca 30 minutes, depending on ambient temperature	
Footprint	L 12.192 m × W 2.438 m × H 2.591 m	
Weight	Approximately 20 t	
Transport dimensions	40 ft container	

Figure 36: AEM Multicore Theorical specification [8]

Comparison between Electrolyzers:

The charts below show a comparison of the main technical and economic parameters of the electrolyzers we've discussed so far. From a technical point of view, we can observe that both PEM and AEM electrolyzers perform best, with high nominal current, long lifetime, and low degradation rate. They also stand out in terms of lower initial investment costs.

Alkaline electrolyzers are certainly competitive, but they suffer from a significantly lower current density.



Between AEM and PEM, AEM electrolyzers currently appear to be more expensive, which seems contradictory to the idea that they could be the ideal solution, as they combine the advantages of both Alkaline and PEM technologies while avoiding the use of rare and expensive materials.

The high cost of AEMs is mainly due to their development stage, which is still between prototype and commercial product. As a result, they are far from benefiting from economies of scale—a phase that PEM electrolyzers are already experiencing, contributing to their decreasing costs.

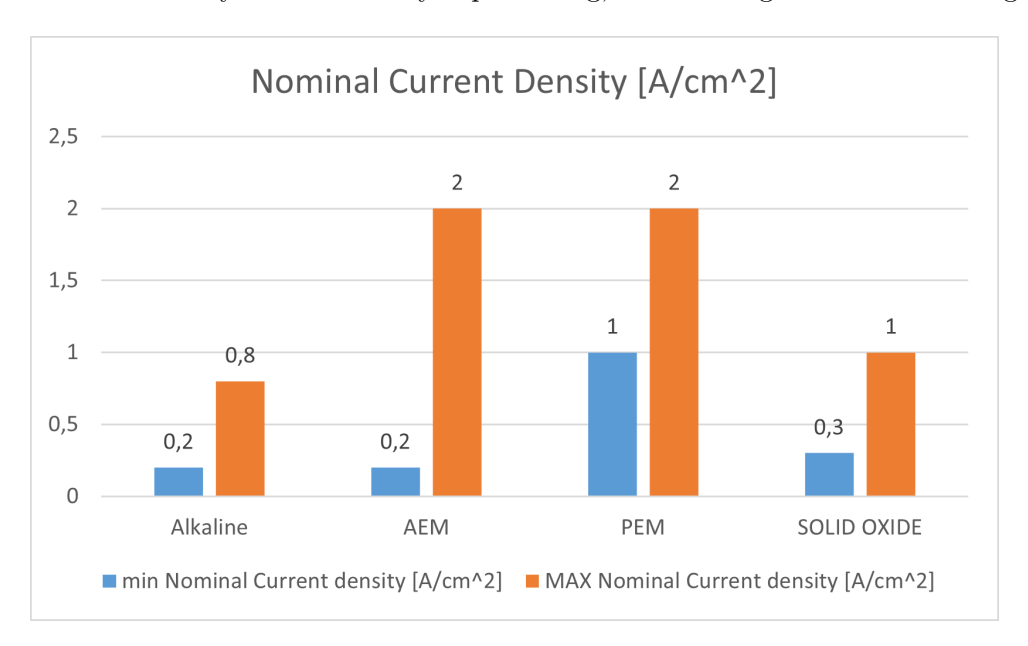


Figure 37: Nominal Current Density

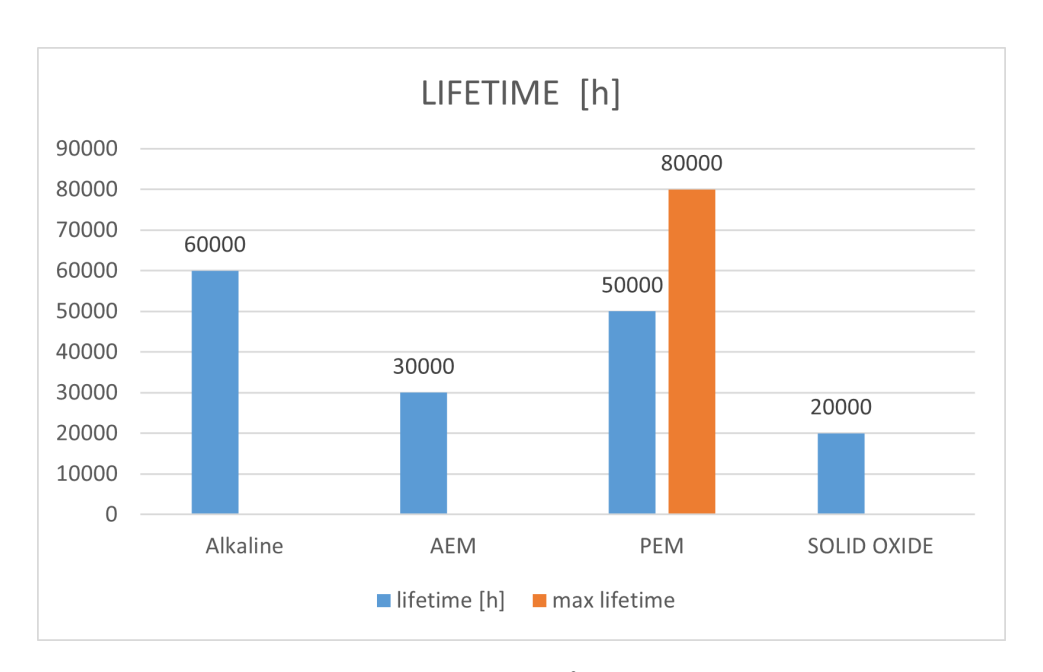


Figure 38: Lifetime



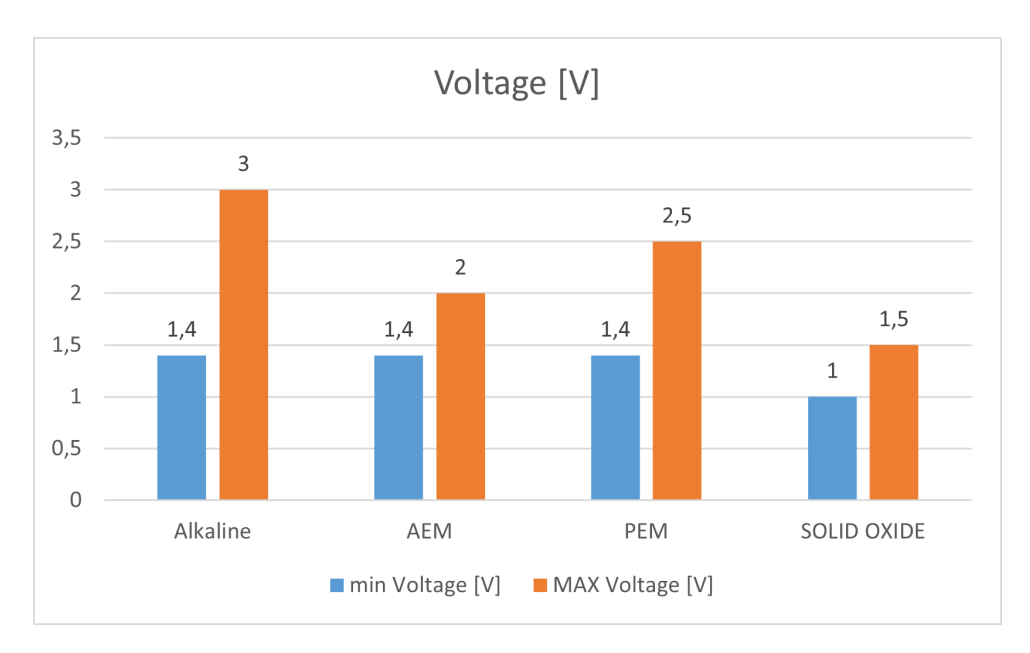


Figure 39: Voltage

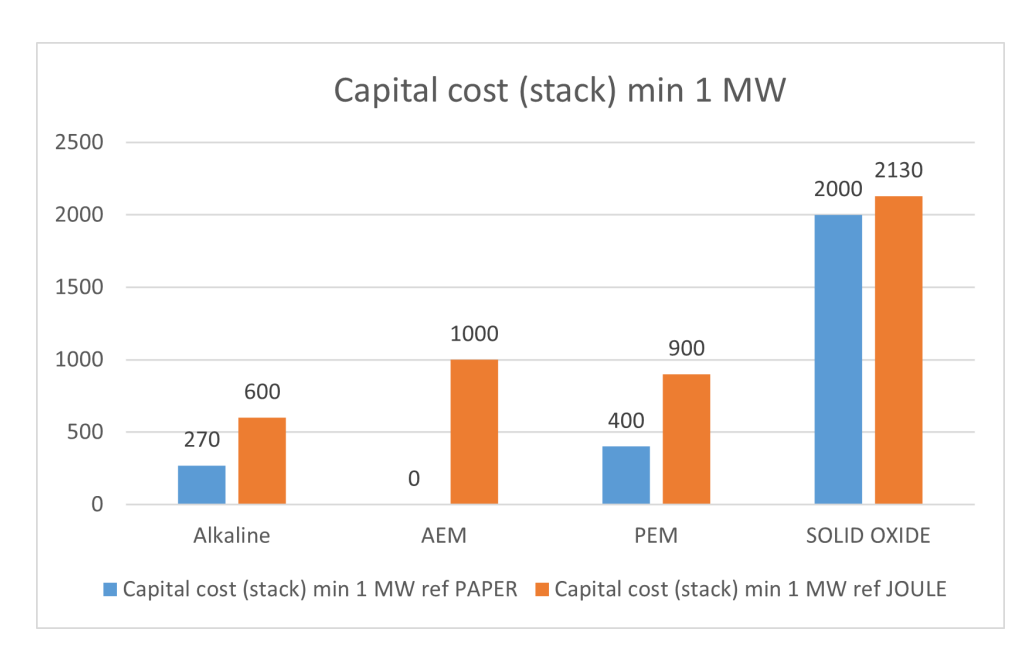


Figure 40: Capital cost (stack) min 1 MW



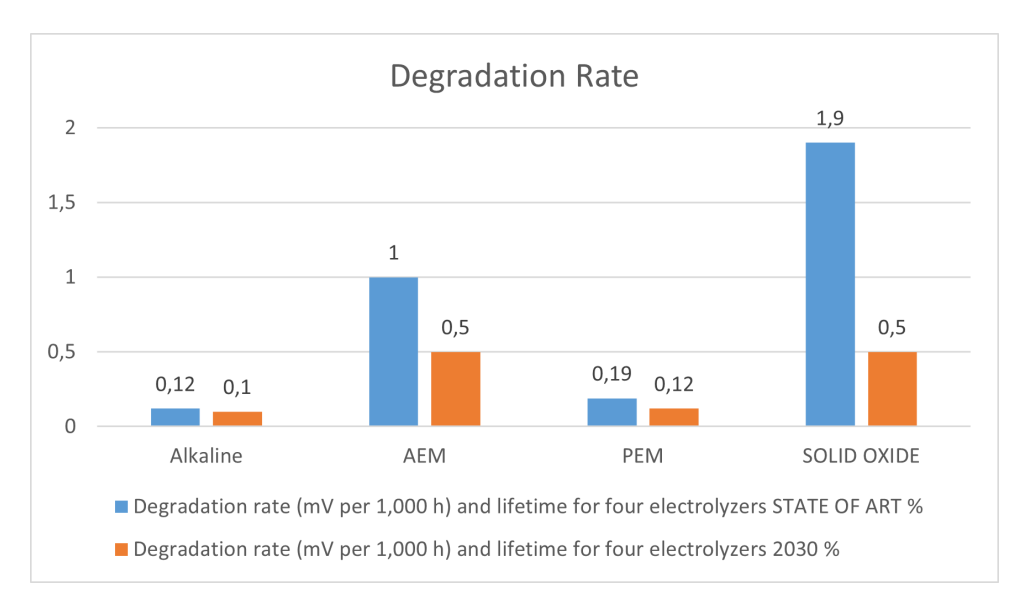


Figure 41: Degradation Rate



4 State of the Art: Storage

Hydrogen storage is a critical component in the development of a sustainable hydrogen economy. As a clean energy carrier, hydrogen offers high energy density by weight and produces only water upon combustion, making it an attractive alternative to fossil fuels. However, its low volumetric density poses significant challenges for storage and transport. Various storage methods have been developed, including gaseous and liquid storage, as well as solid-state storage using metal hydrides. Among these, metal hydrides are particularly promising due to their high volumetric hydrogen densities, safety advantages, and potential for reversible absorption and desorption. These materials can store hydrogen in a compact form, making them ideal for stationary and mobile applications. Nevertheless, issues such as cost, energy requirements for synthesis, material criticality, and recyclability must be addressed to enable large-scale adoption.

In this chapter, we will review the current state-of-the-art hydrogen storage technologies, with a particular focus on metal hydrides. We will analyze their economic and environmental aspects, availability of raw materials, and the potential for future implementation in industrial-scale hydrogen storage systems.

4.1 Physical Based

Physical-based hydrogen storage retains hydrogen in its molecular form using methods like compression and liquefaction. These technologies are already commercially used but face challenges such as energy demand, safety, and space efficiency. Despite their maturity, limitations remain for large-scale deployment. This section reviews current technologies and their development prospects.

4.1.1 Gaseous hydrogen

Gaseous hydrogen is the most common form used for energy storage and industrial applications. It is typically stored at high pressures, ranging from 200 to 700 bar, in specially designed cylindrical or composite tanks. This form of storage is straightforward and allows for quick refueling, making it suitable for mobility and transport sectors. However, due to its low volumetric energy density, high-pressure storage requires robust materials and strict safety measures. Advances in vessel technology and thermal management continue to improve its efficiency and practicality.

There are several types of vessels for storing gaseous hydrogen, classified from Type I to Type IV. Each type has specific characteristics regarding operating pressure and construction materials. Type I and II vessels are mainly used for industrial applications, while Type III and IV vessels, which are lighter and more advanced, are suitable for transportation and can withstand much higher pressures. In particular, Type IV composite cylinders can handle pressures up to 1000 bar.

4.1.2 Liquid Hydrogen

Liquid hydrogen is safe and more compact. It is liquefied at -253° C and then pressurized to 250-350 atm, with a volumetric density of 70 g/L and a boiling point of -253° C. The storage vessels are typically spherical (which reduce the surface area) or cylindrical.

The main challenges are:



49 4.2 Material Based

Type	Characteristics
Type I	17.5-20 MPa (industrial use)
Type II	26.3-30 MPa (industrial use)
Type III	25%-75% lighter, transport use, 450-700 Bar
Type IV	Composite cylinder, carbon fiber, up to 1000 Bar

Table 2: Characteristics of Compressed Hydrogen Storage Vessels

- Energy efficiency of the liquefaction process (with 25-40% losses)
- Thermal insulation (loss of 0.4% per day)

Typically, liquid hydrogen consists of 75% ortho-hydrogen (with parallel proton spins, thus higher energy) and 25% para-hydrogen (with antiparallel proton spins). Ortho-hydrogen decreases from 75% to 0% when the temperature reaches 20 K. The conversion from ortho- to para-hydrogen is crucial because it is exothermic and releases heat. Liquid hydrogen is ideal for marine transportation and storage in isolated locations.

4.1.3 Cryo-Compressed Hydrogen

Cryo-compressed hydrogen partially addresses the volume problem. It requires vessels that are insulated to handle high pressures and low temperatures.

At 1 bar, it has a density of 70 g/L, and at 240 bar, it has a density of 87 g/L when compressing liquefied hydrogen at 20 K.

This method provides a high dormancy period and reduces boil-off losses (evaporation losses over time).

4.2 Material Based

Material-based hydrogen storage refers to methods that store hydrogen through physical or chemical interactions with solid materials, rather than as a gas or liquid. These technologies aim to offer safer, more compact, and potentially more efficient alternatives to traditional storage methods. Common approaches include metal hydrides, chemical hydrogen carriers, and adsorption onto porous materials such as metal-organic frameworks (MOFs). Such systems can enable hydrogen storage at lower pressures and temperatures. However, challenges remain in terms of weight, reversibility, and cost for large-scale applications.

Hydrogen storage can be achieved by attaching hydrogen molecules to solid surfaces or by dissociating them into hydrogen atoms. The main methods are physisorption and chemisorption.

4.2.1 Physisorption

Physisorption occurs at high surface areas and low temperatures (below 77 K) with high pressure required for greater hydrogen capacity. A large surface area enhances absorption, typically requiring a high-pressure cylinder and a cooling system.

One common material used is Carbon Nanotubes (CNTs), which are lightweight and dominated



by Van der Waals interactions (10 $\rm kJ/mol$). These structures are essentially rolled-up graphite sheets in cylindrical form.

Physisorption is promising in terms of storage capacity (7.75 wt%) and volumetric capacity (0.209 kg H_2/L at ambient temperature and 650 atm).

Single-wall nanotubes can store around 3 wt% of hydrogen. Multi-wall nanotubes range between 1.8-2.6 wt% at approximately 10 MPa and ambient temperature. Overall, materials in this category have a storage capacity of 5-9 wt% and volumetric capacities between 40-60 g/L at high pressure and 77 K.

4.2.2 Chemisorption

Chemisorption involves bonding hydrogen chemically with materials such asmetals, chemical hydrides, ammonia, and liquid organic hydrogen carriers (LOHCs).

Advantages: High volumetric density. Disadvantages: High cost and high operating temperature.

- Metal Hydrides Solid-state storage using metal hydrides is achieved by combining binary hydrogen compounds with transition metals (Fe, Cr, Mn, V, Cu, Co, Ni, Au, Pt).
 - Current best materials achieve a volumetric density of 150 kg/m³ (e.g., Mg_2FeH_6 and $Al(BH_4)_3$). Some metal hydrides can reach up to 115 kg/m³.

However, separate hydrogenation is required, making "on-the-fly" refueling impractical. The process is time-consuming, requiring specialized equipment, making it more suitable for long-term storage rather than transport. Additionally, hydrogen desorption requires high activation energy, exceeding that of standard hydrogen release.

- Ammonia Ammonia is a potential hydrogen carrier with a vapor pressure of 9.2 bar at ambient temperature, containing 17.65% hydrogen and a volumetric density 4.5 times higher than liquid hydrogen.
 - Advantages: No CO₂ emissions, co-combustion with existing fuels.
 - Challenges: High energy demand for hydrogen release and potential traces of ammonia in the extracted hydrogen.
- Chemical Hydrogen Storage This method involves absorption in water and materials, which can be either solid or liquid. Storage capacity typically ranges between 6-8 wt%, offering higher energy density than metal hydrides. Examples include boron hydrides and ammonia borane.
 - Strengths: Good volumetric capacities and suitable temperatures due to the presence of lightweight elements.
 - Limitations: High activation energy for absorption and irreversible dehydrogenation reactions, making it a one-time-use solution.
- Liquid Organic Hydrogen Carriers (LOHCs) LOHCs are a promising hydrogen storage and transportation technology. The process consists of two phases: 1. Hydrogenation (storage) 2. Dehydrogenation (release)



Advantages:

- High storage density
- Safe and easy to transport at ambient temperature
- Low operational risk, utilizing existing infrastructure
- Reduced explosion risk

Hydrogenation occurs at high pressure, while hydrogen release happens at low pressure (lower than 5 bar), making LOHCs an efficient and secure solution.

4.3 Comparison of Different Hydrogen Storage Technologies

- Ammonia and Liquid Hydrogen Carriers (LOHCs) have the highest hydrogen content in terms of weight.
- Metals and Chemical Hydrides offer the highest volumetric energy density, but present safety concerns, high energy consumption, and require elevated operating temperatures.
- Sorbent and Carbon-Based Materials provide high storage capacity, but their hydrogen storage potential is not yet fully developed.

Table 3: Comparison of physical-based and physisorption hydrogen storage technologies

Technology	Advantages	Drawbacks
Compressed Gas	Mature technology, fast charging/discharging, simple vessel structure	Limited storage capacity, safety concerns due to high pressure, heat management required
Liquid Hydrogen	High gravimetric and volumetric density, high purity	Energy-intensive and time-consuming, costly, hydrogen boil-off, safety issues
Cryocompressed	High volumetric density	High energy demand for compression and lique- faction
Physisorption (Sorbent/Carbon-Based Materials)	High storage density, lightweight systems	Depends on sorbent geometry/temperature, cooling required, high cost

Table 4: Comparison of chemical-based hydrogen storage technologies

Technology	Advantages	Drawbacks
Metal Hydrides	No need for high pressure, safer operation, thermal integration possible	Low hydrogen capacity due to weight, expensive, high temperature needed for release
Chemical Hydrides	Good volumetric density	Requires thermal management, off-board regeneration
LOHC (Liquid Organic Hydrogen Carriers)	Liquid phase storage, existing infrastructure compatible, storage possible >1 year	High hydrogen input required for dehydrogenation
Ammonia	Inexpensive, can be used directly, compatible with infrastructure	Toxicity and odor management required, 13% H ₂ needed for dehydrogenation and purification

The content of this paragraph is taken from the paper "Hydrogen energy, economy and storage: Review and recommendation" [12]



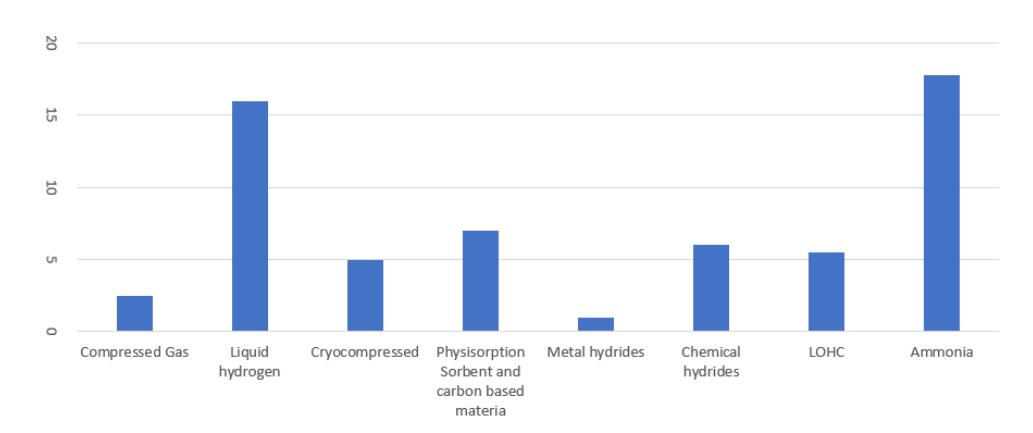


Figure 42: Hydrogen content in different storage technologies (weight %)

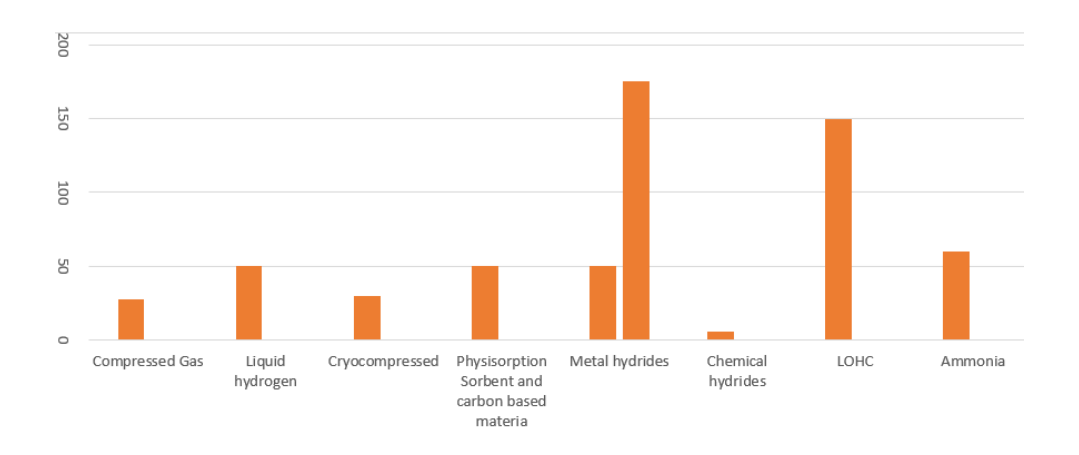


Figure 43: Volumetric energy density of hydrogen storage technologies (MJ/L)



4.4 Focus on Metal Hydrides and Solid Storage

As previously mentioned, green hydrogen produced from renewable sources is highly susceptible to the inherent intermittency of renewable energy generation. Therefore, hydrogen storage becomes a crucial component in ensuring a stable and reliable energy supply.

This section provides an in-depth review and state-of-the-art overview of the main available technologies based on metal hydrides. Although hydrogen has the highest energy density per unit mass of any fuel, its low volumetric density at ambient temperature and pressure results in a relatively low energy content per unit volume.

One promising storage technology applicable across various sectors is hydrogen storage via absorption in metal hydrides. These materials offer high volumetric energy densities and enhanced safety, as hydrogen is chemically bound within the material and stored at relatively low pressures.

Six key types of metal hydrides are commonly investigated: MgH₂, TiFe, TiMn₂, LaNi₅, NaAlH₄, and LiBH₄.

This section will also address important issues related to material durability, activation methods, production costs, availability of raw materials, and environmental impact, with a focus on recyclability.

4.4.1 Material Properties

Metal hydrides are compounds formed by the reaction of hydrogen with metals or metal alloys. When a metal absorbs hydrogen, a metal hydride is formed through an exothermic chemical absorption reaction:

$$M + H_2 \rightarrow MH_x + heat$$

The reverse reaction, which releases hydrogen (desorption), is endothermic:

$$MH_x + heat \rightarrow M + H_2$$

To resume this concept in one balance equation we can say that metal hydrides are formed via the reversible interaction of a hydride-forming metal/alloy, or intermetallic compound (IMC), with H2 gas:

$$M(s) + \frac{x}{2} H_2(g) \xrightarrow{\text{absorption}} MH_x(s) + Q$$

where M is an individual metal, or a multicomponent alloy or IMC. Typical M components include individual metals e for example, rare earths such as La, Ce, Nd or Pr, and elements such as Zr, Ti, Mg, Ca and V e and IMCs, which can include AB5 (e.g. LaNi5, CaNi5), AB2 (e.g. ZrMn2, ZrV2, ZrCr2), AB (e.g. TiFe), and A2B (e.g. Ti2Ni, Zr2Fe) compounds. For a binary IMC, A is typically a hydride-forming element, while B is a transition or non-transition metal/element that does not form a stable hydride under normal conditions. [?]

Two key parameters in comparing hydrogen storage technologies are the gravimetric storage capacity and the volumetric energy density.



The gravimetric capacity is defined as the ratio of the mass of hydrogen absorbed to the total mass of the hydride material, expressed in weight percent (wt%).

The volumetric energy density is typically calculated as:

Volumetric Energy Density =
$$\frac{m_{\rm H_2} \cdot \text{LHV}}{V_{\rm MH}}$$

where:

- $m_{\rm H_2}$ is the maximum absorbed hydrogen mass,
- LHV is the lower heating value of hydrogen (approximately 120 MJ/kg),
- $V_{\rm MH}$ is the volume of the hydride material.

In general, interstitial metal hydrides have gravimetric capacities in the range of 1–2 wt%, whereas complex hydrides can reach significantly higher values. Among them, LiBH₄ stands out with the highest theoretical gravimetric capacity, up to 18.5 wt%.

A comparative table in this section will present key parameters including gravimetric storage capacity, volumetric energy density, operating pressure, and operating temperature for each metal hydride material.

Table 5: Storage capacities and energy densities of different hydrogen storage technologies and metal hydride materials.

Hydrogen storage	Grav. storage capacity ^a [wt%]	$egin{array}{ll} ext{Vol.} & ext{energy} \ ext{density}^b \ [ext{kWh}/ ext{dm}^3] \end{array}$	Operating pressure c [bar]	$\begin{array}{c} \textbf{Operating} \\ \textbf{temperature}^d \\ \textbf{[K]} \end{array}$
CGH_2 350 bar	100	0.8	350	Ambient
CGH_2 700 bar	100	1.3	700	Ambient
LH_2	100	2.2	1–10	20
Metal hydrides				
Elemental MgH ₂	7.6 (5.5)	3.67 (2.65)	_	593
AB TiFe	1.86 (1.5)	4.03 (3.25)	4.1	265
AB ₂ TiMn ₂	1.86 (1.15)	4.09 (2.53)	8.4	252
AB ₅ LaNi ₅	1.49 (1.28)	4.12 (3.53)	1.8	285
Complex hydrides				
LiBH ₄	18.5 (13.4)	4.08 (3.02)	_	573
NaAlH ₄	7.5 (3.7)	3.20 (1.58)	_	473

 $^{^{}a}$ Theoretical values, practical values in parentheses.

The values presented are for the pure substance. For the system (tank) level a weight increase of approximately 50% and a volume increase of 100% is expected for metal hydrides

In order to determine the operating ranges of pressure and temperature for different metal hydride materials, Pressure-Concentration Isotherms (PCI) and Van't Hoff plots (Fig. 2b) are commonly used. The curves in the Van't Hoff plot can be described by the following equation:



^b Based on LHV of hydrogen, theoretical/practical values.

^c Approximate pressure required for absorption.

^d Approximate temperature required for desorption.

^e Not applicable due to chemical stability in standard conditions.

$$\ln\left(\frac{P}{P_0}\right) = -\frac{\Delta H}{RT} + \frac{\Delta S}{R}$$

where:

- R is the universal gas constant,
- T is the absolute temperature,
- P_0 is the reference pressure (typically 1 bar),
- ΔH is the enthalpy change of the absorption reaction,
- ΔS is the entropy change of the desorption reaction.

Low-temperature metal hydrides generally exhibit lower activation enthalpies and are capable of operating at or near ambient temperatures. Among the thermodynamic parameters, the reaction enthalpy ΔH plays a particularly crucial role in thermal management, as it is closely associated with the amount of heat released or required during the absorption and desorption processes.

Since hydrogen absorption is an exothermic process, heat is released during uptake, causing an increase in temperature. However, as described by the Van't Hoff equation, an increase in temperature leads to a rise in equilibrium pressure. Consequently, to maintain hydrogen absorption under elevated temperatures, a higher hydrogen pressure is needed. Without effective thermal management, the system may "self-lock": the hydride heats up excessively and ceases to absorb hydrogen, significantly slowing the filling process.

Similarly, during desorption, it is essential to supply heat to sustain hydrogen release at the desired pressure. If the material is not sufficiently heated, the equilibrium pressure drops, and hydrogen is no longer effectively released. Therefore, proper thermal control is critical to ensuring the efficient operation of metal hydride storage systems.

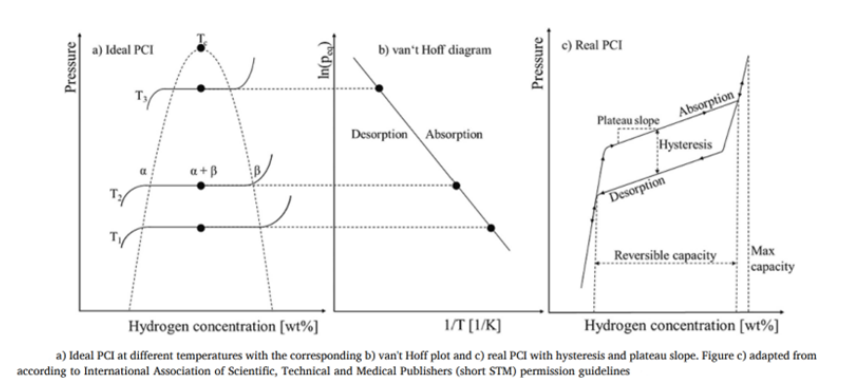


Figure 44: Pressure-Composition-Isotherm (PCI) diagram

The Pressure-Composition-Isotherm (PCI) diagram illustrates the relationship between the hydrogen pressure and the amount of hydrogen absorbed or desorbed at constant temperature. These curves typically exhibit a plateau region, representing a phase where hydrogen is absorbed or released at nearly constant pressure. However, the plateau is not perfectly flat—it usually has



a slope. Moreover, there is a phenomenon of hysteresis: the pressure required for absorption is higher than that for desorption.

The equilibrium pressure (p_{eq}) , defined at the midpoint of the plateau, is a key parameter in understanding metal hydride behavior (see Fig. 2a). For absorption to proceed, the partial pressure of hydrogen gas must exceed the equilibrium pressure at a given temperature. Conversely, desorption occurs when the hydrogen pressure falls below this equilibrium value. Notably, as the temperature increases, the equilibrium pressure also rises, in accordance with thermodynamic principles.

Most interstitial hydrides can operate under near-ambient conditions, typically within the range of 0–100°C and 1–40 bar, depending on the specific application. On the other hand, elemental hydrides such as MgH₂ and complex hydrides may also function at low pressures but require substantially higher operating temperatures, ranging from 100 to 400°C.

One of the key challenges in metal hydride storage systems is the relatively slow hydrogen absorption and desorption kinetics, which directly affects charging and discharging times. These rates vary significantly depending on the material and operating conditions. Current research is focused on improving both the filling and extraction rates, which are often limited by poor heat transfer and contamination within the hydride material.

Efforts to enhance kinetics include optimizing material properties through partial elemental substitution, the use of dopants and catalysts, and improving thermal conductivity—e.g., by incorporating aluminum foam—or redesigning the storage container to enhance heat dissipation.

Contaminants have a significant negative impact on hydrogen storage performance. Common impurities include O₂, H₂O, CO, CO₂, N₂, NH₃, and various hydrocarbons. The effects of these impurities are well documented in the literature and include poisoning (irreversible loss of capacity), kinetic retardation (slower reaction rates), chemical reactions (e.g., corrosion), and inert gas blanketing.

The long-term viability of metal hydride storage is assessed through cyclic stability, which refers to the material's ability to retain its storage capacity over numerous hydrogen absorption/desorption cycles. Degradation over time, caused by both physical and chemical changes, leads to a reduction in storage efficiency.

In terms of safety, while the risk of explosion is significantly lower compared to high-pressure hydrogen gas storage, some metal hydride materials are flammable when exposed to air. This poses a safety concern in the event of a container breach. Other safety risks include material toxicity and the potential for inhalation of fine hydride powders.

4.4.2 Stationary Applications of Metal Hydrides

The use of metal hydrides for stationary hydrogen storage offers several distinct advantages. Chief among these are the high volumetric energy density and the relatively low operating pressures compared to compressed gaseous hydrogen (CGH₂) systems. The typical hydrogen outlet pressure of PEM electrolysers is around 30 bar, which is sufficient for charging metal hydrides directly without the need for additional compression.

The reduced operating pressure contributes not only to improved safety but also to lower system



maintenance requirements. Moreover, avoiding high-pressure components can lead to significant cost reductions. Due to their high energy density and modular scalability, metal hydride systems are suitable for a range of storage capacities—from small-scale residential use to large-scale seasonal applications.

Additionally, since metal hydride systems do not suffer from hydrogen loss during storage, they are well-suited for medium- to long-term energy storage. In seasonal storage applications, the compactness and scalability of metal hydrides can compensate for their lower round-trip efficiency relative to batteries. Although slower reaction kinetics may necessitate a small buffer storage system to manage peak demand, they do not pose a significant drawback in these use cases.

Potential application areas include residential energy systems, off-grid installations, backup power systems, and centralized seasonal hydrogen storage solutions.

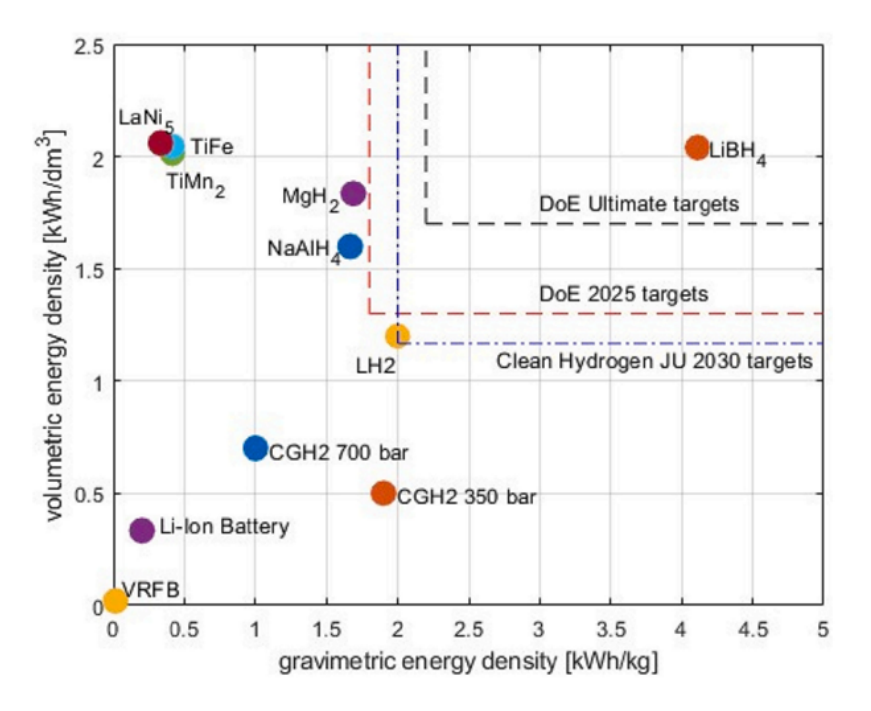


Figure 45: Ratio Gravimetric-Volumetric energy densities

To better evaluate the balance between weight and volume efficiency of different hydrogen storage technologies, the ratio between volumetric and gravimetric energy density can be calculated. This metric helps identify whether a material is more space-efficient or mass-efficient for storing hydrogen.

The ratio is defined as:

$$Ratio = \frac{Volumetric\ Energy\ Density\ [kWh/dm^3]}{Gravimetric\ Energy\ Density\ [kWh/kg]}$$

A lower ratio indicates better gravimetric performance per unit of volume (i.e., more hydrogen stored per unit of weight), while a higher ratio indicates superior volumetric storage at the cost of heavier materials.



Technology / Material	Gravimetric Energy Density [kWh/kg]	Volumetric Energy Density [kWh/dm ³]	$\begin{array}{c} \textbf{Ratio} \textbf{(Vol/Grav)} \\ \textbf{[dm}^3/\textbf{kg]} \end{array}$
LiBH ₄	4.5	2.3	0.51
LaNi ₅	0.9	2.1	2.33
TiFe	1.0	2.0	2.00
$TiMn_2$	1.1	1.9	1.73
MgH_2	1.5	1.6	1.07
NaAlH ₄	1.4	1.5	1.07
LH_2	2.5	1.1	0.44
CGH_2 700 bar	2.0	0.7	0.35
CGH_2 350 bar	1.7	0.5	0.29
Li-ion Battery	0.6	0.4	0.67
VRFR (Redox Flow)	0.2	0.1	0.50

Table 6: Volumetric to gravimetric energy density ratio of selected hydrogen storage technologies

Although this ratio is an interesting parameter, in our specific Power-to-X application we will limit the material selection criteria to energy per unit volume, cost, technological readiness, compatibility with the system, material availability, and safety.

The volumetric and gravimetric energy densities of various hydrogen storage systems—including compressed gaseous hydrogen (CGH₂), liquid hydrogen (LH₂), and metal hydrides—are shown with system-level penalties applied: a 50% weight increase and a 100% volume increase over material values. For comparison, lithium-ion and vanadium redox flow batteries (VRFB) are also included. The 2025 and ultimate targets set by the U.S. Department of Energy (DOE) are represented by dashed lines, while the 2030 targets of the European Clean Hydrogen Joint Undertaking (CH JU), continuing the Fuel Cells and Hydrogen Joint Undertaking, are indicated by a dash-dotted line.

One important aspect to consider in large-scale hydrogen storage is compliance with the Seveso III Directive (2012/18/EU), which regulates major accident hazards involving dangerous substances. This directive specifies quantitative thresholds for substances stored at a single facility. Hydrogen is explicitly listed in Annex I of the directive, with threshold quantities of 5 tonnes (lower-tier) and 50 tonnes (upper-tier).

A facility storing 5 tonnes or more of hydrogen is classified as a lower-tier establishment and must fulfill specific safety obligations. Exceeding 50 tonnes qualifies a site as an upper-tier establishment, which imposes stricter safety requirements. These limits reflect the extreme flammability and high risk associated with hydrogen.

Many metal hydride materials used for hydrogen storage (e.g., sodium alanate) also pose hazards. They are often flammable solids that may react violently with water, releasing hydrogen and forming corrosive byproducts. As such, the hydride materials themselves are considered dangerous. The Seveso III Directive applies to hydrides classified as flammable, toxic, or water-reactive, based on the applicable hazard category thresholds—typically ranging from a few to several dozen tonnes.

This means that even before reaching the hydrogen threshold, a facility may already be subject to Seveso regulation based on the mass of hydride material stored. For instance, hundreds of kilograms of metal hydride may be required to store just a few kilograms of hydrogen. Therefore, the effective hydrogen storage capacity may be constrained by the Seveso threshold of the hydride



compound itself. Conversely, if the storage material is not classified as hazardous, it would not trigger Seveso obligations on its own.

Another implication of Seveso III is the need to consider siting and land-use planning. Article 13 of the directive requires authorities to regulate land use around hazardous sites to ensure appropriate distances from residential areas, public spaces, critical infrastructure, and transportation corridors. This implies that large-scale hydrogen storage facilities should be located in isolated industrial zones or at sufficient distance from populated areas.

Facilities falling under Seveso regulation must follow a defined authorization process. Operators are required to submit a formal notification to the competent authorities (in Italy, via the portal defined under Legislative Decree 105/2015), providing detailed information about stored substances, quantities, activities, and the local environment. All Seveso establishments must implement a Major Accident Prevention Policy (MAPP), as mandated by Article 8.

In the case of upper-tier sites, a full Safety Report (Article 10) is required, including an in-depth analysis of potential accident scenarios and the technical and organizational measures in place to prevent or mitigate such events. These facilities must also develop an Internal Emergency Plan (Article 12) and provide relevant data for an External Emergency Plan coordinated by local authorities, civil protection agencies, and fire services. These steps involve substantial documentation and risk assessment that must be factored into the engineering planning process, including time and budget estimates. Public consultation (Article 15) and technical review by national or regional authorities are often prerequisites for project approval.

The directive also necessitates the integration of high safety standards in system design. Preventive measures must be implemented to minimize the likelihood of accidental hydrogen release and to reduce the consequences of possible incidents. This includes:

- Forced ventilation and gas detection systems to prevent hazardous accumulations,
- Use of intrinsically safe electrical equipment (ATEX certified) in storage areas,
- Installation of safety valves and automatic shut-off systems in case of leaks or fire.

In systems using solid-state hydrides, design must prevent unwanted reaction triggers such as water ingress or overheating that could cause material decomposition or self-ignition. Redundant containment systems and physical separation are often used. Hydrogen tanks may be buried or shielded with protective barriers, while hydride modules may be compartmentalized to prevent chain reactions.

Internal safety distances are also maintained between hydrogen or hydride storage systems and other equipment to reduce the risk of domino effects. All safety measures must be incorporated in the early design phase and will be scrutinized during the Safety Report assessment by relevant authorities. Compliance with recognized standards (e.g., ISO/TR 15916 for hydrogen safety, ASME/ANSI codes for pressure vessels, NFPA/API standards for separation distances) greatly facilitates the approval process by demonstrating adherence to best engineering practices.

From a risk management perspective, detailed analysis of accident scenarios—such as flash fires, vapor cloud explosions (VCE), jet fires, and internal explosions in hydride tanks due to air mixing—is required. This analysis, often in the form of a Quantitative Risk Assessment (QRA),



informs the design, safety features, and emergency planning.

Facilities under Seveso jurisdiction are subject to periodic inspections by regulatory bodies such as fire departments and environmental agencies (e.g., ARPA, ISPRA). These inspections ensure compliance with declared safety measures and promote a culture of continuous safety improvement.

As for mobile applications, I will simply note that the weight percentage relative to the total vehicle mass remains one of the main obstacles, currently making this solution unsuitable for mobile hydrogen storage.

4.4.3 Various classes of metal hydrides

The most prominent representatives of the different classes of metal hydrides have been selected for analysis. From the elemental hydrides group, magnesium hydride (MgH₂) is the most studied. For interstitial hydrides, TiFe, TiMn₂, and LaNi₅ serve as examples of the AB, AB₂, and AB₅ subgroups, respectively. Among complex hydrides, sodium alanate (NaAlH₄) is one of the most widely discussed, while lithium borohydride (LiBH₄) is noted for having the highest theoretical gravimetric capacity of any hydride material.

Tailoring the properties of metal hydrides through enhancement techniques is common practice. The most promising strategies include:

- Doping with catalytic elements,
- Alloying or substituting with different elements,
- Particle or grain size reduction (e.g., ball milling),
- Severe plastic deformation (SPD),
- Annealing treatments.

1. Magnesium Hydride (MgH₂)

Magnesium hydride is one of the most extensively studied materials for hydrogen storage due to its high theoretical gravimetric capacity (7.6 wt%). It can be synthesized through direct reaction with hydrogen at temperatures above 400°C or via advanced methods such as high-energy ball milling. However, it suffers from slow absorption/desorption kinetics and requires elevated temperatures for hydrogen release. Additionally, magnesium is highly susceptible to surface oxidation, which hinders hydrogenation. Therefore, thermal or mechanical activation is needed to remove the oxide layer. Various strategies have been explored to improve performance, including doping with transition metals (e.g., Ti, Fe, Ni), incorporating carbon nanotubes or graphene, and nanosizing the particles to increase surface area. A promising approach is confining the material in nanoporous matrices to prevent particle agglomeration during cycling. Despite these improvements, large-scale production remains costly due to the energy-intensive treatments involved.



2. Titanium-Iron (TiFe)

TiFe is a well-known intermetallic hydride recognized for its reversible hydrogen storage properties. It is typically produced through arc or induction melting under an inert atmosphere using high-purity titanium and iron. One of the main limitations is the challenging activation process prior to the first hydrogenation, which usually involves cycling between room temperature and 400–450°C under high hydrogen pressure (around 65 bar). Air exposure leads to the formation of a surface oxide layer (TiO₂) that impedes hydrogen diffusion. However, mechanical treatments such as ball milling, severe plastic deformation, and catalytic doping (with elements like Mn, V, Pd) have been successfully applied to facilitate activation. TiFe exhibits two pressure plateaus in PCI diagrams, although the second often diminishes with repeated cycling. With a storage capacity of around 1.7 wt%, it is not particularly competitive in gravimetric terms but remains attractive due to its cycle stability and relatively low cost.

3. Titanium–Manganese (TiMn₂)

TiMn₂ is a widely used intermetallic hydride, appreciated for its good absorption/desorption kinetics at room temperature and ease of activation. It is generally synthesized via arc melting or induction furnaces under argon, followed by annealing at 1000° C to enhance alloy homogeneity. The Ti/Mn ratio can vary, but TiMn_{1.5} is often considered optimal for balancing storage capacity and maintaining a flat pressure plateau in PCI curves. Notable drawbacks include a relatively high plateau pressure and pronounced hysteresis. Performance can be enhanced by partially substituting Ti or Mn with elements such as Zr, V, Cr, or Al. For instance, Zr can lower the plateau pressure, while V improves both capacity and operating pressure. Mechanical processing, including milling, further improves kinetics. TiMn₂ is also more affordable and does not require complex activation, making it a promising material for vehicular and portable hydrogen systems.

4. Lanthanum-Nickel (LaNi₅)

LaNi₅ is a classic and reliable material for reversible hydrogen storage. It is well known for easy activation, excellent cycle stability, and a flat pressure plateau, which is advantageous in applications requiring stable operation. Production methods include induction or arc melting, as well as chemical reduction of oxide mixtures with CaH₂. Activation requires only a few hydrogenation cycles at temperatures below 100°C and moderate pressures (<100 bar). However, intensive mechanical treatment (e.g., ball milling) tends to reduce storage capacity, likely due to the formation of overly stable hydride phases at grain boundaries. LaNi₅ is less sensitive to oxygen compared to other hydrides, thanks to the ability of nickel to regenerate the active surface after each cycle. Performance improvements are typically achieved through partial substitution of Ni with Al, Mn, or Co, and La with Ce, Nd, or mischmetal. Al addition notably reduces the plateau pressure, while Co enhances cycle life. LaNi₅ remains a dependable option for stationary storage systems and low-power devices.

5. Sodium Alanate (NaAlH₄)

NaAlH₄ is a complex hydride that has garnered considerable attention as a reversible hydrogen storage material, especially after the discovery that titanium-based catalysts (e.g., TiCl₃) can greatly enhance its reversibility. In its pure form, NaAlH₄ shows slow kinetics and requires high temperatures (200–400°C) and pressures for recharging. It is synthesized economically by milling NaH with Al in an inert atmosphere, followed by hydrogen exposure. Hydrogen is released in two primary steps, with a theoretical capacity of approximately 5.5 wt%. The addition of catalytic



dopants (e.g., Ti, Sc, Ce) improves absorption rates and reduces operating temperatures. Advanced approaches, such as using carbon-based supports (graphene, nanotubes) or metal-organic frameworks (MOFs), have also been explored to improve performance. Nevertheless, NaAlH₄ is sensitive to moisture and may release flammable gases, necessitating controlled handling environments. While promising for mobile applications, further optimization is needed to ensure stable and efficient cycling.

6. Lithium Borohydride (LiBH₄)

LiBH₄ is known for its exceptionally high theoretical hydrogen storage capacity (18.5 wt%), but its practical use is hindered by slow kinetics and extreme operating conditions. Hydrogen desorption occurs in multiple steps, with most of the hydrogen released between 400 and 680°C. Rehydrogenation requires high pressures (>70 bar) and elevated temperatures, making it unsuitable for conventional applications without modification. To overcome these limitations, strategies such as doping with transition metals (Fe, Ti, Ni), halide catalysts (e.g., TiCl₃, ZnF₂), and nanoscaling via physical deposition or confinement in porous matrices have been investigated. Partial anion or cation substitution has also shown potential in lowering desorption temperatures. However, LiBH₄ is extremely reactive with moisture and may ignite upon air exposure, requiring strict atmospheric controls. Despite these challenges, it remains a highly promising candidate for long-term, high-density hydrogen storage applications.

Property	$\mathrm{MgH_2}$	TiFe	${ m TiMn_2}$
H ₂ Capacity (%wt)	7.6	~1.7	~1.8
Desorption Temp. (°C)	>300-400	80-200	20-50
Desorption Pressure (bar)	>10-30	10-20	10-30
Activation	Difficult (oxide layer)	Complex (thermal cy-	Easy
		cles)	
Kinetics	Slow	Good after activation	Good
Advantages	High capacity, low cost	Economical, good cy-	Simple activation, good
		cling stability	kinetics
Disadvantages	High T, surface oxida-	Difficult activation, oxi-	High plateau, hysteresis,
	tion, slow kinetics	dation blocks H ₂	O_2 -sensitive
Improvements	Doping (Ti, Fe), CNTs,	Doping (Mn, V), Pd	Substitution (Zr, V, Cr),
	nanosizing, nanoconfine-	coating, mechanical	milling, annealing
	ment	treatments	

Table 7: Comparison of MgH₂, TiFe, and TiMn₂ metal hydrides.

4.4.4 Economic and environmental factors

The main driver for economic assessments is cost, which includes raw material prices, manufacturing processes (including energy demand and process complexity), quality control, recycling, and profit margins. While raw material costs are somewhat traceable, the contributions from other cost components are harder to quantify. Enhancing domestic mining and production of critical raw materials is a key strategy for increasing self-sufficiency. Europe holds significant reserves of titanium (notably in Norway), nickel (Norway and Russia), magnesium and boranes (Balkan region, especially Greece), lithium (Portugal, France, Austria, Germany, Serbia), and some rare-earth elements like lanthanum (found in Turkey, Greece, Balkans, and recently discovered in Arctic Sweden). Despite this, the EU remains highly dependent on imports, particularly from China.

Waste reduction and recycling are crucial strategies for both sustainability and cost-effectiveness. Recycling involves both using secondary raw materials in hydride synthesis and recovering the



Property	LaNi ₅	NaAlH ₄	${ m LiBH_4}$
H ₂ Capacity (%wt)	~1.4	5.5 theoretical, \sim 5 prac-	18.5 theoretical, ~ 9
		tical	practical
Desorption Temp. (°C)	<100	30-150	400-600
Desorption Pressure (bar)	2–3	60-150	>70
Activation	Very easy	Moderate (requires dop-	Difficult
		ing)	
Kinetics	Very good	Slow without catalyst	Very slow
Advantages	Flat plateau, stable, air-	Decent density, re-	Extremely high theoreti-
	resistant	versible with catalyst	cal capacity
Disadvantages	Limited capacity, toxic,	High T/P, slow, reactive	High T/P, poor re-
	sensitive to milling	with H ₂ O	versibility
Improvements	Substitution (Al, Mn,	Doping ($TiCl_3$, $ScCl_3$),	Doping (Fe, Ti),
	Co, Ce), annealing	carbon materials, MOFs	nanoconfinement, ionic
			substitutions

Table 8: Comparison of LaNi₅, NaAlH₄, and LiBH₄ metal hydrides.

hydride after its end-of-life. Noteworthy examples include recycled aluminum from cans and automotive sources for NaAlH, achieving performance comparable to high-purity aluminum. Promising studies on LiBH synthesis using recycled boranes show encouraging results. Recycled Mg/Al wastes have demonstrated good hydrogen storage capacities and improved thermal properties, while TiFe alloys produced from scrap iron and titanium show nearly equivalent storage capacities to pure TiFe, helping reduce costs.

Although recycling of rare-earth elements is still in early stages, recovery rates for nickel and rare-earths from NiMH batteries are promising. Most metal hydrides can be recovered using metallurgical processes (pyro-, hydro-, or electrometallurgy), and ideally re-activated for reuse. However, hydrogen remaining in the tank (either physically or chemically bound) must be carefully removed through venting or heating and vacuum pumping.

Life-cycle CO equivalent emissions are another critical factor. Materials like MgH have relatively low emissions per kg of hydrogen stored, due to low extraction impacts and high capacity. In contrast, TiFe and TiMn have higher carbon footprints due to titanium's high CO cost and energy-intensive activation steps. Although LaNi's raw materials have high extraction emissions, the alloy is easier to activate. A study comparing metal hydride tanks with Type III and IV gaseous tanks revealed higher production GHG emissions for hydrides but comparable total emissions when compression energy for gases is considered.

Manufacturing costs depend on synthesis method (e.g., ball milling, thermal activation), production scale, equipment costs (CAPEX), operating costs (OPEX), and additive materials. Highpurity hydride materials are significantly more expensive; for instance, storage-grade LiBH can cost 50% more than lower-purity forms, and LiAlH up to 200% more. Lab-scale prices are misleadingly high—NaAlH (87 €/10g), LiBH (219 €/10g), LaNi (84 €/10g)—but large-scale production could lower prices by orders of magnitude. Mg remains the cheapest material in terms of hydrogen stored per euro.

To compete with gaseous storage (about 1000 €/kg H), metal hydrides must reach target costs under 10 €/kg. However, metal hydrides have 10 times the volumetric energy density compared to 80 bar gaseous systems, potentially justifying higher costs through space savings. The criticality of elements also influences material choice. According to the EU's Critical Raw Materials list, B, La, Li, Mg, Ni, and Ti are all deemed critical, while NaAlH is free from these elements.



With rising global demand for these materials, especially for climate targets, and geopolitical uncertainties, supply risks are increasingly important.

Ultimately, while metal hydrides face economic and technical challenges, their recyclability, compactness, and environmental potential make them promising for certain hydrogen storage applications, especially if future developments can optimize recycling processes and scale production efficiently.

Table 9: Economic and environmental aspects of selected metal hydrides (Part 1)

Hydride Material	Key Ele-	Gravimetric Ca-	$\mathrm{CO_2} \mathrm{eq} (\mathrm{kg/kg})$	Lab-Scale Price	CRM (EU)
	ments	pacity (wt%)			
NaAlH ₄	Na, Al	Moderate	Low-Moderate	€87/10g	No
LiBH ₄	Li, B	High	Moderate	€219/10g	Yes (Li, B)
LaNi ₅	La, Ni	Low	High (La: 11, Ni: 6.5)	€84/10g	Yes (La, Ni)

Table 10: Economic and environmental aspects of selected metal hydrides (Part 2)

Hydride Material	Key Ele- ments	Gravimetric Capacity (wt%)	CO ₂ eq (kg/kg)	Lab-Scale Price	CRM (EU)
TiFe	Ti, Fe	Low-Moderate	Moderate (Ti: 8.1, Fe: 1.5)	Not available	Yes (Ti)
TiMn ₂	Ti, Mn	Moderate	Moderate (Ti: 8.1, Mn: 1.0)	€79/25g	Yes (Ti)
MgH_2	Mg	High	Low (Mg: 5.6)	Cheapest per H_2 stored	Yes (Mg)

The content of this paragraph is taken from the paper "A review on metal hydride materials for hydrogen storage" [13]



5 Case study and Methodology

5.1 Design of the PtX Plant

This chapter describes the development and validation of the Power-to-X (PtX) plant model used for the simulation and subsequent cost analysis. The objective of this plant is the production and storage of green hydrogen, which can subsequently be used as a fuel in hard-to-abate industrial sectors, specifically in this case, the glass manufacturing industry. The model was built using an object-oriented approach in Python to ensure a clear structure and facilitate future extensions.

5.1.1 Power-to-X Overview

The model simulates a system consisting of three main subsystems: a photovoltaic (PV) array for power generation, a Proton Exchange Membrane (PEM) electrolyzer for hydrogen production, and a metal-hydride storage unit. The objective is to efficiently convert solar energy into storable chemical energy in the form of hydrogen, which can then be supplied to the industrial process. The diagram below illustrates the general structure of a Power-to-X system.

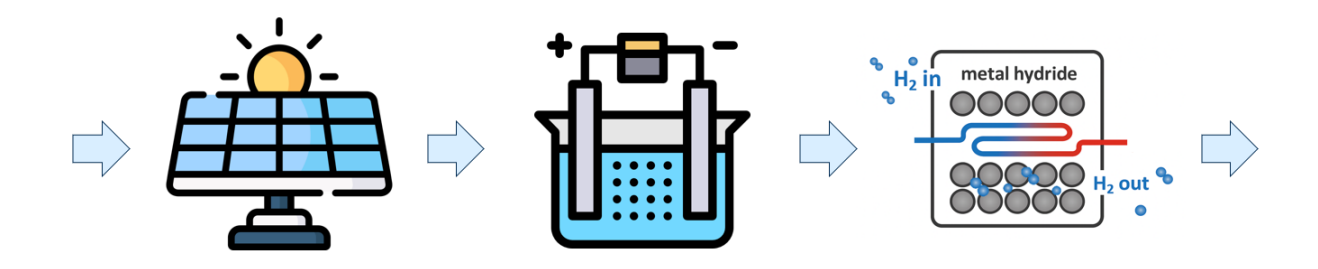


Figure 46: Power to X

The Power-to-X (PtX) concept is a technology that converts electrical energy into chemical energy, primarily in the form of hydrogen. This hydrogen can be utilized for various purposes, such as an alternative fuel for transportation, a feedstock for chemical synthesis, or, as in the specific case of this study, as a clean fuel for a glass industrial furnace. This application is crucial for decarbonizing hard-to-abate sectors, which are difficult to electrify directly.

5.1.2 Software Environment

Python was chosen as the development environment for its versatility, computational efficiency, and widespread adoption as one of the most recognized and widely used programming languages globally. Python's strengths include its suitability for handling large datasets—such as the meteorological data that will be integrated into the model—and its pivotal role in the implementation of artificial intelligence algorithms, a feature that may prove valuable for potential future developments of the PtX model. The initial approach focused on creating a dynamic model in Python, using as a reference a validated Simulink model from a previous Master's thesis [14].



5.1.3 First Dynamic Electrolyzer Model

After defining the software environment, the following section describes the mathematical modeling and physical structure of the PtX plant, which constitutes the foundation for the subsequent simulations and cost analysis. The model was initially developed as a complete dynamic system to capture the transient behavior of the electrolyzer. To solve this behavior, a fixed-point iteration method was employed across all time- and temperature-dependent variables, iterating within a for loop using a variable time step dt and time horizon. The simulation was performed on a daily basis (24 hours) with a fixed time step of dt = 1 second, ensuring accurate resolution of the transient dynamics.

An important insight emerged from experimenting with different values of dt in the code, which proved to be a crucial turning point in the development of the final model.

Constant	Value
Faraday constant F	$96485\mathrm{C/mol}$
Ideal gas constant R	$8.314 \mathrm{J/(mol \cdot K)}$
Stefan–Boltzmann constant σ_{SB}	$5.67 \times 10^{-8} \mathrm{W/(m^2 \cdot K^4)}$
Molar mass of water M_{H_2O}	$0.01801528\mathrm{kg/mol}$
Reference pressure P_{el}	$101325\mathrm{Pa}$
Membrane density ρ_{me}	$1980\mathrm{kg/m^3}$
Equivalent weight of membrane EW_{me}	$1100\mathrm{g/mol}$
Higher heating value of H ₂ (HHV)	$1.416 \times 10^{8} \mathrm{J/kg}$
Lower heating value of H ₂ (LHV)	$1.199 \times 10^8 { m J/kg}$
Molar mass of hydrogen M_{H_2}	$0.00201568\mathrm{kg/mol}$
Gibbs free energy ΔG	$236480\mathrm{J/mol}$
Reaction enthalpy ΔH	$285830 \mathrm{J/mol}$
Electrons transferred z	2

Table 11: Physical constants used in the electrolyzer dynamic model.

The governing equations of the model can be grouped into five categories. For clarity, each set is presented together with its physical meaning. In addition, all equations are explained component-by-component in a complete and logical manner in the three subsequent subsections (Photovoltaic System, Electrolyzer, and Hydrogen Storage). As discussed, this is a transient process model that serves as the foundation for the final techno-economic analysis.

Electrochemical Potentials. These relations define the fundamental driving forces of electrolysis:

$$E_0 = \frac{\Delta G}{zF}$$
 Nernst potential at standard conditions (from Gibbs free energy),
$$(6)$$

$$V_{TN} = \frac{\Delta H}{zF}$$
 Thermoneutral voltage, including electrical and thermal contributions,
$$(7)$$

$$E_n = E_0 + \frac{RT}{2F} \ln \left(P_{H_2} \sqrt{P_{O_2}} \right)$$
 Nernst potential at operating gas pressures. (8)



Currents and Efficiencies. These equations describe how the electrical current translates into hydrogen and oxygen flows:

$$i = \frac{I}{n_{cells} A_{cell}}$$
 Current density (A/m²), (9)

$$i_{loss} = 0.01 i$$
 Fraction of current lost due to parasitic effects, (10)

$$\eta_F = 1 - \frac{i_{loss}}{i}$$
 Faradaic efficiency, (11)

$$\dot{N}_{O_2} = \frac{n_{cells} i}{4F} \eta_F$$
 Molar flow of O_2 , (12)

$$\dot{N}_{H_2} = \frac{n_{cells} i}{2F} \eta_F \qquad \text{Molar flow of H}_2. \tag{13}$$

Pressures and Gas Flows. They govern gas accumulation and water transport:

$$P_{O_2} = \frac{\dot{N}_{O_2}RT}{V_{an}}$$
 Partial pressure of O₂ in the anode chamber, (14)

$$P_{H_2} = \frac{\dot{N}_{H_2}RT}{V_{ca}}$$
 Partial pressure of H₂ in the cathode chamber, (15)

$$\dot{N}_{H_2O,an} = k_{ao}(P_{O_2} - P_{el})y_{H_2O,an} \quad \text{Anode-side water molar flow}, \tag{16}$$

$$\dot{N}_{H_2O,ca} = k_{co}(P_{H_2} - P_{el}) \cdot 0.05$$
 Cathode-side water molar flow. (17)

Membrane Water Content and Transport. The PEM's hydration state strongly affects conductivity:

$$P_{sat} = -2846.4 + 411.24T_C - 10.554T_C^2 + 0.16636T_C^3 \quad \text{Saturation vapor pressure of water},$$
(18)

$$a_{an} = \frac{P_{H_2O,an}}{P_{sat}}, \quad a_{ca} = \frac{P_{H_2O,ca}}{P_{sat}}$$
 Relative humidities at anode and cathode, (19)

$$\sigma_m = (0.005139\lambda_m - 0.00326)e^{1268\left(\frac{1}{303} - \frac{1}{T}\right)}$$
 Protonic conductivity, (20)

$$R_{ohm} = \frac{t_{me}}{\sigma_m}$$
 Ohmic resistance of the membrane. (21)

Voltage Losses. The total cell voltage accounts for several contributions:

$$V_{an} = \frac{RT}{2\alpha_{an}F} \sinh^{-1}\left(\frac{i}{2i_{0,an}}\right)$$
 Activation overpotential (anode), (22)

$$V_{ca} = \frac{RT}{2\alpha_{ca}F} \sinh^{-1}\left(\frac{i}{2i_{0,ca}}\right)$$
 Activation overpotential (cathode), (23)

$$V_{cell} = E_n + V_{an} + V_{ca} + iR_{ohm}$$
 Total cell voltage, (24)

$$V_{stack} = n_{cells} V_{cell}$$
 Total stack voltage. (25)



Thermal Model and Energy Balances. In proton exchange membrane (PEM) electrolyzers, the conversion of electrical power into hydrogen is not perfectly efficient: a significant fraction of the input energy is dissipated as heat due to overpotentials, ohmic losses, and auxiliary system inefficiencies. The stack temperature is a key operational variable, as it directly affects electrochemical kinetics, efficiency, and durability of the membranes. To correctly capture these effects, the digital twin incorporates a dynamic thermal model that updates the temperature of the stack at each simulation step, based on first-principles energy balances. This allows the system to account for the transient coupling between electricity consumption, hydrogen generation, and heat transfer to the surroundings.

The governing equations can be grouped as follows:

$$P_{\text{stack}} = V_{\text{stack}} \cdot I$$
 Electrical power absorbed by the stack, (26)

$$\eta_{\rm el} = \frac{\dot{m}_{\rm H_2} \cdot \rm LHV_{\rm H_2}}{P_{\rm stack}}$$
Electrolyzer efficiency (LHV basis), (27)

$$Q_{\text{gen}} = P_{\text{stack}} (1 - \eta_{\text{el}})$$
 Heat generated by irreversible losses, (28)

$$Q_{\text{loss}} = (h_c + h_r) A_{\text{ext}} (T - T_{\text{amb}})$$
 Heat lost to the environment by convection and radiation, (29)

$$\frac{dT}{dt} = \frac{Q_{\text{gen}} - Q_{\text{loss}}}{C_{\text{th}}}$$
 Dynamic temperature evolution of the stack. (30)

Equation (26) defines the absorbed electrical power as the product of stack voltage and current. Equation (27) relates the chemical power of the produced hydrogen (based on its lower heating value, LHV) to the absorbed electrical power, defining the instantaneous efficiency. Equation (28) quantifies the heat generated internally, equal to the fraction of input power not converted into hydrogen. Equation (29) represents the heat lost to the environment, including convective and radiative contributions. Finally, Equation (30) closes the dynamic balance, linking the net thermal power to the time derivative of the stack temperature through the effective thermal capacity $C_{\rm th}$.

In this way, the thermal model provides a transient prediction of the stack temperature evolution, closely coupled with the electrical and electrochemical behaviour of the electrolyzer. By simulating the heating due to inefficiencies and the cooling due to external heat exchange, the model allows one to evaluate operating stability under different load conditions and ambient environments. Such a description is crucial, as excessive temperature excursions may reduce efficiency, accelerate degradation of the membranes, or limit hydrogen productivity.

It is important to note that, thanks to this first transient model, it was possible to verify that the thermal transient of the electrolyzer is negligible both in terms of characteristic time scale (on the order of a few tens of seconds) and in terms of temperature variations (limited to a few degrees). For this reason, and in order to significantly reduce computational cost without compromising the reliability of the results, subsequent simulations were carried out under the assumption of a fixed stack temperature.

The polarization curve obtained from the dynamic simulation is reported in Figure 47. It shows excellent agreement with literature data, confirming the validity of the implemented equations.



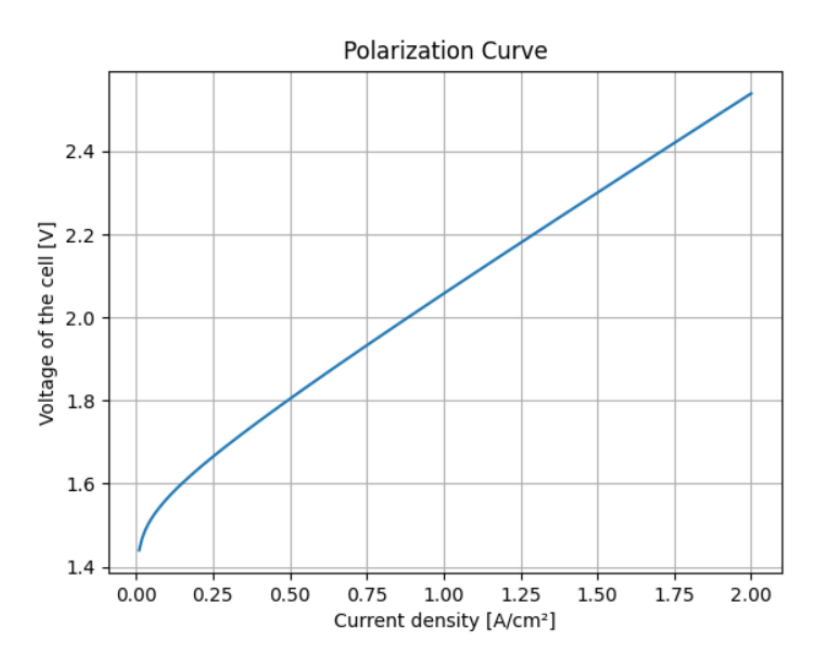


Figure 47: Polarization curve obtained from the dynamic model.

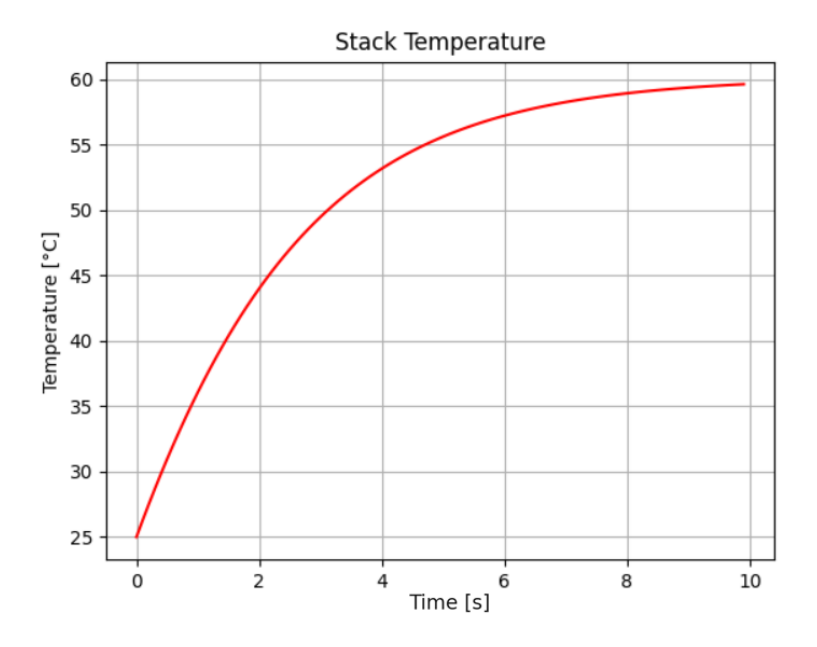


Figure 48: Transient temperature profile of the electrolyzer stack

The thermal transient curve shows that the stack temperature reaches the operating setpoint within approximately 10 seconds, a timescale that is negligible compared to the long-term horizons (days to years) considered in this study. This behavior has no meaningful impact on cumulative hydrogen production or energy balances at the plant scale. Consequently, the model was simplified by fixing the operating temperature at a nominal value instead of solving the transient thermal equation at every time step. This choice significantly reduces computational cost while



maintaining the accuracy of the results under steady-state conditions. In summary, the model's predictive reliability is preserved, while unnecessary short-term dynamics are omitted.

The model, although highly detailed and consistent with both literature polarization curves and the Cummins 500 datasheet, was later simplified. Thermal transients from ambient conditions to the nominal operating temperature of 60 °C occur in just a few seconds, a negligible timescale for lifetime simulations of industrial plants. Therefore, the iterative thermal loop was omitted and a constant operating temperature was assumed. This reduced the computational cost significantly while preserving model accuracy.

Simulation of the Cummins 500

The HyLYZER® 500 is a PEM water electrolyzer with a nominal hydrogen production capacity of 500 Nm³/h (1080 kg/day). It delivers hydrogen at 30 bar without the need for a compressor, while ensuring a purity level of 99.998% with very low oxygen and nitrogen impurities. This unit represents a compact and robust benchmark for large-scale green hydrogen generation. The developed digital twin aims to replicate the operation of the HyLYZER 500 under realistic conditions. When the model is executed with a fixed current input, the simulated output matches the technical specifications with high accuracy, confirming the validity of the approach.



FEATURES

	HyLYZER® - 400	HyLYZER® - 500
Technology	PEM water electrolysis	
Hydrogen production	400 Nm³/h (862 kg/day)	500 Nm ³ /h (1080 kg/day)
H ₂ delivery pressure	30 bar _g (435 psig) without a compressor	
H ₂ quality max impurities	99.998% $O_2 < 2$ ppm, $N_2 < 12$ ppm (higher purities optional); Atm. Dew point: -75°C	

Figure 49: HyLYZER-500.



Before structuring the code according to the principles of object-oriented programming, two preliminary simulations were carried out to verify the consistency of the model with the technical specifications of the commercial Cummins 500 electrolyzer. These tests were essential to validate the reliability of the implemented equations and to ensure that the digital twin could accurately reproduce the nominal performance of the system.

The first simulation was performed under constant irradiance conditions of $1000 \,\mathrm{W/m^2}$, representing the standard test case scenario. The second simulation considered a variable irradiance profile, corresponding to an ideal clear-sky day, in order to assess the system's response to fluctuating inputs. In both cases, the model equations remain unchanged and will be discussed in detail in the following subsections dedicated to each component of the PtX plant (PV system, electrolyzer, and hydrogen storage). Here, we limit ourselves to reporting the input data and the simulation results for the two scenarios.

These tables highlight the differences in system performance under the two conditions: constant irradiance at $1000\,\mathrm{W/m^2}$, variable irradiance representing an ideal sunny day. In this case, the irradiance profile is modeled as a sinusoidal function that starts from zero at sunrise, gradually increases to a peak of $1000\,\mathrm{W/m^2}$ at noon, and then decreases back to zero by 18:00, thus providing a simplified yet representative description of a clear-sky daily cycle.

Table 12: Results for constant irradiance simulation at 1000 W/m	n²	2	
--	----	---	--

Output Parameter	Value			
Average stack current [A]	5638.04			
Current density $[A/cm^2]$	0.78			
Average cell voltage [V]	1.8558			
E_0 [V]	1.2255			
Average stack voltage [V]	399.00			
Average absorbed power [MW]	2.500			
Total H ₂ production [kg/day]	1083.05			
Average efficiency [%]	60.13			

Table 13: Results for variable irradiance simulation (ideal sunny day).

Output Parameter	Value
Average absorbed power [MW]	0.737
Total H_2 production [kg/day]	364.28

The results confirm that the model is capable of reproducing the nominal performance of the Cummins 500 electrolyzer under constant irradiance, while also responding consistently to a time-varying solar input. This provides confidence in the robustness of the digital twin before extending the analysis to longer simulation horizons.

5.2 Object-Oriented Programming Approach

To ensure flexibility, scalability, and transparency, the computational model developed in this work was implemented in Python following the principles of object-oriented programming (OOP). Python was chosen not only for its widespread adoption and powerful numerical libraries, but also



for its ability to support a modular coding structure. In this context, OOP provides an effective framework for representing complex energy systems by breaking them down into well-defined components.

Object-oriented programming (OOP) is a paradigm widely used in software engineering that organizes code around objects rather than functions. Each object represents an entity with its own attributes (data) and methods (operations), which together define its behavior. This approach improves modularity, reusability, and clarity, making it particularly well suited for modeling complex systems such as energy conversion plants.

The model is organized in a modular and well-structured manner, where each physical subsystem is encapsulated within its own class. In this way, the digital twin of the plant is built in a clear, scalable, and reusable form, facilitating both the simulation process and future developments. The overall code structure is organized around a main script, which manages the time iteration and coordinates the interaction among the different subsystems. The time-based loop allows the simulation of the entire plant's dynamics over a given period, capturing the evolution of the physical variables and their interdependencies.

Three main components are included in the model: a photovoltaic (PV) system, an electrolyzer, and a hydrogen storage unit. Each of these components has been implemented as an independent class containing the relevant physical laws and operating principles necessary to replicate its behavior. In addition, a separate data file provides the required input parameters, which serve as the boundary conditions and technical specifications for the simulation.

The photovoltaic system class models the conversion of solar radiation into electrical power, taking as input meteorological and system data and returning the electricity produced at each time step. The electrolyzer class uses this electricity to perform water electrolysis, generating hydrogen. Its inputs are the power supplied and the technical parameters of the device, while the output is the hydrogen produced as a function of efficiency and operating conditions. The hydrogen storage class accounts for the accumulation of hydrogen over time, balancing the inflows from the electrolyzer with the current storage level and possible withdrawals, thus providing information on the available hydrogen stock.

The interaction between these components is governed by the main script, which ensures the temporal consistency of the simulation and the logical flow of inputs and outputs. At each iteration, the PV system supplies electricity, the electrolyzer converts part of it into hydrogen, and the storage unit updates its state according to the production balance. This modular structure not only ensures an orderly and transparent implementation but also makes the code flexible and easily extendable. Additional functionalities or new components can be integrated into the system with minimal changes to the existing framework.

In summary, the OOP design establishes the foundation for the digital twin representation of the PtX plant, which is further detailed in the following section.

5.3 Model of the PtX

The model described in this section represents the final and complete implementation of the digital twin of the PtX plant. As a first validation step, the code was executed with a constant current input in order to verify its consistency with the technical data of the Cummins 500 electrolyzer, as previously discussed. The simulation successfully reproduced the expected behavior,



73 5.3 Model of the PtX

confirming the accuracy of the implemented equations.

Subsequently, the model was tested using a theoretical solar irradiance profile over a 12-hour period to verify its capability of handling variable inputs. This preliminary daily simulation demonstrated that the program is able to correctly propagate fluctuations in irradiance into the electrical output, hydrogen production, and storage dynamics. Once these validations were completed, the model was extended to longer time horizons. For monthly, annual, and lifetime simulations, meteorological datasets from ARPA were employed, providing average values of irradiance and temperature representative of real operating conditions.

The code was developed following the principles of Object-Oriented Programming (OOP), as introduced in the previous section. This choice ensures a clear, modular, and extendable structure, while facilitating future improvements. The computational framework was therefore divided into distinct modules, each dedicated to a specific subsystem of the plant: the photovoltaic (PV) array, the proton exchange membrane (PEM) electrolyzer, and the hydrogen storage unit. In addition, two auxiliary modules were implemented: the main script, responsible for orchestrating the execution flow, and the plotting module, dedicated to generating graphical representations of the results.

This section also presents the main physical formulas employed for the modeling of the different components, providing a clear overview of the theoretical foundations underlying the implemented calculations. Specific simulation modules were later developed to evaluate the system's performance over different time horizons (daily, monthly, annual, and lifetime). Finally, a dedicated module was created to perform the cost analysis, using the outputs of the simulations as input parameters.

The main script acts as the orchestrator of the simulation environment. Its primary function is to coordinate the interactions among the different subsystems of the plant—PV generator, electrolyzer, and hydrogen storage unit—according to a time-iteration scheme. The script governs the initialization of system parameters, the calculation of the irradiance profile, the execution of the simulation loop, the collection of results, and their visualization.

At the beginning, the required Python libraries (NumPy, Pandas, Matplotlib) are imported, together with the subsystem classes defined in separate files. The SystemParameters class provides the general configuration of the plant. Once the temporal variables and the irradiance profile are defined, the three subsystem classes are instantiated. Each class contains the physical models necessary for constructing the digital twin.

The core of the simulation is handled within the loop, where at each time step the PV model computes the available electrical power, the electrolyzer converts part of it into hydrogen according to its efficiency and operational state, and the storage unit updates its level of hydrogen accordingly. This sequential interaction guarantees temporal consistency and reflects the physical flow of energy and mass within the system.

After the iterative phase, the main script compiles the results into a structured DataFrame, which contains the time evolution of all relevant variables: electrolyzer current and voltage, hydrogen flow rate, cumulative hydrogen production, storage state of charge, and overall system efficiency. These outputs are then passed to the Plotting class, which generates the graphical representation of the results. Diagnostic calculations are also performed, reporting average values of current, voltage, efficiency, and total hydrogen produced, to provide a quick validation of the



simulation outcomes.

It is important to highlight that this main script was originally designed for a first daily simulation, evaluating the plant behavior under simplified irradiance conditions. Longer-term simulations, based on ARPA meteorological datasets, were performed in separate scripts to account for seasonal and long-term variations. In summary, the main script acts as the core orchestrator, integrating the inputs and outputs of each subsystem into a coherent temporal evolution, in line with the modular philosophy of the OOP approach.

5.3.1 Photovoltaic System

Once the general simulation framework was defined, the focus shifted to the implementation of the photovoltaic (PV) subsystem, which provides the primary energy input to the PtX plant. The PhotovoltaicSystem class models the conversion of solar irradiance into electrical power available for the electrolyzer and, when applicable, for the electrical grid. It is designed to capture the essential dynamics of a PV field by applying standard physical relations and efficiency factors, while keeping the implementation computationally efficient for time-domain simulations.

The class takes as input the irradiance profile and the ambient temperature, and computes the instantaneous PV power as a function of the incident solar radiation and cell temperature. It also includes a method for generating the irradiance profile. For daily simulations, a sinusoidal approximation of the solar curve is adopted, providing a simplified but representative description of solar input.

Meteorological Input

Parameter	Description
G	Solar irradiance (W/m^2), location dependent

The PV model accounts for temperature effects on module efficiency through a temperature coefficient, as well as for derating factors and auxiliary system losses. The available PV power is then split between the electrolyzer (up to its maximum allowable input power) and the electrical grid, with any surplus energy being exported. Table 14 summarizes the main parameters used in the PV subsystem model.

Table 14: Input parameters for the photovoltaic (PV) subsystem.

Parameter	Symbol	Value	Unit / Description
PV surface area	A_{PV}	20000	m^2
PV module efficiency	η_{PV}	0.22	- (fraction)
Irradiance at STC	$G_{ m STC}$	1000	$ m W/m^2$
Rated PV power	$P_{\mathrm{PV,rated}}$	4.4×10^{6}	W (calculated as $A_{\text{PV}} \cdot \eta_{\text{PV}} \cdot G_{\text{STC}}$)
PV derating factor	$f_{ m PV}$	0.9	- (fraction)
Temperature coefficient of power	α_P	-0.004	1/K
Cell temperature at STC	$T_{c, \rm STC}$	25	$^{\circ}\mathrm{C}$
Maximum electrolyzer power input	$P_{\rm reale}$	2.5×10^6	W
Auxiliary systems efficiency	$\eta_{ m aux}$	0.9	- (fraction)



75 5.3 Model of the PtX

Governing Equations

The central function of the PhotovoltaicSystem class is updatepvpower, which computes the instantaneous photovoltaic power at each time step. The model accounts for: (i) the influence of ambient temperature on module temperature, (ii) the correction of efficiency through the temperature coefficient, and (iii) auxiliary system losses.

The irradiance profile for a daily simulation is approximated as:

$$G(t) = G_{\text{peak}} \cdot \max\left(0, \sin\left(\frac{\pi(t_{\text{hr}} - 6)}{12}\right)\right),\tag{31}$$

where $t_{\rm hr}$ is the time expressed in hours and $G_{\rm peak}$ is the maximum daily irradiance.

The cell temperature is estimated as:

$$T_c = T_{\text{amb}} + 0.03 \cdot G(t),$$
 (32)

where T_{amb} is the ambient temperature.

The theoretical PV power output is then calculated by:

$$P_{\text{PV,teo}} = f_{\text{PV}} \cdot P_{\text{PV,rated}} \cdot \left(\frac{G(t)}{G_{\text{STC}}}\right) \cdot \left(1 + \alpha_P \cdot (T_c - T_{c,\text{STC}})\right), \tag{33}$$

which is subsequently corrected for auxiliary system efficiency:

$$P_{\text{PV}} = \eta_{\text{aux}} \cdot P_{\text{PV,teo}}.\tag{34}$$

The allocation of PV power is governed by the electrolyzer's maximum admissible input:

$$P_{\text{PV}\to\text{Electrolyzer}} = \min(P_{\text{PV}}, P_{\text{reale}}),$$
 (35)

$$P_{\text{PV}\to\text{Grid}} = \max(P_{\text{PV}} - P_{\text{reale}}, 0). \tag{36}$$

Outputs. The outputs of this class are threefold: 1. the PV power delivered to the electrolyzer, 2. the surplus PV power injected into the grid, and 3. the theoretical PV power without auxiliary losses.

In summary, the PhotovoltaicSystem class provides a simplified but effective digital twin of a PV field. It captures the dependence of power production on irradiance and temperature, applies realistic constraints such as the maximum admissible power for the electrolyzer, and ensures that any excess energy is properly accounted for. This enables dynamic simulation of the PV subsystem within the overall PtX model, reflecting both physical principles and operational constraints.

5.3.2 Electrolyzer

The next component is the electrolyzer class, which converts the PV-generated electricity into hydrogen according to electrochemical principles. The Electrolyzer class encapsulates the dynamic behaviour of a PEM electrolyzer operated under time-varying electrical input. It receives



the global simulation parameters and the time vector from the main script, preallocates all state and output arrays, and advances its internal state at each time step according to standard electrochemical relations.

Inputs to this component are the DC electrical power routed from the PV field at each time step and the previous cell voltage, which is used as a stabilising reference for the next-step calculation. The outputs are time series of stack current, cell and stack voltages, stack power, instantaneous hydrogen production rate, voltage contributions, and instantaneous efficiency.

The core routine of the class converts available electrical power into stack current, computes the current density, and applies a pragmatic cutoff for low-current operation to avoid non-physical hydrogen production. Once a meaningful operating point is established, the model evaluates the principal electrochemical contributions that determine the instantaneous cell voltage: - Faradaic efficiency, which penalizes parasitic losses at low current density, - anodic and cathodic activation overpotentials, modeled through a simplified Butler–Volmer inverse hyperbolic sine relation, - the thermodynamic equilibrium potential, computed from the Nernst relation, and - an ohmic drop, proportional to current density and membrane resistance.

Hydrogen generation is computed from the electrical current by Faraday's law, converted from moles per second to kilograms per second. Finally, the instantaneous efficiency is reported as the ratio between the chemical power of hydrogen produced (based on its lower heating value) and the absorbed electrical power.

In summary, the Electrolyzer class provides a compact and computationally efficient digital twin of a PEM electrolyzer. It preserves numerical robustness under zero-input or low-load conditions, exposes diagnostic variables for analysis and plotting, and integrates seamlessly within the time-iterated orchestration managed by the main script.

Governing Equations. The physical behaviour is governed by standard electrochemical relations.

Current and Current Density:

$$I_k = \frac{P_{\text{in},k}}{n_{\text{cells}} \cdot V_{k-1}}, \qquad i_k = \frac{I_k}{A_{\text{cell}}}, \tag{37}$$

where $P_{\text{in},k}$ is the PV power input at time step k, V_{k-1} is the reference cell voltage from the previous step, and A_{cell} is the active cell area.

Faradaic Efficiency:

$$\eta_F \approx 1 - \frac{0.01 \, i_{k,\text{cm}^2}}{i_{k,\text{cm}^2}} \simeq 0.99,$$
(38)

an empirical relation that captures parasitic losses at low current densities.

Activation Overpotentials:

$$V_{\rm an} = \frac{RT}{2\alpha_{\rm an}F} \operatorname{arcsinh}\left(\frac{i_{k,\rm cm^2}}{2i_{0,\rm an}}\right),\tag{39}$$

$$V_{\rm ca} = \frac{RT}{2\alpha_{\rm ca}F} \operatorname{arcsinh}\left(\frac{i_{k,\rm cm^2}}{2i_{0,\rm ca}}\right),\tag{40}$$



77 5.3 Model of the PtX

where $i_{0,an}$ and $i_{0,ca}$ are the anode and cathode exchange current densities.

Nernst Potential and Cell Voltage:

$$E_n = E_0 + \frac{RT}{2F} \ln \left(\frac{P_{\rm H_2} \sqrt{P_{\rm O_2}}}{P_{\rm H_2O,an}} \right),$$
 (41)

$$V_{\text{cell}} = E_n + V_{\text{an}} + V_{\text{ca}} + i_k R_{\Omega}, \tag{42}$$

$$V_{\text{stack}} = n_{\text{cells}} \cdot V_{\text{cell}}.$$
 (43)

Hydrogen Production:

$$\dot{n}_{\rm H_2} = \frac{n_{\rm cells} \cdot I_k}{2F} \, \eta_F,\tag{44}$$

$$\dot{m}_{\rm H_2} = \dot{n}_{\rm H_2} \cdot \frac{M_{\rm H_2}}{1000},\tag{45}$$

where $M_{\rm H_2}$ is the molar mass of hydrogen.

Instantaneous Efficiency:

$$\eta_{\text{inst}} = \frac{\dot{m}_{\text{H}_2} \cdot \text{LHV}_{\text{H}_2}}{P_{\text{in},k}} \times 100 \, [\%]. \tag{46}$$

Input Parameters. Table 15 reports the initialization seeds and internal thresholds of the Electrolyzer class, while Table 16 lists the main physical and electrochemical constants.

Table 15: Class-level inputs, thresholds, and initialization used by the Electrolyzer model.

Quantity	Symbol	Value	Unit / Notes
Initial cell voltage seed	$V_{\text{cell},0}$	2.23	V
Initial stack current seed	I_0	6239.76	A
Initial H_2 mass flow seed	$\dot{m}_{ m H_2,0}$	11	kg/s (seed; overwritten)
Minimum current density for production	$i_{ m min}$	1.0×10^{-4}	A/m^2 (below this, no production)
Parasitic-loss factor for η_F	_	0.01	- (empirical coefficient)
Current density conversion	_	$i_{\rm cm^2} = i/10^4$	$ m A/cm^2$



Parameter	Symbol	Value	Unit / Description
Number of cells	$n_{\rm cells}$	215	_
Active cell area	A_{cell}	0.7225	m^2
Universal gas constant	R	8.314	$\mathrm{J/(mol \cdot K)}$
Operating temperature	T	333.15	K
Charge transfer coefficient (anode)	$\alpha_{ m an}$	2.0	_
Charge transfer coefficient (cathode)	$\alpha_{ m ca}$	0.5	_
Faraday constant	F	96485	C/mol
Exchange current density (anode)	$i_{0,\mathrm{an}}$	2×10^{-7}	$ m A/cm^2$
Exchange current density (cathode)	$i_{0,\mathrm{ca}}$	2×10^{-3}	$\mathrm{A/cm^2}$
Standard cell potential	$\dot{E_0}$	1.224	V
H ₂ partial pressure	$P_{ m H_2}$	3.0×10^{6}	Pa (30 bar)
O_2 partial pressure	P_{O_2}	3.0×10^{6}	Pa (30 bar)
Anode-side H ₂ O partial pressure	$P_{\rm H_2O,an}$	101325	Pa (1 bar)
Area-specific ohmic resistance	R_{Ω}	0.000139	$\Omega \cdot \mathrm{m}^2$
Hydrogen molar mass	$M_{ m H_2}$	2.016	g/mol
Hydrogen lower heating value	$\mathrm{LHV}_{\mathrm{H}_2}^{\mathrm{I}}$	1.199×10^{8}	J/kg

Table 16: Electrochemical and thermophysical input parameters for the PEM electrolyzer.

5.3.3 Hydrogen Storage

The last major subsystem is the hydrogen storage unit, modeled as a metal-hydride (MH) tank. The HydrogenStorage class simulates the dynamic accumulation and release of hydrogen under time-varying inflows from the electrolyzer, while enforcing a simplified day-night operating policy. The model encapsulates four main processes: (i) hydrogen absorption and desorption constrained by Johnson-Mehl-Avrami (JMA) kinetics, (ii) thermodynamic equilibrium relations based on the Van't Hoff and Sieverts laws, (iii) a lumped thermal balance of the tank including reaction enthalpy and water-loop heat exchange, and (iv) inventory management governed by maximum storage capacity.

Inputs to this component are the hydrogen inflow from the electrolyzer at each time step and the simulation parameters defining the tank's physical, kinetic, and thermodynamic properties. Outputs are time series of stored hydrogen mass, state of charge, absorbed and released flow rates, tank temperature, and the chemical energy content of the stored hydrogen. These quantities are used both for downstream analysis and for graphical visualization of the system's behaviour.

Input Parameters. Tables 17 and 18 summarize the thermochemical, kinetic, and thermal parameters adopted in the hydrogen storage model.



79 5.3 Model of the PtX

Parameter	Symbol	Value	Unit / Description
Reference reaction enthalpy	$\Delta H_{ m ref}$	32500	J/mol (positive for desorption)
Reaction heat capacity change	$\Delta C_p^{\mathrm{rxn}}$	0	$\mathrm{J/(mol \cdot K)}$
Reference temperature	T_{ref}	298.15	K
Reaction entropy	ΔS	100	$ m J/(mol \cdot K)$
Universal gas constant	$R_{\rm gas}$	8.314	$ m J/(mol \cdot K)$
Arrhenius pre-exponential	$\overset{\circ}{A}$	7.3×10^{4}	h^{-m}
Activation energy	E_a	22000	m J/mol
JMA exponent	$m_{ m JMA}$	0.55	_
Maximum H ₂ capacity	$m_{\rm H_2,max}$	200	kg
Hydrogen molar mass	$M_{ m H_2}$	2.016	m g/mol
Hydrogen lower heating value	$\mathrm{LHV}_{\mathrm{H}_2}^-$	1.199×10^{8}	J/kg

Table 17: Thermochemical and kinetic parameters for the hydrogen storage system.

Table 18: Thermal mass and heat-exchanger parameters for the hydrogen storage system.

Parameter	Symbol	Value	Unit / Description
Hydride bed mass	$m_{ m MH}$	10869.6	kg
Effective heat capacity	$c_{p,\mathrm{eff}}$	506.33	$\mathrm{J/(kg \cdot K)}$
Water mass flow rate	$\dot{m}_{ m w}$	5	$\mathrm{kg/s}$
Water specific heat	$c_{p,\mathrm{w}}$	4180	$\mathrm{J/(kg \cdot K)}$
Cold-side inlet temperature	$T_{\rm in,cold}$	298.15	$K(25^{\circ}C)$
Hot-side inlet temperature	$T_{ m in,hot}$	353.15	K (80°C)

Governing Equations. The hydrogen storage dynamics are determined by thermodynamic equilibrium, reaction kinetics, and thermal balances.

Kinetics (JMA model):

$$k_{\text{JMA}}(T) = A \exp\left(-\frac{E_a}{RT}\right), \qquad \frac{d\alpha}{dt} = k_{\text{JMA}} \, m \, t^{m-1} (1-\alpha) \left[-\ln(1-\alpha)\right],$$
 (47)

where α is the conversion fraction (state of absorption).

Equilibrium Pressure (Van't Hoff and Sieverts laws):

$$P_{\rm eq}(T) = \exp\left(-\frac{\Delta H_{\rm ref}}{RT} + \frac{\Delta S}{R}\right), \qquad k_{\rm Sieverts}(T) = \sqrt{P_{\rm eq}(T)}.$$
 (48)

Temperature-Dependent Enthalpy:

$$\Delta H_{\rm rxn}(T) = \Delta H_{\rm ref} + \Delta C_p^{\rm rxn}(T - T_{\rm ref}). \tag{49}$$

Thermal Balance:

$$\Delta E = Q_{\text{reaction} \to \text{tank}} + Q_{\text{HX} \to \text{tank}}, \tag{50}$$

$$\Delta T_{\text{tank}} = \frac{\Delta E}{m_{\text{MH}} c_{p,\text{eff}}},\tag{51}$$



where $Q_{\text{reaction}\to \text{tank}}$ accounts for exothermic/endothermic reaction heat and $Q_{\text{HX}\to \text{tank}}$ represents water-loop heat exchange.

Stored Energy:

$$E_{\text{chem}} = m_{\text{H2,stored}} \cdot \text{LHV}_{\text{H2}}. \tag{52}$$

Operating Policy

The storage system follows a simple day–night logic:

- Daytime (06:00–18:00): absorption is prioritized, with inflows from the electrolyzer stored up to the kinetic and capacity limits.
- Nighttime (18:00–06:00): hydrogen is released at a constant target rate, designed to deplete the inventory over 12 hours, while still constrained by kinetics and available stored mass.

This ensures a realistic cycling of charge/discharge that reflects solar-driven operation.

Outputs. The primary variables stored over the simulation are listed in Table 19.

Table 19: Primary outputs stored over time by the HydrogenStorage model.

Output	Symbol	Unit / Description
State of charge	SOC_t	% (relative to $m_{\rm H_2,max}$)
Stored hydrogen	$m_{\mathrm{H}_2,t}$	kg
Chemical energy content	$E_{\mathrm{chem},t}$	MJ (from LHV of H_2)
Tank temperature	$T_{\mathrm{tank},t}$	°C (internally updated in K)
Absorbed flow	$\dot{m}_{\mathrm{abs},t}$	$\mathrm{kg/s}$
Released flow	$\dot{m}_{\mathrm{rel},t}$	$\mathrm{kg/s}$

In summary, the hydrogen storage subsystem provides a compact, computationally efficient digital twin of a metal–hydride tank. It captures the essential features of absorption/desorption thermodynamics and kinetics, incorporates a lumped-parameter thermal model, and enforces a transparent day–night policy. Together with the PV and electrolyzer components, it completes the simulation framework of the PtX plant.



6 Scenarios

6.1 Approach for Simulations

Building upon the computational framework developed in Chapter 5, this chapter applies it to, this chapter applies the computational framework to different simulation horizons and analyses. The objective is to evaluate the technical, environmental, and economic performance of the PtX system

Once the correct operation of the plant had been verified through a daily simulation, the next step involved gathering meteorological data from the ARPA Veneto website. The plant was geographically located at the Zignago Vetro facility in the town of Fossalta di Portogruaro, which hosts one of the company's main production sites.

Following a systematic approach, simulations were performed in three stages: first on a monthly basis, then on an annual basis, and finally using long-term meteorological data spanning a period of 25 years. The input meteorological parameters considered were the average temperature and the average monthly solar irradiance.

From these datasets, the hydrogen production over the plant's entire lifetime was estimated. This lifetime hydrogen yield then served as the basis for carrying out the subsequent cost analysis, enabling an evaluation of the economic feasibility of the proposed system under real climatic conditions.

6.1.1 Daily Simulations (Plant Scale)

At this stage of the work, the computational framework was consolidated and prepared for long-term analyses. To facilitate future developments and ensure clarity, as already mentioned before, the code was developed following the principles of Object-Oriented Programming (OOP). The framework was organized into distinct modules, each dedicated to a specific subsystem of the plant: the photovoltaic (PV) field, the proton exchange membrane (PEM) electrolyzer, and the hydrogen storage unit. Two additional modules were introduced: the main script, responsible for coordinating the execution flow, and a plotting module dedicated to generating graphical representations of the results. The detailed description of the OOP implementation has already been provided in Chapter 5.3 and is only briefly recalled here.

Building on this structure, specific simulation modules were implemented to evaluate system performance across different time horizons: daily validation, annual operation, and lifetime analysis. A dedicated module was also developed to perform the cost analysis, using the outputs of the technical simulations as input parameters.

The daily simulation represents the first validation step of the framework. It is performed over a single-day horizon using an ideal clear-sky irradiance profile, which rises from sunrise, peaks at noon, and decreases to zero at sunset. This controlled scenario allows the model to be tested under smooth boundary conditions, avoiding the stochastic variability of real meteorological data. At each time step, the PV subsystem computes the available electrical power, which is then fed into the electrolyzer to generate hydrogen, while the storage unit manages absorption and release according to the predefined operating policy. The outputs include instantaneous quantities such as current, voltage, and hydrogen flow, as well as cumulative hydrogen production over the day.



6 Scenarios 82

The main purpose of this validation is to ensure the numerical stability of the time-iterated code, verify the correct interaction among subsystems, and confirm that the electrolyzer reproduces datasheet-consistent operating points. Once these aspects were validated at the plant scale, the framework was extended to longer horizons, namely annual and lifetime simulations.

6.1.2 Annual simulation

This script extends the daily digital-twin framework to an annual horizon using monthly meteorological data. The goal is to estimate the yearly hydrogen output of the PV-electrolyzer-storage system while preserving the object-oriented architecture previously described. The approach is based on a representative-day method: for each month, a 24-hour simulation is executed with monthly average ambient temperature and a sinusoidal irradiance profile scaled to match the month's measured global irradiation. The monthly hydrogen yield is then obtained by multiplying the daily result by the number of days in that month, and the annual total is the sum of the twelve contributions.

The script begins by declaring the monthly series used as inputs: average near-surface air temperature in degrees Celsius and global solar irradiation in megajoules per square metre per month. These data were acquired from the ARPAV Centro Meteorologico di Teolo and correspond to the year 2023, the latest available. The arrays are passed, month by month, to the physical components, thereby linking the digital twin to observed climatic conditions without changing the components' internal models.

Table 20: Monthly mean air temperature at 2 m in 2023 (°C).

Year	Jan	Feb	Mar	Apr	May	Jun	Jul	Aug	Sep	Oct	Nov	Dec	Mean
2023	6.2	5.5	10.1	11.9	18.2	22.6	24.4	23.8	21.3	16.9	8.5	5.8	14.6

The time discretization mirrors the daily setup used previously: a 60-second time step over a 24-hour window that runs from 06:00 to 06:00 of the following day. The irradiance profile is generated by a sinusoidal function with a nominal 12-hour daylight duration and is scaled so that the integral of the daily curve matches the month's measured irradiation. This preserves the monthly energy balance while keeping the transient behaviour physically plausible.

For each month, the three component classes are re-instantiated, thus resetting their internal states. The PV model converts the irradiance profile and ambient temperature into electrical power; the electrolyzer converts DC power into hydrogen according to its electrochemical operating map; the metal-hydride storage updates its state by applying the day–night policy constrained by kinetics and thermal balance. This coupling is identical to the daily simulation, but now executed twelve times with month-specific boundary conditions.

At the end of each day-simulation the script aggregates the hydrogen mass flow into a daily production figure and scales it by the number of days in the month to obtain the monthly production. The monthly series is then plotted as a bar chart and summed to yield the annual production.

$$m_{H_2,\text{month}} = \left(\sum_{k=1}^{N} \dot{m}_{H_2}(k) \cdot \Delta t\right) \cdot D_{\text{month}}$$
 (53)



From a modelling standpoint, the underlying physical laws remain those already discussed for each component. The PV output accounts for irradiance and temperature effects on module performance; the electrolyzer maps electrical input to hydrogen output via thermodynamic potential, activation overpotentials, ohmic losses, and Faradaic conversion; the storage follows metal-hydride equilibrium, kinetics, and a lumped thermal balance with a simple operating policy. No explicit equations are printed here because they are defined within the component classes; the present script focuses on feeding month-specific boundary conditions and aggregating results over the annual horizon.

Two remarks improve clarity of use. First, components are re-created each month, so there is no carry-over of storage state across months; this is consistent with the representative-day philosophy but can be relaxed in future work if seasonal coupling of the storage is needed. Second, the irradiance profile assumes twelve hours of daylight for all months, which preserves monthly energy but simplifies the diurnal shape; it can be replaced by hour-by-hour irradiance if higher temporal fidelity is required.

Overall, this annual driver provides a compact and transparent way to quantify the yearly hydrogen yield of the plant under observed meteorological conditions while keeping the simulation cost low and the codebase fully modular.

6.1.3 Lifetime simulation (25-Year Series)

While the annual simulation provides a one-year estimate, the lifetime simulation extends the analysis over 25 years to assess inter-annual variability and long-term performance trends. Building upon the representative-day methodology introduced for single-year studies, the model was extended to a lifetime horizon of twenty-five years. The simulation replicates the annual procedure for each calendar year from 1999 through 2023, using observed monthly meteorological data as boundary conditions. The resulting time series of hydrogen production and photovoltaic energy serve as inputs to the techno-economic assessment and the environmental analysis discussed later in this thesis, including the estimation of avoided CO emissions and the displacement of natural gas consumption.

The driver function sets the temporal scope, the discretization for the representative day, and the per-month boundary conditions. The object-oriented architecture remains unchanged: at each month of each year the three component classes are instantiated, the daily time loop is executed, and the results are aggregated to monthly and annual figures.

Meteorological inputs are provided as two matrices indexed by year and month. For each year, the script reads the monthly mean air temperature in degrees Celsius and the monthly global irradiance in megajoules per square metre. These values are mapped to the component models without changing their internal physics, thereby keeping the digital twin consistent while adapting to year-specific boundary conditions.

For each month, the representative-day irradiance curve is constructed as a sinusoid with twelve hours of daylight. Its peak value is chosen so that the daily integral of the curve equals the month's measured global irradiation divided by the number of days. The monthly mean temperature sets the ambient condition used by the PV model.

At the end of the daily loop, hydrogen mass flow is integrated to obtain the daily production and then scaled by the number of days in the month to obtain the monthly production. This



6 Scenarios 84

value is accumulated over the twelve months to obtain the annual total for that year:

$$m_{H_2,\text{year}} = \sum_{j=1}^{12} m_{H_2,\text{month}}(j)$$
 (54)

In parallel, the script aggregates the photovoltaic electrical energy delivered to the electrolyzer. The daily electrical energy is obtained by integrating the power time series; the monthly and annual values are computed by multiplication and summation, and finally a multi-year average is reported.

$$E_{\text{avg,year}} = \frac{1}{N} \sum_{i=1}^{N} E_{\text{year}}(i)$$
 (55)

Several modelling choices ensure transparency and computational efficiency. The representative-day assumption preserves the monthly energy budget while simplifying the intra-day pattern, which is sufficient for lifetime-scale scenarios. Components are re-instantiated at each month so that the storage state does not carry over between months, consistent with the aggregation method; this can be relaxed in future work if seasonal storage coupling is required. Numerical safeguards are in place for low-power conditions and start-up phases.

The multi-year outputs obtained with this driver constitute the quantitative basis for the subsequent cost analysis, the CO reduction assessment, and the natural gas displacement study. Those post-processing scripts use the annual hydrogen production and electrical energy series reported here and will be analysed in the following sections.

6.2 Post-processing of Simulation Results: CO Reduction and Methane Savings

Beyond the purely technical performance, the model outputs were post-processed to quantify environmental and economic indicators, which are crucial for assessing the viability of the PtX system. The first post-processing module consumes the yearly hydrogen production obtained from the lifetime simulation that replicates the annual procedure for each calendar year from 1999 to 2023. Its purpose is to translate usable hydrogen into equivalent methane savings and avoided carbon dioxide emissions. The script adopts fixed energy equivalences and an emission factor for natural gas combustion, applies them to the annual hydrogen output, and aggregates the results both by year and over the full lifetime.

Table 21: Energy and emission constants used in the CO₂ and methane savings module.

Quantity	Value
Methane energy content (LHV)	$10.7\mathrm{kWhSm^{-3}}$
Hydrogen energy content (LHV)	$33.33{\rm kWhkg^{-1}}$
CO_2 emission factor for CH_4	$2.024{\rm kgCO_2Sm^{-3}}$
Annual methane consumption (reference)	$84,543,271 \text{ Sm}^3/\text{yr}$

For each year in the analysis window the module reads the mass of usable hydrogen in kilograms,



converts it into electrical energy on a lower heating value basis, and then computes the equivalent volume of methane that would deliver the same energy. The avoided carbon dioxide is evaluated by applying the specific emission factor per standard cubic metre of methane and reporting the result in tonnes. A compact loop builds a tabular dataset, computes lifetime totals, and produces diagnostic bar charts.

$$E_{H_2}(t) = m_{H_2}(t) \cdot \text{LHV}_{H_2}$$
 (56)

$$V_{CH_4,\text{saved}}(t) = \frac{E_{H_2}(t)}{\text{LHV}_{CH_4}}$$
(57)

$$CO_2$$
, avoided $(t) = V_{CH_4, \text{saved}}(t) \cdot f_{CH_4}$ (58)

The script concludes with two figures that display, year by year, the methane saved and the avoided carbon dioxide. These graphics provide a direct visual link between the variability of yearly hydrogen production and its environmental impact, while the lifetime totals summarise the cumulative benefit over the twenty-five year horizon.

6.3 Economic Analysis: LCOE, LCOH, NPC and Payback Period

The second post-processing module implements the economic assessment. Using the lifetime outputs of the simulation as technical inputs, it evaluates the levelised cost of electricity for the photovoltaic field, the levelised cost of hydrogen for the combined system, the net present cost of the project, and the discounted payback under two distinct revenue models: savings from displaced methane and hydrogen sales at an exogenous market price. The same core routine is run repeatedly under multiple scenarios to reflect plausible future cost trends.

Table 22: Key economic parameters used in the analysis.

Plant PV rating	$4400~\mathrm{kW}$
Plant PEM rating	$2500~\mathrm{kW}$
Methane price	2
Hydrogen market price	4 €/kg
Discount rate	4.9% (real)

The heart of the module is a function that computes the net present cost (NPC) by summing the initial investment, the discounted stream of annual operating expenses, and any discounted replacement cost. The levelised cost of electricity is obtained by dividing the NPC by the discounted lifetime energy, while the levelised cost of hydrogen divides the same NPC by the total hydrogen produced over the lifetime. This choice of denominator for hydrogen is conservative and transparent; an alternative would be to discount the annual hydrogen output as well, which can be considered in sensitivity analyses.



6 Scenarios 86

$$NPC = CAPEX + \sum_{t=1}^{N} \frac{OPEX_t + RC_t}{(1+r)^t}$$
 (59)

$$LCOE = \frac{NPC}{\sum_{t=1}^{N} \frac{E_t}{(1+r)^t}}$$

$$(60)$$

$$LCOH = \frac{NPC}{\sum_{t=1}^{N} H_{2,t}}$$

$$(61)$$

Three scenarios are defined to reflect learning-curve cost reductions for photovoltaic and PEM technologies. Each scenario specifies capital costs per kilowatt and the operating expenditure model.

Table 23: Scenario assumptions for CAPEX and OPEX in the economic analysis.

	2025	2030	2050
PV CAPEX [€/kW]	1200	1000	600
PEM CAPEX [€/kW]	1500	1000	800
PV OPEX [€/kW·yr]	24	24	24
PEM OPEX [% of CAPEX]	3%	3%	2%

The module also implements a discounted cash-flow routine for payback analysis. In the first revenue model the project accrues savings proportional to the annual methane displaced, using an externally provided series in cubic metres per year multiplied by the methane price. In the second model revenues come from selling hydrogen at a fixed market price per kilogram. In both cases a discount factor is applied year by year and the break-even year is identified as the first year in which the cumulative discounted cash flow turns non-negative.

$$NPV_t = -CAPEX + \sum_{i=1}^{t} \frac{(R_i - OPEX_i)}{(1+r)^i}$$
 (62)

Break-even year =
$$\min\{t : NPV_t \ge 0\}$$
 (63)

The analysis is then executed for all scenarios. Lifetime-average PV electricity and total lifetime hydrogen production, previously computed by the 1999–2023 simulation, enter as technical inputs that remain constant across scenarios. The outputs include LCOE for the PV plant alone, LCOH for the combined system, the total net present cost, the discounted cost streams, and the discounted payback curves under the two revenue models.

Table 24: Lifetime technical outputs used for economic analysis.

Average annual PV electricity	3,972,934 kWh
Total hydrogen production (25 yrs)	2,194,133 kg
Analysis horizon	25 years



Finally the module produces a set of figures that compare the discounted annual energy across scenarios, the discounted operating and replacement costs, and the levelised costs. Two additional graphs document the discounted cash flows and the break-even year for both revenue models. These plots make it straightforward to understand how learning-curve cost reductions shift the economics of the project. In the broader workflow of the thesis, this module and the preceding environmental module are run multiple times with different price assumptions and savings series to generate a suite of scenarios that reflect plausible futures for equipment costs and energy markets.

This economic layer completes the digital-twin workflow. The simulation engine generates consistent multi-year technical outputs. The environmental module quantifies avoided emissions and fuel displacement. The economic module translates technical performance into levelised metrics and discounted payback under multiple scenarios. Together they provide the quantitative basis for discussing the conditions under which the project becomes attractive from both an environmental and an industrial perspective.



7 Results

7.1 Daily Simulation

The first two figures produced by the simulation of the digital twin correspond to the photovoltaic (PV) module class. They represent, respectively, the power output and the electrical current of the PV system.

As expected, and in agreement with what is widely reported in the literature, both power and current follow a sinusoidal-like profile over the course of the day. The values start from zero at sunrise, increase steadily until reaching a maximum around solar noon—when irradiance is at its peak—and then symmetrically decrease back to zero at sunset. During nighttime hours, the output remains null, consistently with the absence of solar radiation.

This behavior confirms the physical consistency of the model, since the curves correctly reproduce the expected diurnal solar cycle. Moreover, the similarity between the shapes of the power and current profiles highlights the direct relationship between irradiance, power generation, and current flow in the PV system.

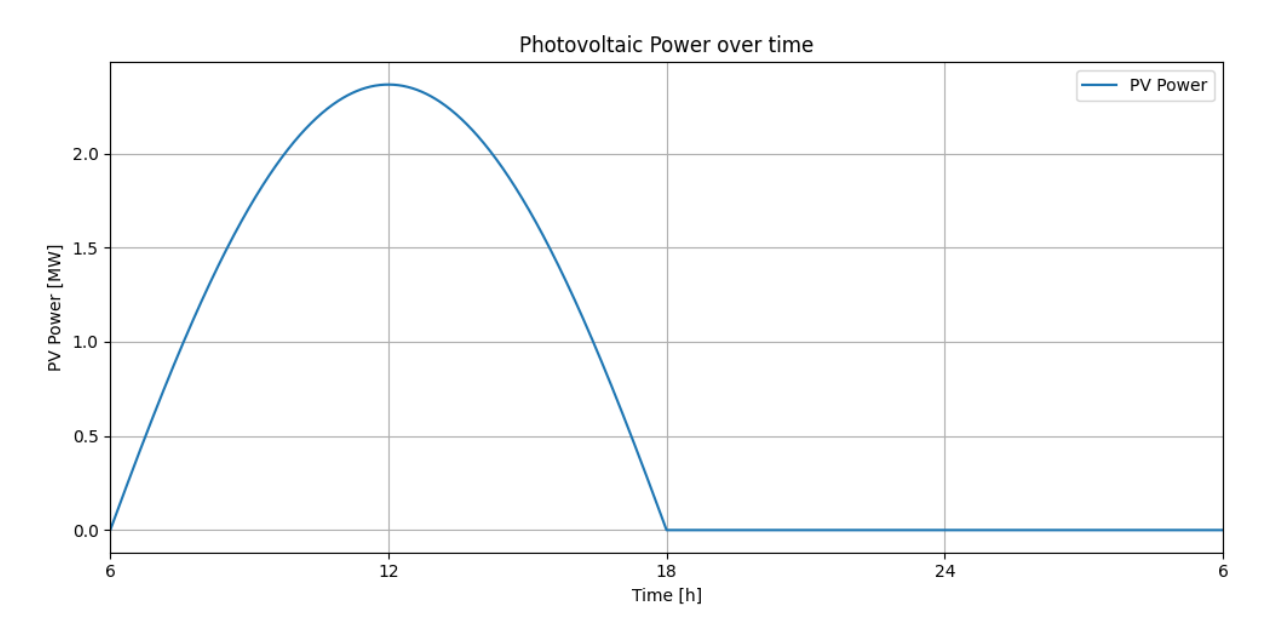


Figure 50: Photovoltaic Power over time



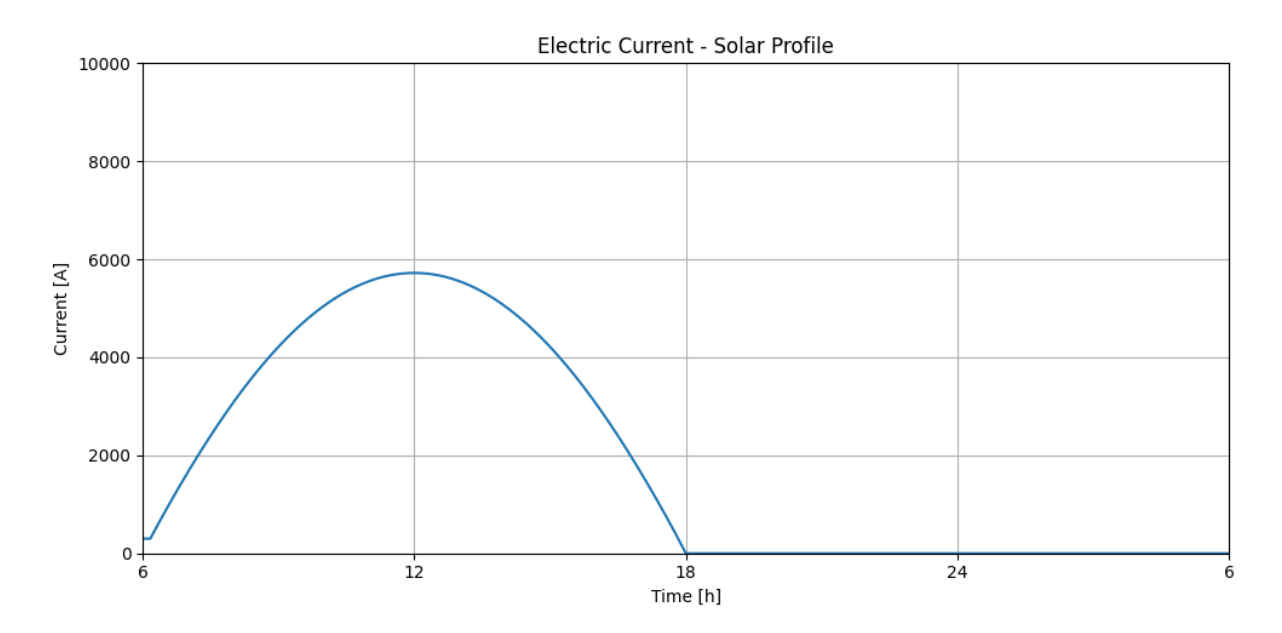


Figure 51: Electric Current

The other key results produced by the digital twin involve the PEM electrolyzer module. In these plots, the instantaneous hydrogen production rate is computed as a function of time. As expected, given that in our simulation the PEM electrolyzer is directly and exclusively connected to the photovoltaic (PV) field, the hydrogen production follows a sinusoidal diurnal profile: it increases throughout the morning, reaches its maximum around solar noon, and decreases again towards sunset, while remaining null during the night.

A second plot shows the cumulative hydrogen production over the day. The total daily output reaches slightly above 350 kg of H₂, which is fully consistent with expectations. This result aligns with the fact that the digital twin was designed to reproduce the behavior of the commercial CUMMINS HyLYZER[®] 500 electrolyzer, which is rated for up to 1000 kg of H₂ per day under conditions of continuous 24-hour power supply.



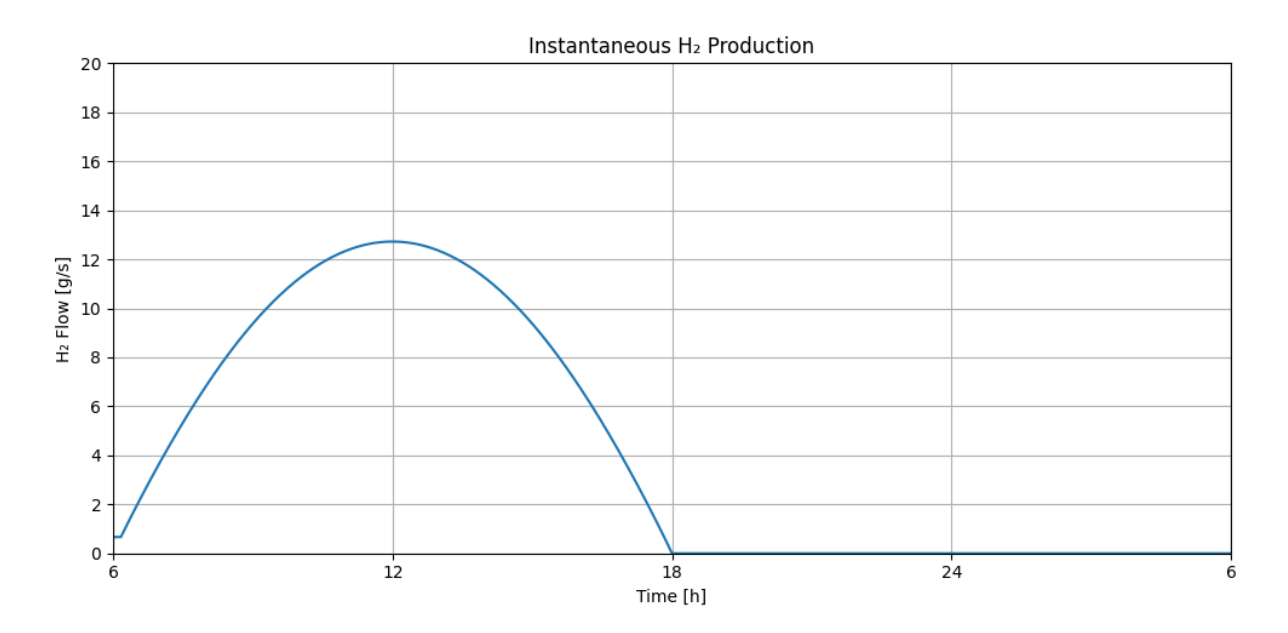


Figure 52: Instantaneous H2 production

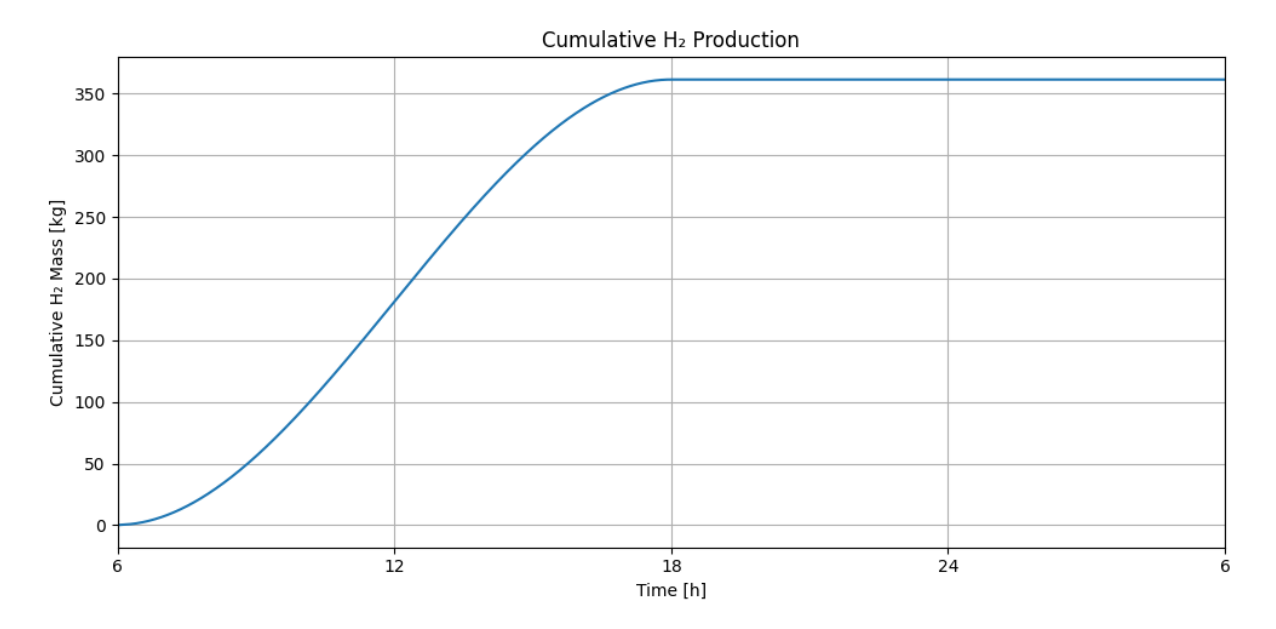


Figure 53: Comulative H2 production

The results obtained for the PEM electrolyzer digital twin are in strong agreement with the scientific literature, suggesting that the model is both reliable and physically consistent with the system it aims to reproduce. This strengthens confidence in the robustness of the simulation framework.

Three figures are particularly significant and are discussed below:

Polarization curve – The simulated polarization curve is in excellent agreement with experimental trends reported in the literature, both under nominal and varying operating conditions. This



correspondence also confirms that the temperature-dependent effects integrated into the model are consistent with the underlying electrochemical physics.

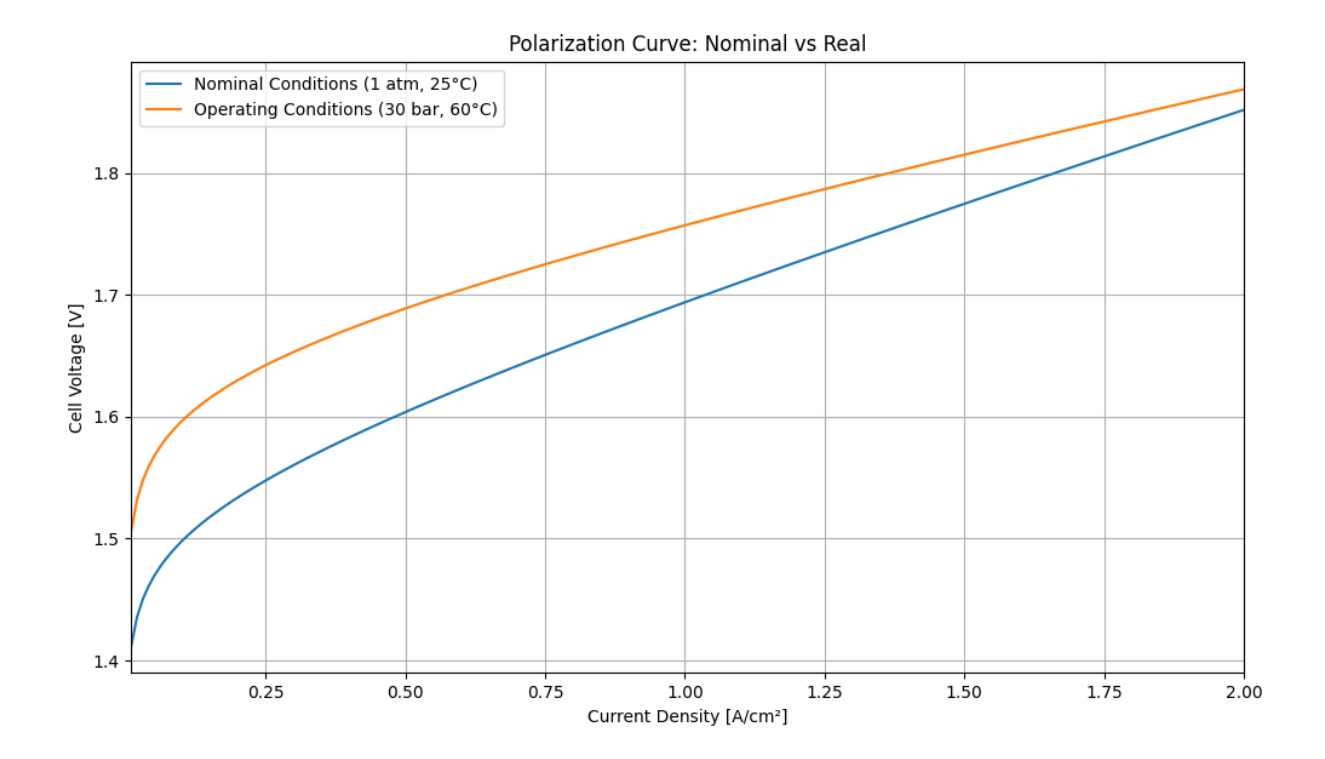


Figure 54: Polarization Curve

Cell voltage profile – The evolution of the cell voltage during operation matches the expected behavior for a commercial PEM unit. The accuracy of this result demonstrates that the model correctly captures the characteristic performance of a single PEM cell under dynamic conditions.



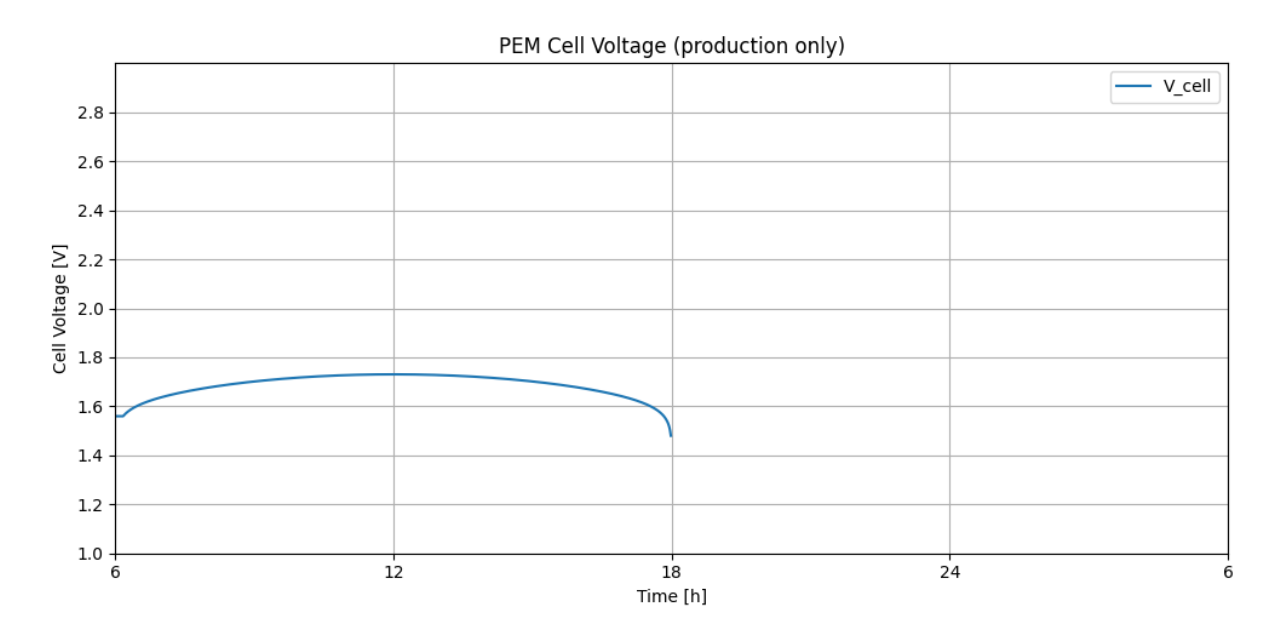


Figure 55: PEM Cell Voltage

Overall system efficiency – The global efficiency, calculated using the formulas introduced in the methodology and case study sections, reaches values close to those reported for commercial PEM electrolyzers, typically in the range of 60–70%. Such consistency with industrial benchmarks reinforces the validity of the digital twin.

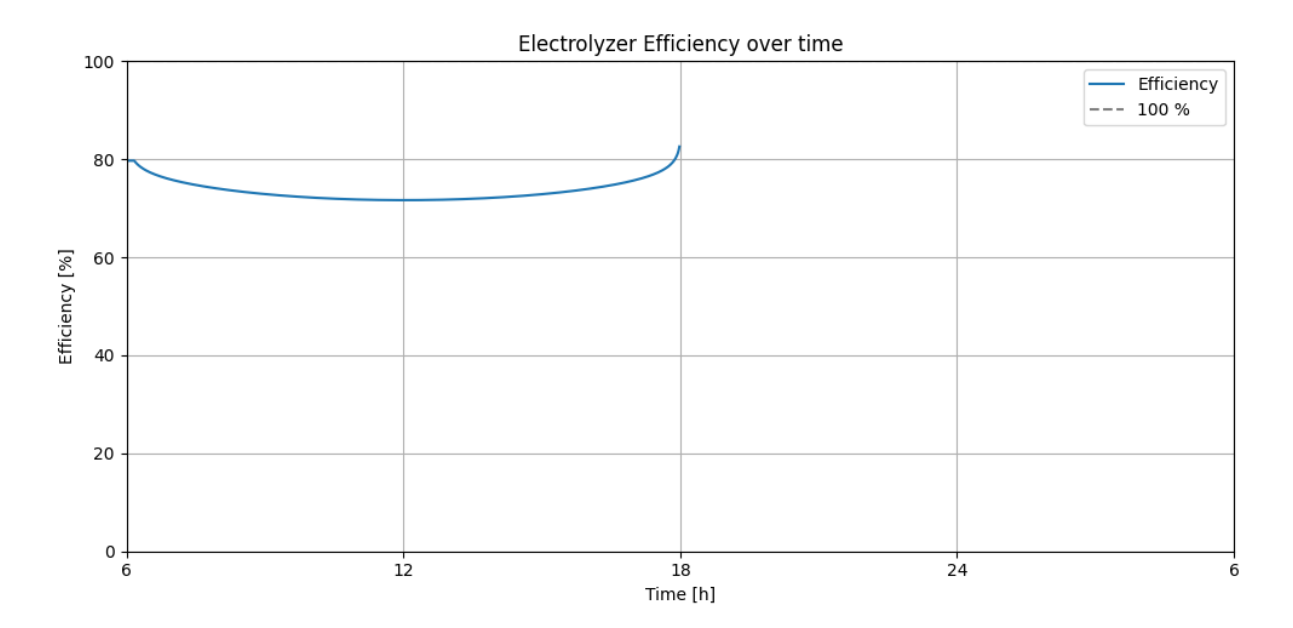


Figure 56: Electrolyzer Efficiency

Taken together, these results indicate that the model not only reproduces the expected physical behavior of the electrolyzer but also provides a credible basis for scenario analysis and technoeconomic assessments. This suggests that the digital twin can be confidently employed to inves-



tigate both operational strategies and potential improvements in future PEM-based hydrogen production systems.

Among the simulation results, it is also worthwhile to discuss the figure comparing the cumulative electrical energy absorbed by the PEM electrolyzer with both the daily electrical energy consumption and the chemical energy stored in the produced hydrogen. The latter is calculated using both the Lower Heating Value (LHV) and the Higher Heating Value (HHV) of hydrogen.

This representation offers an alternative and insightful way of visualizing the efficiency of the electrolyzer, as it directly contrasts the input electrical energy with the chemical energy embodied in the hydrogen output. In addition, the same plot highlights the cumulative hydrogen production over the simulation period, providing a clear link between energy conversion efficiency and total hydrogen yield.

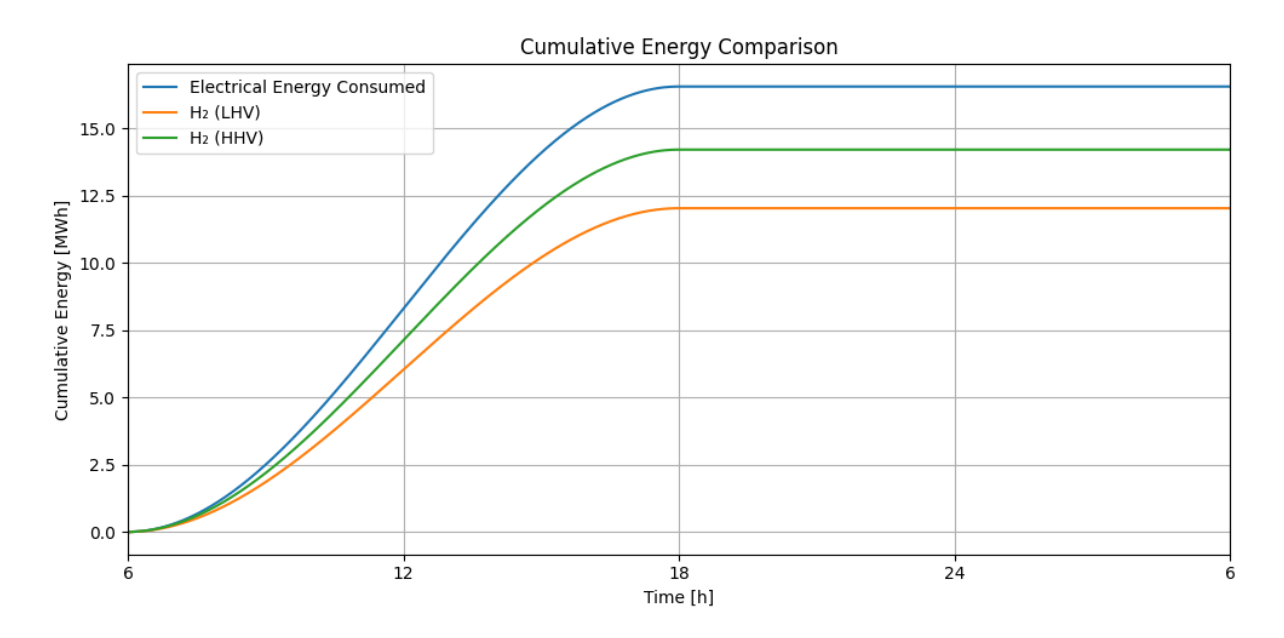


Figure 57: Cumulative Energy Comparison

The following figures describe the behavior of the storage system within the digital twin during the simulated daily cycle. In this scenario, half of the hydrogen produced by the PEM electrolyzer is consumed directly by the industrial furnace, while the remaining 50

The first graph illustrates the state of charge (SOC) of the storage system. The SOC increases gradually during the day as hydrogen is absorbed, reaching its maximum value in the late afternoon. Once charging stops, the stored hydrogen is progressively released during the night, leading to a corresponding linear decrease in SOC until it returns to zero in the early morning hours. This profile is fully consistent with the imposed operational strategy and reflects the expected dynamic balance between daytime production and nighttime release.



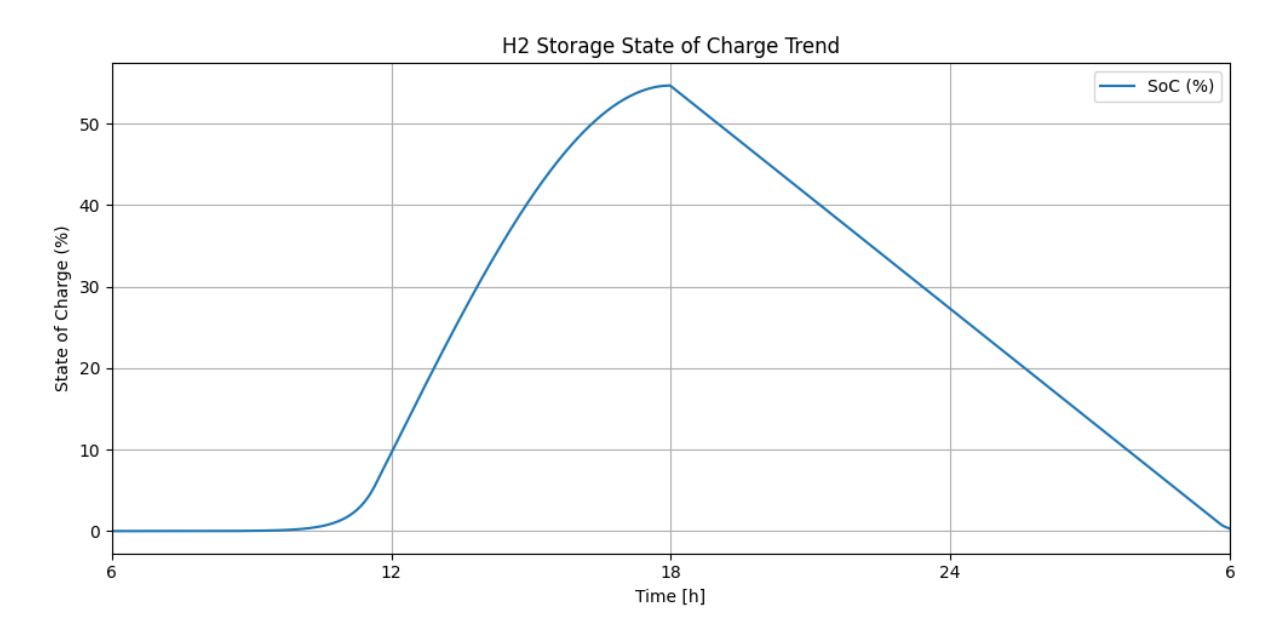


Figure 58: H2 Storage State of the Charge

The second figure presents the cumulative hydrogen quantity stored in kilograms, which follows the same trend as the SOC, confirming the direct correlation between the absorbed hydrogen and the storage level. The peak value corresponds to approximately half of the daily hydrogen production, in line with the initial assumption that the remaining half is directly consumed.

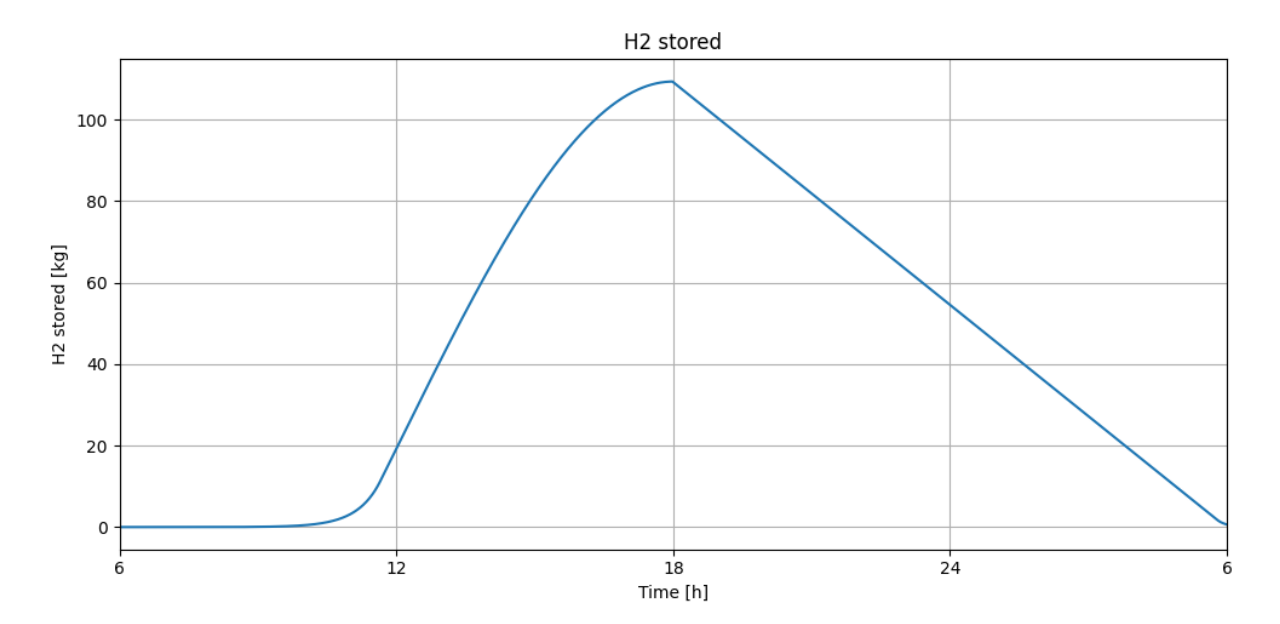


Figure 59: H2 Stored

Finally, the third plot shows the temperature evolution of the storage tank. During the charging phase, the absorption of hydrogen leads to a slight cooling effect, which is physically consistent with the endothermic nature of the process. Conversely, during the discharging phase at night,



the tank exhibits a marked temperature rise, stabilizing at a higher level as hydrogen is released. This thermal behavior highlights the importance of effective thermal management in storage systems, since temperature strongly influences both absorption and desorption rates.

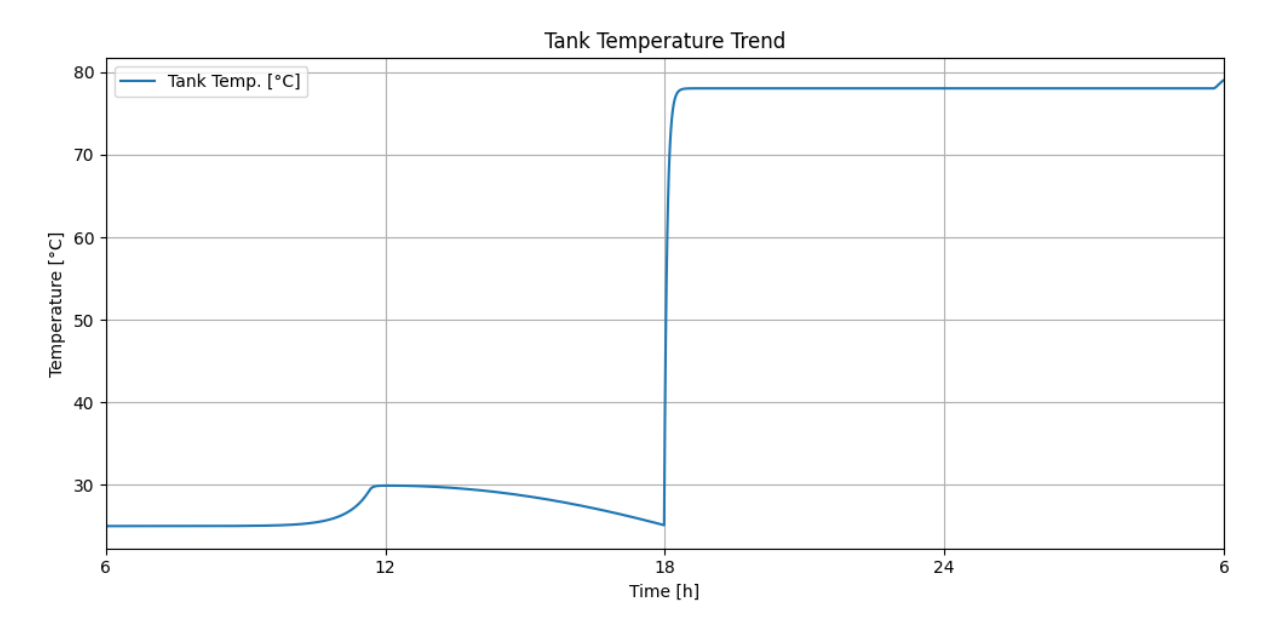


Figure 60: Tank Temperature

7.2 Yearly Simulation

Overall, these results confirm that the storage module not only reproduces the expected physical trends but also provides valuable insights into the daily interaction between hydrogen production, direct consumption, and storage dynamics. The combined analysis of SOC, stored mass, and temperature offers a comprehensive picture of how the storage system can support the continuous supply of hydrogen in applications where demand extends beyond the hours of solar production.



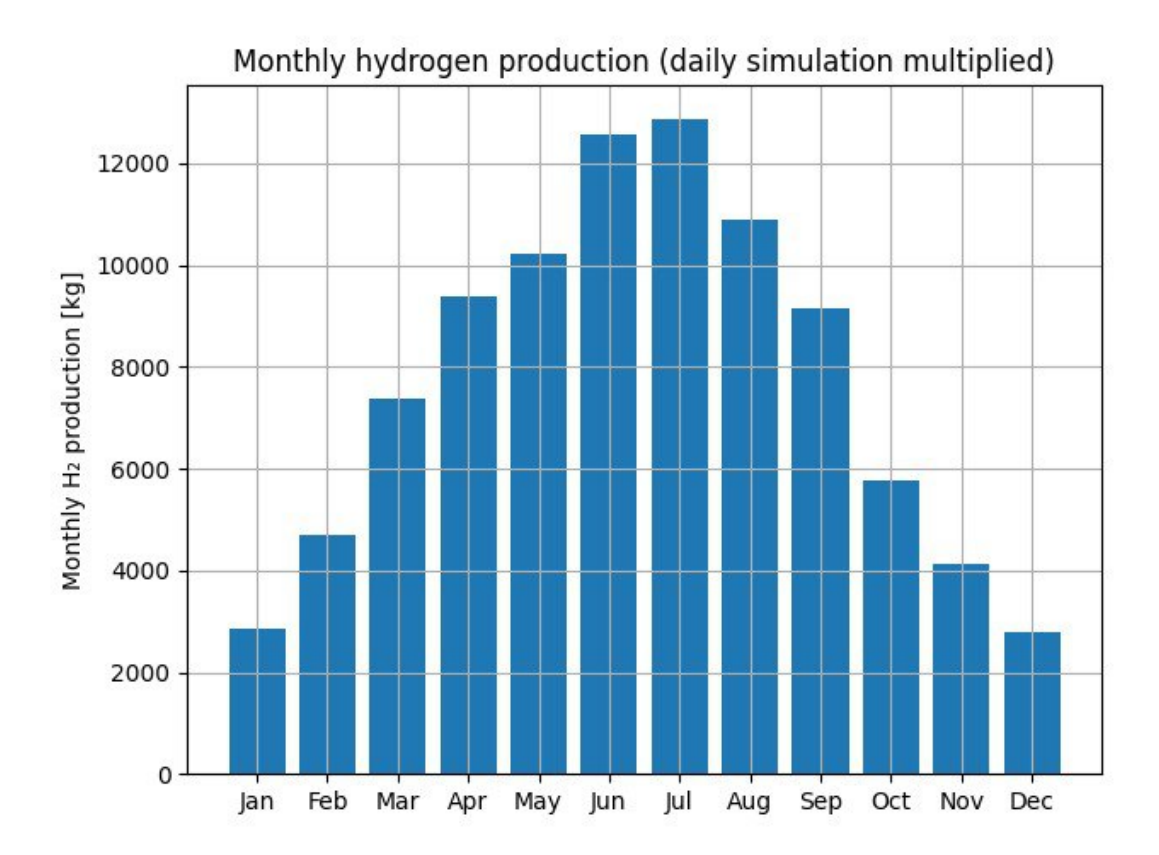


Figure 61: Monthly Hydrogen production

7.3 Lifetime Simulation Results

Using the same simulation approach, the lifetime savings in methane consumption were calculated, assuming that the hydrogen produced by the system is directly supplied to the industrial furnace. From this calculation, it was also possible to determine the corresponding reduction in CO emissions.

The results indicate that over the plant's operational lifetime, approximately 6.83 million cubic meters of methane would be displaced, leading to a cumulative avoidance of nearly 13,833 tonnes of CO2. When normalized by the photovoltaic (PV) surface area, the avoided emissions correspond to about 692 kg of CO2 per square meter of PV panel.

It is worth noting that, although inter-annual variations in both irradiance and temperature naturally occur, the seasonality of the solar resource is essentially annual rather than multi-annual. An analysis of the past 25 years shows no significant long-term trends in irradiance or temperature that would affect hydrogen production on the scale of the system considered.

This indicator is particularly meaningful, as it highlights the central role of the PV field as the system's primary bottleneck. In fact, under the present configuration, the electrolyzer produces only about one-third of the hydrogen it would be capable of generating if supplied continuously with electricity. Consequently, the scalability and effectiveness of the system are strongly tied to the availability and expansion of solar resources.



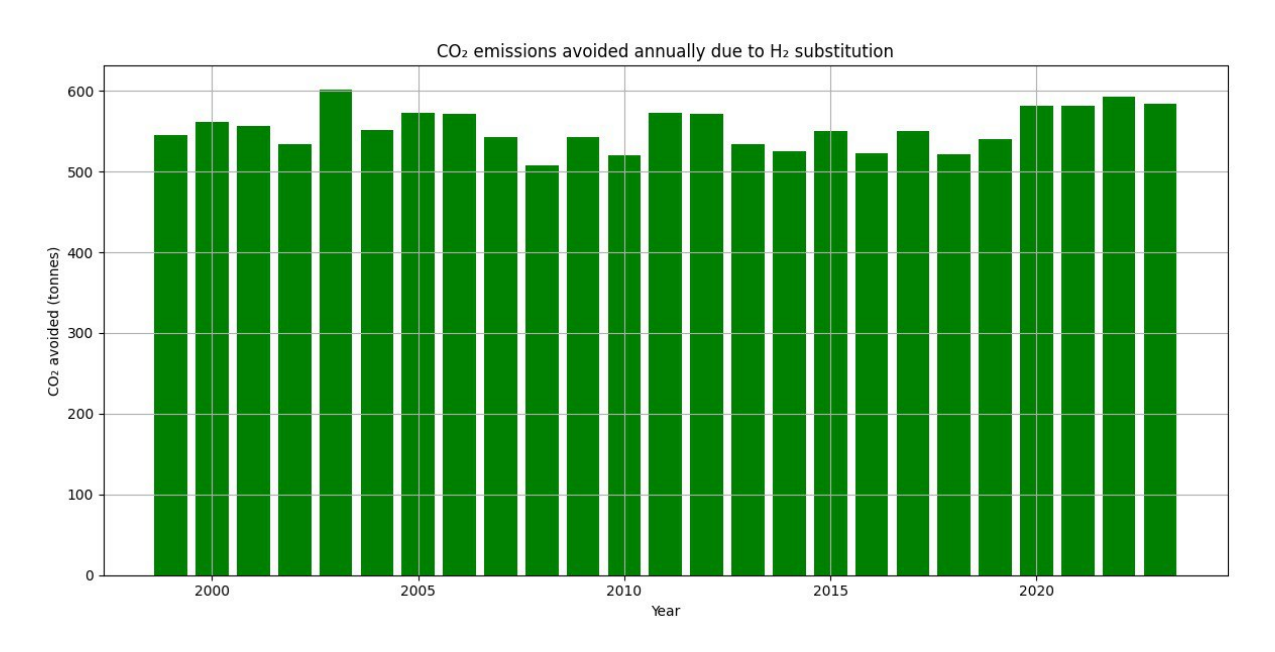


Figure 62: CO2 emissione avoided annually

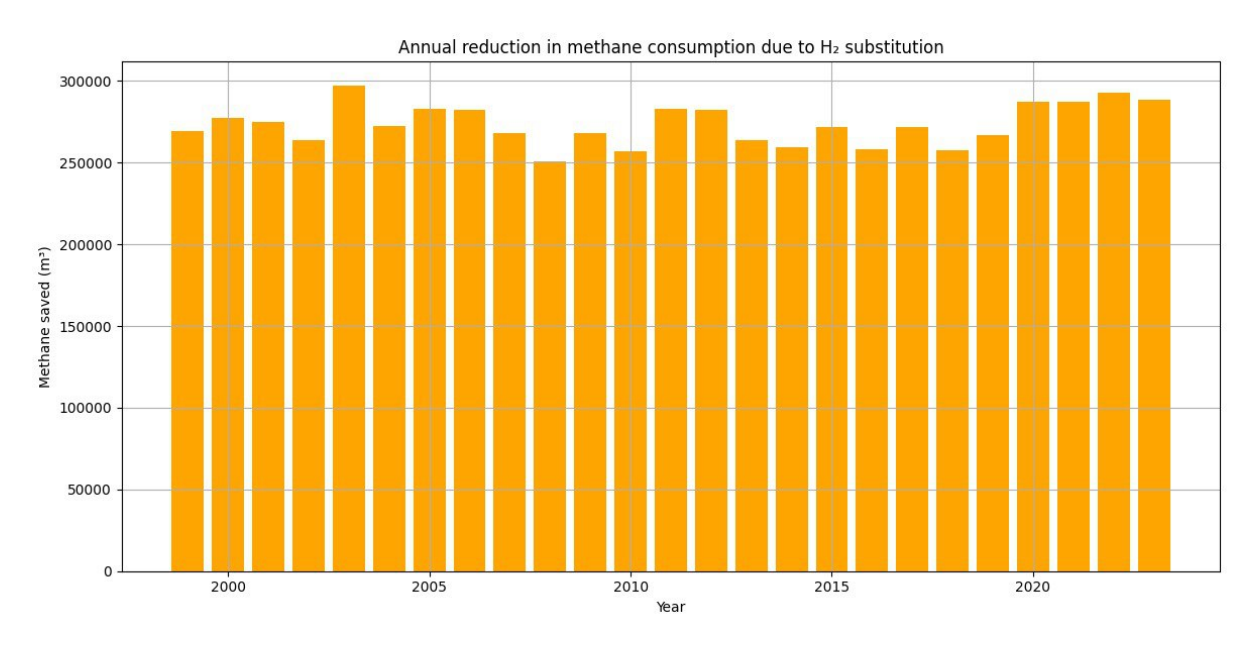


Figure 63: Annual reduction in methane consumption



7.4 Economic Results

The final set of figures to be discussed are arguably the most relevant, as they address the cost analysis of the system. As previously explained, the assessment was carried out under different market and technological scenarios (natural gas prices ranging from &0.40 to &2.00 per m³; hydrogen market prices of &4.00, &6.00, and &8.00 per kg; and projected CAPEX/OPEX values for PV and PEM technologies in 2025, 2030, and 2050).

It is important to emphasize once again that, for both the annual and lifetime simulations, the storage component was not included in the cost analysis. The reason is the lack of reliable economic data for large-scale metal hydride storage systems, which remain at a pre-commercial stage of development. For this reason, and in order to keep the analysis realistic and robust, the storage module was deliberately excluded.

This was made possible thanks to the object-oriented structure of the simulation framework, which allows individual components to be easily decoupled from the system. Such flexibility ensures that the results remain as reliable and representative as possible of an actual industrial deployment. Indeed, this modeling choice is fully aligned with the real-world case of the Zignago Vetro H Glass project, where the electrolyzer will be directly connected to the industrial furnace without large-scale hydrogen storage.

7.5 Economic Analysis of Scenarios

The economic feasibility of the PtX system is assessed through levelized cost indicators, namely the Levelized Cost of Electricity (LCOE) for the photovoltaic subsystem and the Levelized Cost of Hydrogen (LCOH) for the integrated PV-PEM plant. These parameters normalize the total discounted cost of the investment over its expected lifetime against the cumulative useful energy output. They are widely adopted in techno-economic assessments as they allow a direct comparison between different technologies and scenarios.

We can repeat here that the general expression for the Levelized Cost of Electricity is:

$$LCOE = \frac{NPC_{PV}}{\sum_{t=1}^{N} \frac{E_t}{(1+r)^t}},$$
(64)

where NPC_{PV} is the net present cost of the photovoltaic system (CAPEX, OPEX, and possible replacements), E_t the electricity produced in year t, r the discount rate, and N the plant lifetime.

Similarly, as wrote before the Levelized Cost of Hydrogen is expressed as:

$$LCOH = \frac{NPC_{PV+PEM}}{\sum_{t=1}^{N} H_{2,t}},$$
(65)

where NPC_{PV+PEM} is the net present cost of the coupled PV and electrolyzer system, and $H_{2,t}$ the annual hydrogen production (kg).



These formulations ensure that both metrics incorporate time-value-of-money effects and capture the impact of CAPEX/OPEX trajectories on the final unitary cost of energy and hydrogen.

For the discounted cash flow analysis, two sets of market scenarios were considered: (i) natural gas price evolution, which determines the economic value of avoided methane consumption; (ii) hydrogen selling price, which represents revenues in case of direct market integration.

Table 25: Scenario inputs for DCF under varying natural gas price, including CAPEX and OPEX for PV and PEM.

Year	PV CAPEX [€/kW]	PEM CAPEX [€/kW]	$\begin{array}{c} \textbf{OPEX} \\ [\texttt{C}/\text{kW}\cdot\text{yr} + \%\text{CAPEX}] \end{array}$	NG price [€/m³]
2025	1200	1500	$24 + 3\% \ 24 + 3\% \ 24 + 2\%$	0.40
2030	1000	1000		0.40
2050	600	800		0.40
2025	1200	1500	$egin{array}{l} 24 + 3\% \ 24 + 3\% \ 24 + 2\% \end{array}$	0.80
2030	1000	1000		0.80
2050	600	800		0.80
2025	1200	1500	$egin{array}{l} 24 \ + \ 3\% \ 24 \ + \ 2\% \end{array}$	1.20
2030	1000	1000		1.20
2050	600	800		1.20
2025	1200	1500	$24 + 3\% \ 24 + 3\% \ 24 + 2\%$	2.00
2030	1000	1000		2.00
2050	600	800		2.00

Note: PV CAPEX, PEM CAPEX, and OPEX values are scenario assumptions; storage excluded.

Note: PV CAPEX, PEM CAPEX, and OPEX values are scenario assumptions; storage excluded.

Table 26: Scenario inputs for DCF under varying hydrogen selling price, including CAPEX and OPEX for PV and PEM.

Year	PV CAPEX [€/kW]	PEM CAPEX [€/kW]	OPEX [€/kW·yr + %CAPEX]	$egin{array}{c} \mathbf{H_2 \ price} \ [rac{1}{3}] \end{array}$
2025	1200	1500	$24 + 3\% \ 24 + 3\% \ 24 + 2\%$	4
2030	1000	1000		4
2050	600	800		4
2025	1200	1500	$egin{array}{l} 24 + 3\% \ 24 + 3\% \ 24 + 2\% \end{array}$	6
2030	1000	1000		6
2050	600	800		6
2025	1200	1500	$24 + 3\% \ 24 + 3\% \ 24 + 2\%$	8
2030	1000	1000		8
2050	600	800		8

Note: PV CAPEX, PEM CAPEX, and OPEX values are scenario assumptions; storage excluded.

Results: LCOE and LCOH

The following tables summarize the modeled values of LCOE and LCOH for the three technology scenarios.



TD 11 07	7 / T 1 1 1	TOOIL		1 1 1 .	•
Table 27:	Modeled	LCOH	across	technology	scenarios.

Scenario Year	LCOH [€/kg]	Trend
2025	≈ 5.5	Upper bound of current expectations
2030	≈ 4.3	Improved competitiveness
2050	3.0	Competitive with fossil alternatives

Discussion. The results clearly indicate a strong downward trajectory for both LCOE and LCOH. In particular, the LCOE of photovoltaic energy decreases from about €120/MWh in 2025 to €73/MWh in 2050, while the modeled LCOH drops from €5.5/kg to just above €3/kg in the same period. These trends confirm the crucial role of technological learning curves and cost reductions in driving the competitiveness of green hydrogen. Moreover, they highlight that the economic feasibility of large-scale hydrogen production is strongly dependent on future CAPEX/OPEX trajectories of both PV and PEM technologies.

The first graph that we analize in this section is the Levelized Cost of Electricity (LCOE) shows a clear decreasing trend across the three time horizons. In 2025, the LCOE is close to $\mathfrak{C}120/\mathrm{MWh}$, reflecting the still relatively high CAPEX values for PV installations. By 2030, this cost drops to around $\mathfrak{C}105/\mathrm{MWh}$, driven by expected technological learning curves and cost reductions in photovoltaic components. The most significant improvement is observed in 2050, with the LCOE reaching nearly $\mathfrak{C}73/\mathrm{MWh}$, which is consistent with long-term projections for mature renewable technologies. This steady decline confirms that PV electricity costs will play an increasingly favorable role in reducing the overall cost of hydrogen production.

Table 28: Modeled LCOE across technology scenarios.

Scenario Year	LCOE [€/MWh]	Trend
2025	≈ 120	High CAPEX, early stage PV
2030	≈ 105	Learning curve reduction
2050	≈ 73	Mature renewable technology

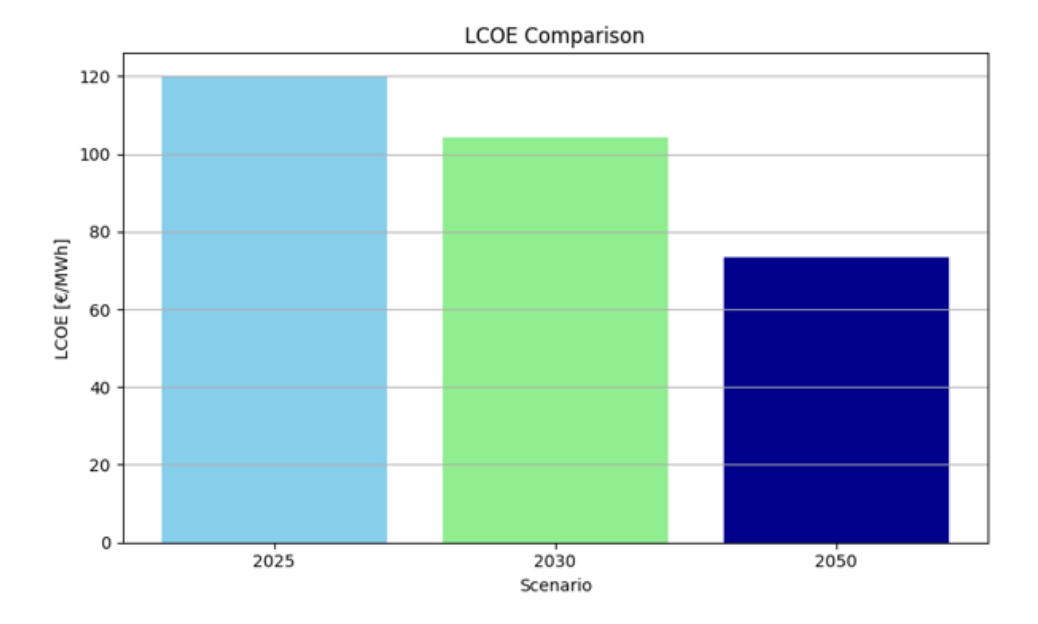


Figure 64: Levelized Cost of Electricity (LCOE)



The Levelized Cost of Hydrogen (LCOH) also follows a pronounced downward trajectory. In 2025, the modeled cost of hydrogen is about $\mathfrak{C}5.5$ per kilogram, which places it at the upper bound of current market price expectations. By 2030, the value decreases to roughly $\mathfrak{C}4.3/\mathrm{kg}$, marking a substantial improvement due to both declining electricity costs and reduced PEM electrolyzer CAPEX. The lowest value is reached in 2050, at just above $\mathfrak{C}3/\mathrm{kg}$, which would make green hydrogen cost-competitive with fossil-based alternatives in many industrial applications. This result highlights the strong impact of future technological progress and cost reductions on the economic viability of hydrogen as a large-scale energy carrier.

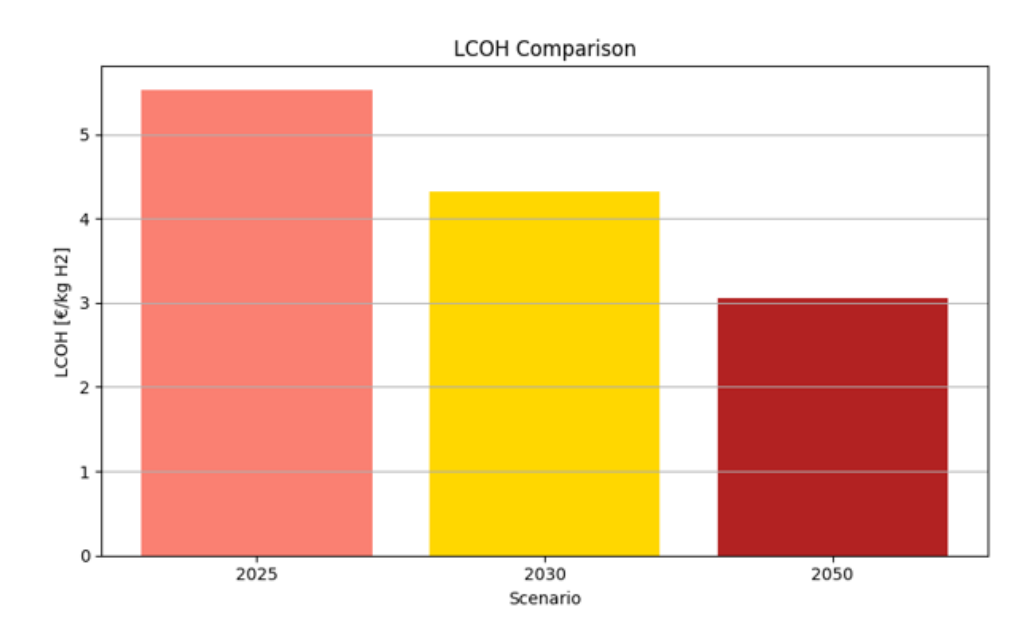


Figure 65: Levelized Cost of Hydrogen (LCOH)

The discounted cash flow analysis clearly highlights the strong dependence of project profitability on the assumed natural gas price and on the selected technological scenario. At the lowest gas price of $€0.40/\text{m}^3$, all three scenarios (2025, 2030, and 2050) remain consistently negative over the entire 25-year horizon, meaning that under such market conditions the investment cannot be recovered. When the price increases to $€0.80/\text{m}^3$, the trajectories improve, particularly for the 2050 scenario, which approaches break-even but still does not cross into positive values.

A significant change occurs at $\textcircled{-}1.20/\text{m}^3$, where the 2050 case nearly reaches cash-back within the plant lifetime, while the 2030 case shows reduced losses compared to 2025. Finally, at the highest natural gas price assumption of $\textcircled{-}2.00/\text{m}^3$, both the 2050 and 2030 scenarios achieve positive net present values. In particular, the 2050 case reaches break-even after approximately 8 years, while the 2030 case follows at around 19 years. The 2025 case, however, remains only marginally below zero even at this favorable market condition, highlighting the difficulty of achieving profitability under current cost structures.

Overall, these results emphasize that economic feasibility is contingent upon both future technological cost reductions and sufficiently high fossil gas prices. In other words, the combination of lower CAPEX/OPEX in future years and increasing methane prices is critical to ensure a positive business case for green hydrogen integration in industrial applications.



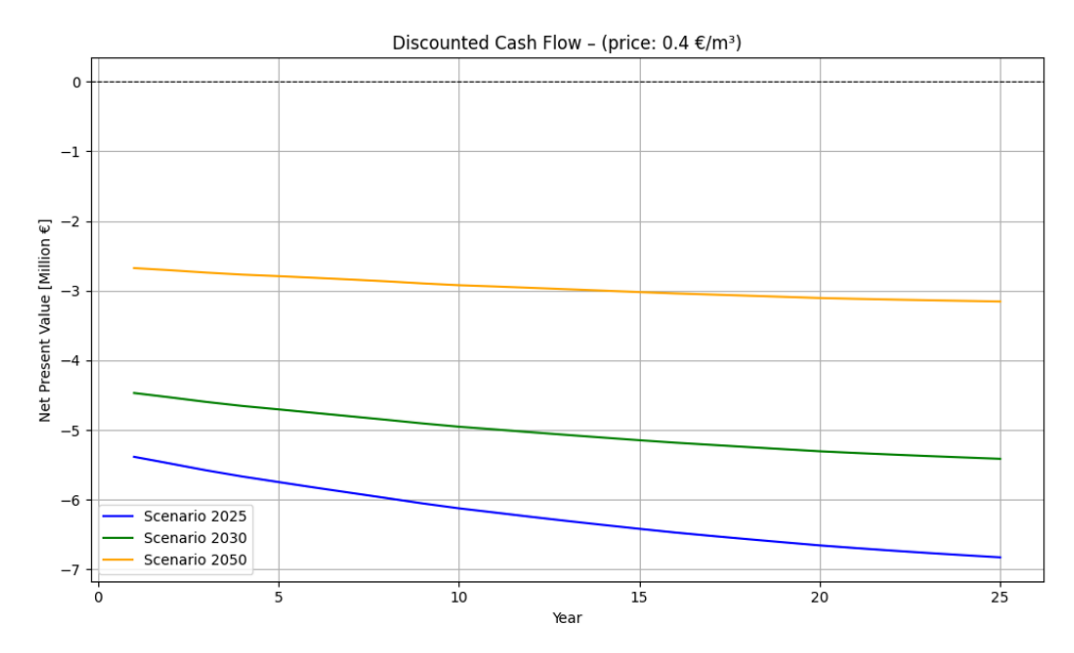


Figure 66: Discounted Cash Flow 0.4~€/m3 of CH4

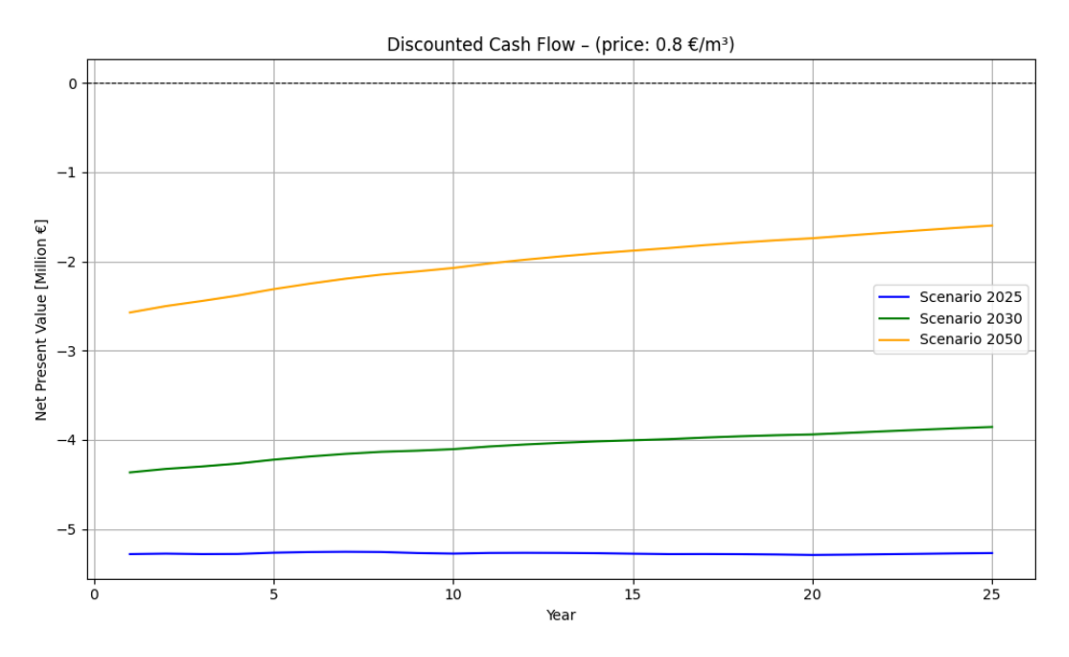


Figure 67: Discounted Cash Flow 0.8 €/m3 of CH4



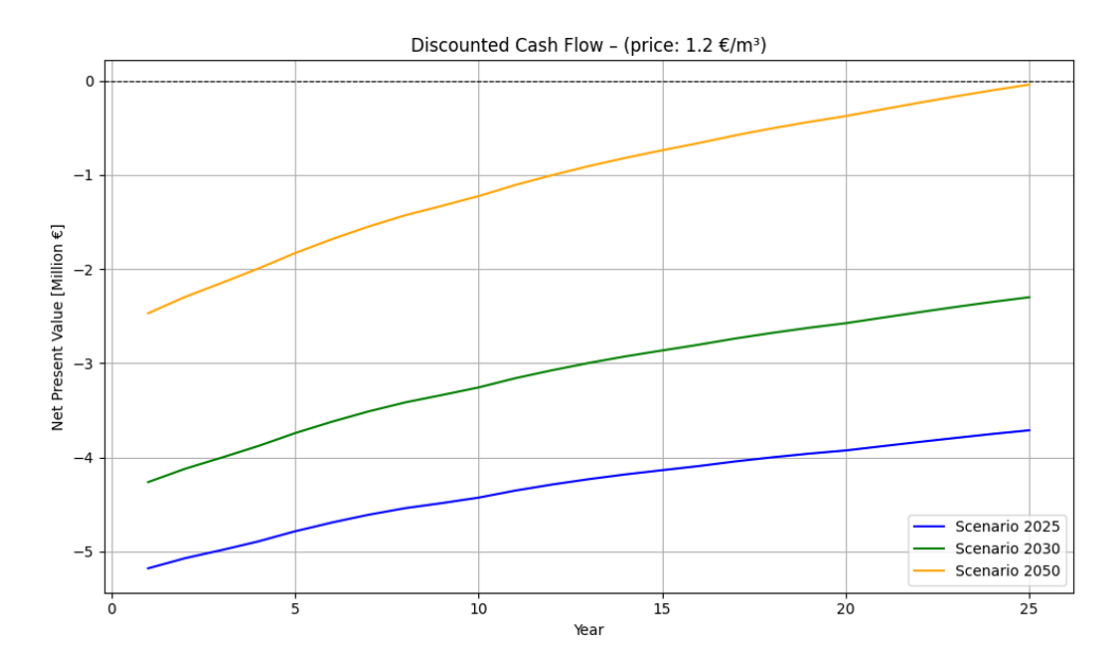


Figure 68: Discounted Cash Flow 1.2 €/m3 of CH4

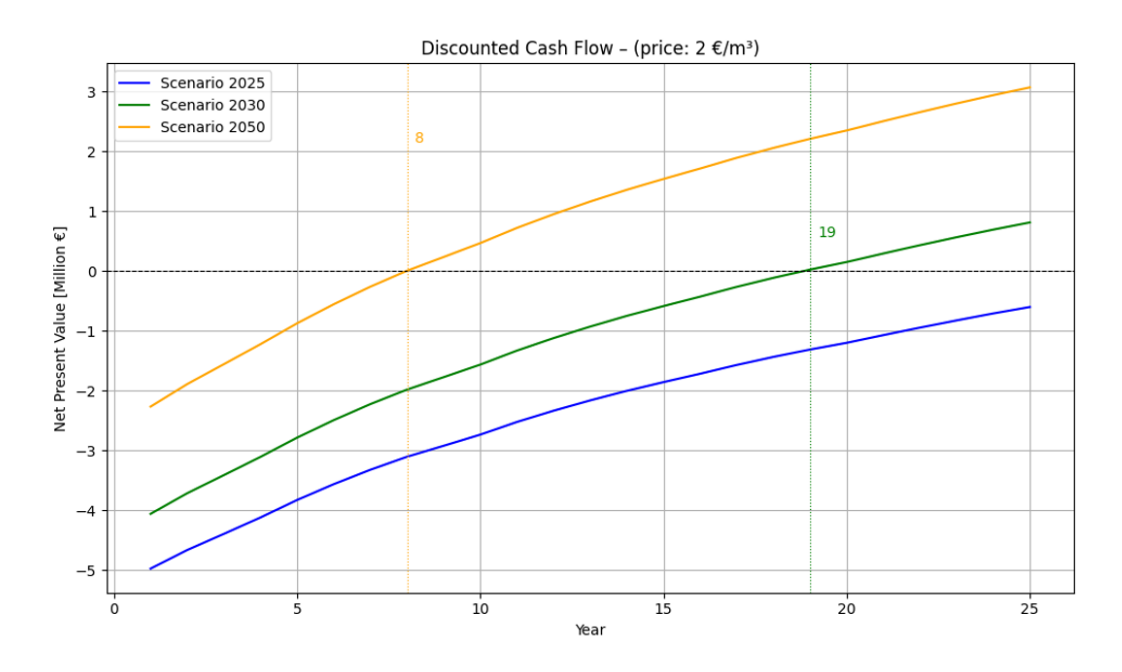


Figure 69: Discounted Cash Flow 2 €/m3 of CH4

The discounted cash flow analysis under different hydrogen sales prices provides further insights into the economic viability of the system. At the highest price assumption of $\mathfrak{C}8/\mathrm{kg}$, all three cost scenarios achieve break-even within the plant's lifetime. The 2050 cost trajectory reaches positive net present value after approximately 6 years, while the 2030 case requires about 12 years and the 2025 case around 16 years. This confirms that high hydrogen prices can ensure profitability even under current or near-term cost structures, although with different payback periods.

At the intermediate price of €6/kg, the results become more differentiated. The 2050 scenario still reaches break-even, though later, around year 9, while the 2030 case barely achieves positive values only after about 21



years. The 2025 case, however, remains below zero throughout the entire 25-year horizon, indicating that with present-day costs hydrogen priced at $\mathfrak{C}6/\mathrm{kg}$ is insufficient to recover the investment.

At the lowest assumed price of $\mathfrak{C}4/\mathrm{kg}$, only the 2050 scenario approaches break-even, and even then only after roughly 21 years of operation. Both the 2025 and 2030 cases remain negative for the full duration, showing that under such market conditions hydrogen production is not economically feasible with current or mid-term technology costs.

Overall, these results demonstrate that economic viability depends strongly on both technological progress and market prices. In a parallel way to the natural gas substitution case, only a favorable combination of reduced CAPEX/OPEX and sufficiently high hydrogen selling price ensures a competitive business case.

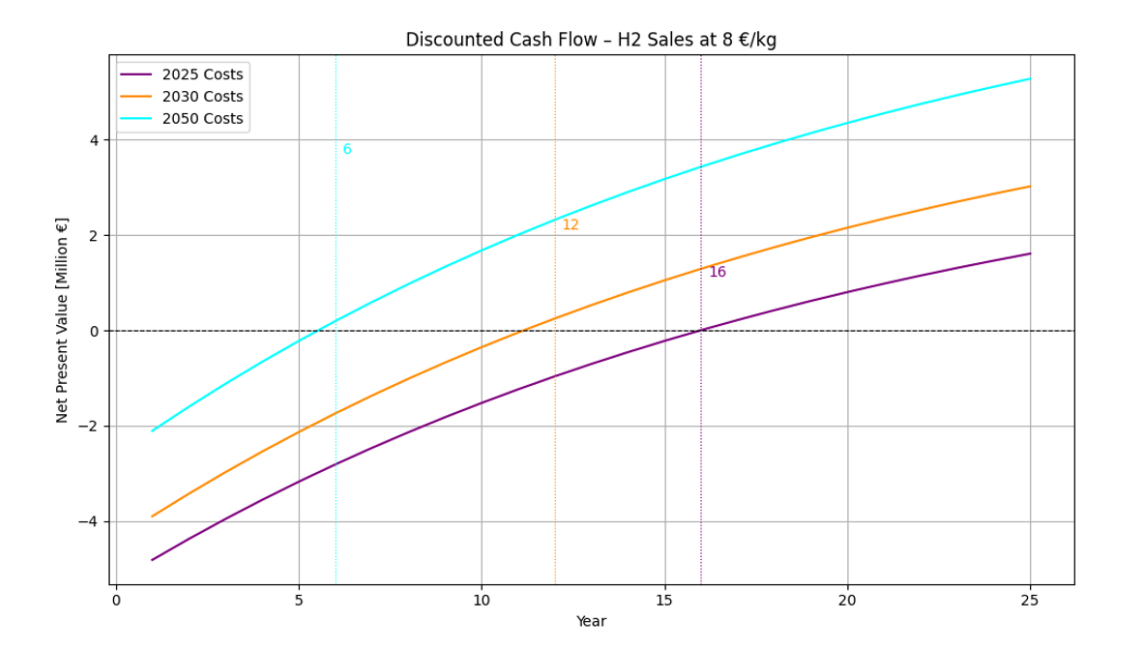


Figure 70: Discounted Cash Flow 8 €/m3 of H2



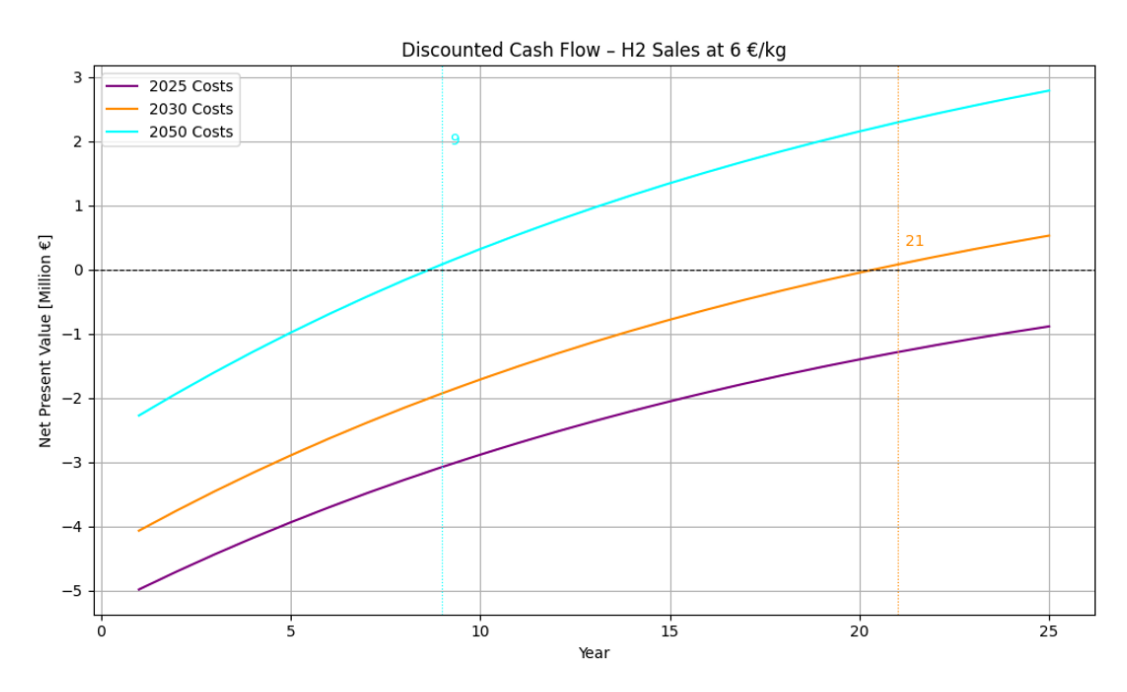


Figure 71: Discounted Cash Flow 6 €/m3 of H2

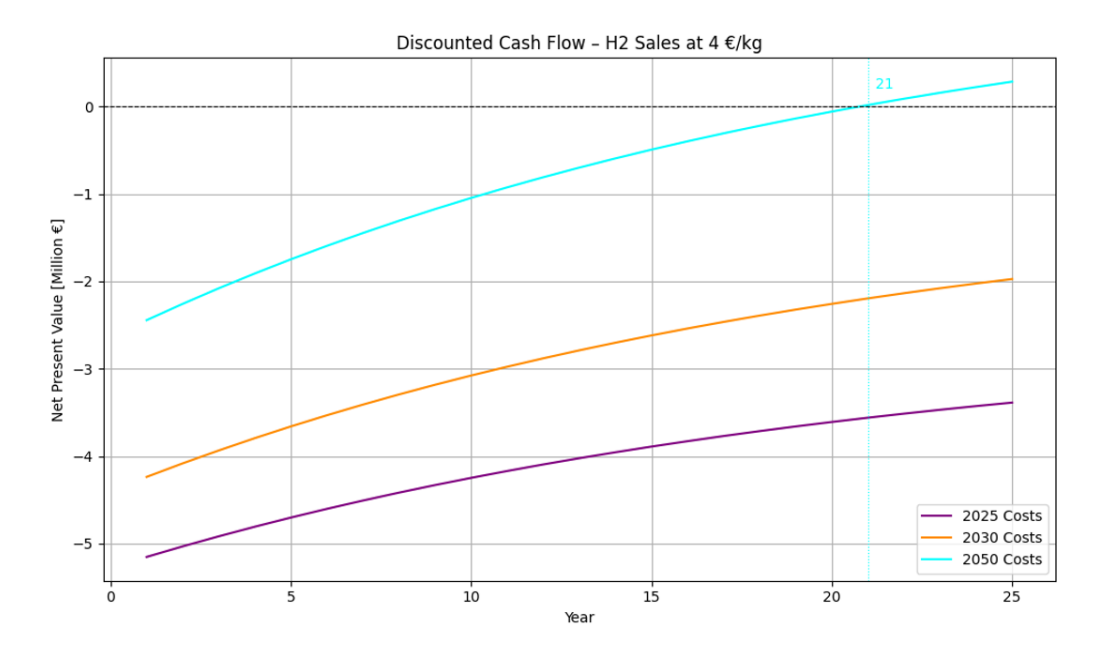


Figure 72: Discounted Cash Flow 4 €/m3 of H2



8 Conclusion 106

8 Conclusion

The objective of this thesis was to carry out a comprehensive techno-economic analysis of renewable energy systems integrated with PEM electrolyzers and green hydrogen storage, combining a state-of-the-art review, the development of an object-oriented computational framework, and its application to plant-scale simulations and economic assessments.

The review phase confirmed that PEM electrolyzers represent the most promising technology for this type of application, thanks to their low-temperature operation, compactness, scalability, and high technology readiness level. Their coupling with photovoltaic generation allows the production of fully renewable hydrogen with virtually zero emissions, but at the same time highlights a structural bottleneck: because solar energy is intermittent, the electrolyzer, one of the costliest components of the system, operates at a fraction of its capacity. This low utilization rate significantly penalizes economic performance, while grid connection would undermine the objective of producing 100% green hydrogen.

A major achievement of this work has been the development of two computational models in Python, both based on fixed-point iteration with temporal discretization. The first included a thermal dynamic description, which for the first time in this context enabled the transient thermal behavior of a PEM electrolyzer to be simulated. This led to the realization that thermal transients are negligible both in time and magnitude, justifying a second, simplified model at constant temperature that drastically reduces computational cost.

Another important result is the demonstration of the framework's ability to handle a large meteorological database spanning 25 years, confirming Python's suitability for data-intensive energy system analyses. The results proved the reliability of the models when compared with manufacturer datasheets and literature, with polarization curves and efficiencies consistent with reference data. On the economic side, the Levelized Cost of Hydrogen was found to decrease steadily from around $\mathfrak{C}5.5/\mathrm{kg}$ in 2025 to just above $\mathfrak{C}3/\mathrm{kg}$ in 2050, values that align with market expectations and indicate the future competitiveness of green hydrogen. Profitability, however, remains highly dependent on external factors: only in favorable conditions, such as hydrogen prices around $\mathfrak{C}8/\mathrm{kg}$ or natural gas prices near $\mathfrak{C}2/\mathrm{m}^3$, do the scenarios reach payback within the plant's lifetime, with break-even achieved after a few years in the most optimistic 2050 case, but remaining unattainable in the near term without additional support.

Beyond the economic aspects, the environmental results are particularly significant. Over its 25-year operational lifetime, the system would displace approximately 6.8 million cubic meters of methane and avoid nearly 13,800 tonnes of CO₂, corresponding to about 692 kg of CO₂ per square meter of PV panel. These figures highlight the importance of green hydrogen in decarbonizing hard-to-abate sectors such as the glass industry, one of the most polluting and least electrifiable sectors of all. The research thus demonstrates the dual role of computational modeling: as a tool for understanding technical feasibility and as a means to quantify the environmental benefits of renewable hydrogen integration. At the same time, it points out the limitations of the present work, such as the exclusion of large-scale hydrogen storage from the economic analysis due to lack of reliable data and the absence of direct experimental validation on a commercial electrolyzer. The study also confirms that under current cost conditions, green hydrogen production is not yet economically viable without public incentives or regulatory support. Looking forward, the framework developed here provides a solid foundation for extensions that incorporate industrial case studies beyond the H₂Glass project and that evaluate the role of green hydrogen in enabling deep decarbonization of energy-intensive processes. In conclusion, this thesis has shown that while technical feasibility is already well established, economic viability requires both technological progress and supportive policies, and that the deployment of hydrogen in hard-to-abate sectors can deliver substantial environmental benefits in the transition to a sustainable energy future.





9 Acknowledgments

Eccomi qui quindi, dopo cinque anni.

Ricordo perfettamente la sera prima della prima lezione: si era organizzata una festa d'autunno in tavernetta in occasione della vendemmia, una bellissima festa con tutti quelli che allora erano i miei amici più stretti.

Il giorno dopo la sveglia è suonata presto. Iniziava il Poli, nessuno sapeva davvero cosa volesse dire questo nome pesante, serio e da pronunciare quasi con un po' di rispetto e paura. Ma era solo un nome per me, che ho sempre amato in realtà le sfide e il mettermi alla prova, un nome che andava sfidato.

Il Poli è iniziato nello stesso posto dove sta finendo: a casa dei miei genitori. All'epoca perché, per il COVID, i primi mesi di lezione sono stati fatti a distanza; oggi perché sono appena tornato dall'Erasmus e con la vita che sta di nuovo per cambiare completamente e il posto che si può chiamare casa.

E quindi è proprio da loro che vorrei iniziare questi ringraziamenti.

Grazie Mamma per ciò che sei e che sei stata in questi anni, grazie per la vicinanza, le attenzioni concrete e i sacrifici che hai fatto per permettermi di fare questo percorso. Grazie per la possibilità di parlare e per l'essere stata sempre presente in ogni situazione, per avermi supportato e stimato in tutto quello che ho fatto in questi anni.

Grazie Papà per la presenza silenziosa ma attenta, per l'essere stato quel qualcuno a cui chiedere consiglio quando ne avevo bisogno e grazie per l'esempio di persona che sei, grazie per i bei momenti passati insieme e per i valori e le passioni che mi hai trasmesso.

Grazie Eli per essere qualcosa di più di una sorella, per essere un'amica, per tutto ciò che abbiamo condiviso in questi anni: i viaggi, le gite, le sciate, le serate. Sei stata davvero la sorellona di cui avevo bisogno, che mi ha sempre aperto la strada e che ho sempre seguito, come si seguono le tracce degli sci di quello davanti, come un apripista, e che continuerò a fare.

Grazie a Nonna Carla per l'amica che sei, una seconda mamma, per tutti i pranzi e i caffè in cui mi hai ascoltato e accolto in questi anni, per avermi ascoltato ripetere interi esami universitari e avermi sempre stimato e supportato in tutte le mie scelte. Sei un esempio umano incredibile. Grazie per il bene che mi vuoi e per avermi insegnato cosa vuol dire voler bene.

Il percorso di laurea è stato un viaggio bellissimo ma sicuramente anche un percorso duro e pieno di ostacoli, e senza le persone che ho incontrato come compagni di viaggio non avrei mai potuto affrontarlo, e siete proprio voi ad aver reso però così bello e ricco questo viaggio.

Ci tengo quindi a ringraziarvi uno a uno.

L'inizio del Poli è stato segnato da questa modalità online dovuta alla situazione di quel momento e questo lo ha reso ancora più duro umanamente per me e qui vanno i primi grandi grazie.

Grazie agli amici di sempre che erano già presenti a quella festa d'autunno e saranno presenti alla festa di laurea magistrale e ormai credo e spero saranno presenti per sempre nella mia vita.

Grazie Samu, siamo cresciuti insieme e stiamo diventando persone simili: questo ci unisce in una maniera unica. Grazie per tutti i momenti condivisi, per essere stato uno di quegli amici che si contano sulle dita delle mani, grazie per i momenti passati insieme a Torino, per lo studio insieme e le birre al pub, per le giornate a Villar, per esserci sempre stato ad ascoltarmi.

Grazie Buni, per essere stato quella persona con cui sono completamente me stesso, per tutte le cazzate sparate insieme e le conversazioni serie fatte con "l'amico psicologo", grazie per tutti i momenti di divertimento e di sport passati insieme, per le feste e per i viaggi. Sei sempre stato la persona in grado di strapparmi quella risata che ti alleggerisce.

Grazie Lollo, la nostra amicizia è qualcosa di speciale, grazie per tutte le passioni che condividiamo. In questo



9 Acknowledgments 108

sei la persona che io conosca più simile a me, grazie per l'esempio umano che sei per me e per i viaggi, le serate a scalare che rendevano speciale una qualsiasi sera settimanale, le sciate e le chiacchierate.

Ci sono poi quegli amici che ormai è come se ci fossero da sempre, con cui il percorso è iniziato alle superiori ed è continuato insieme anche all'università.

Grazie Andre per essere stato il compagno di viaggio e di studi ormai da dieci anni. Abbiamo condiviso tanti momenti, grazie per le giornate a studiare insieme in biblioteca e le serate distensive, grazie per essere quella persona a cui va sempre uno sguardo quando devo prendere una decisione, per la stima che provo per te.

Grazie Agnese, come dire... questo grazie è forse uno dei più grandi di tutti, uno forse non basta nemmeno. Sei davvero un'amica speciale e incredibile, grazie per il supporto che mi hai dato durante il primo anno del Poli, per le giornate a casa tua, i pranzi e lo studio insieme. Un pezzettino di questa laurea è sicuramente dovuto anche a te, grazie per quel messaggio che non ti aspetti ma che ormai arriva sempre: "Careee come stai?". Grazie per il bene sincero e gratuito che mi hai voluto in questi anni. Grazie.

Grazie J per il pezzo di strada che abbiamo condiviso insieme, per le risate e i pomeriggi di studio che ormai sembrano un ricordo, grazie per i momenti di riflessione seria e per i consigli.

Grazie Ele per ciò che sei stata per me, per gli aperitivi e i caffè insieme, grazie per la tua capacità di ascoltare e la bellissima, leggera presenza nel gruppo.

Grazie a Fra Picca e Fra Morelli per tutti i momenti passati insieme, per le serate, le sciate e le cene di Natale tutti insieme.

Grazie a Pute e Samu per essere state quelle presenze centrali e cruciali nel nostro gruppo, con la vostra spinta organizzativa e attiva. Grazie per essere state quelle persone con cui ho parlato di cose serie e subito dopo riso per una stupidaggine mille volte in questi anni.

Il mio primo anno di Poli è stato, almeno come persone, un anno bonus di liceo, ma alcune cose sono sicuramente cambiate: sono iniziate le sessioni studio e il mio studiare sempre in giro con tanti amici diversi.

Grazie ai ragazzi dell'aula studio dell'oratorio San Paolo, grazie a Caso, grazie a Giulia.

Grazie a Biolly per essere un amico importantissimo con cui sono cresciuto, grazie per i campionati di calcio insieme e per le innumerevoli sessioni studio a Santo.

La mia esperienza al Poli è però davvero cambiata a metà del terzo anno, con un amico speciale, un amico tramite cui ho conosciuto quelli che sarebbero poi diventati e che sono tutt'ora tra le persone a cui tengo di più e con cui abbiamo condiviso e continuiamo a condividere tantissimo.

Grazie Rick, sei stato davvero un compagno di avventure, grazie per il tuo spirito positivo e attivo, per le mille cose organizzate insieme, per lo studio, per l'aiuto che mi hai dato nel passare gli esami più difficili, per l'attenzione e l'interesse con cui mi hai sempre cercato, per le innumerevoli notti passate sul tuo divano quando facevo avanti e indietro, per le ormai numerosissime vacanze condivise insieme e per tutte le serate al Comala a giocare a ping-pong, per le birre al pub e le chiacchierate serie sul futuro. Ho conosciuto pochissime persone come te in vita mia, Rick, grazie.

E proprio tramite Rick ho conosciuto e mi sono buttato completamente, da quel momento, nel mondo Poli, di cui ho capito la bellezza e la ricchezza umana che mi ha piano piano assorbito completamente, facendomi circondare di bellissime persone.

Grazie ad Azzurra per essere stata un'amica e compagna di studio per tante giornate, per i tuoi preziosissimi appunti e per tutte le volte che mi hai ascoltato ripetere cose che palesemente sapevi già. Grazie per tutte le risate che ci hai fatto fare alle serate Sangria, e grazie per essere stata un pezzo importantissimo della conclusione della mia triennale.

Grazie a Matteo, grazie per l'amico che sei diventato in questi anni, per tutti i viaggi e le vacanze al mare e in montagna insieme, per le serate Sangria, per le chiacchierate serie, le grigliate e le feste a Bagnolo, per le sciate e



le giornate in montagna. Ti stimo davvero molto come persona.

Grazie a Berti, ecco, questo è un altro di quei grazie speciali. Come dici tu, ci siamo trovati davvero su tutto tranne che sulla musica, cosa che poi non è vera perché anche a te piace(va) Tedua. Sei diventato davvero una delle persone con cui ho condiviso di più in questi anni: dalle chiacchierate tornando da Monginevro, in cui viaggi di ore passavano in minuti, ai confronti su argomenti profondi e sulla vita, fino al parlare usando letteralmente solo meme e vecchi video. Condividiamo una quantità infinita di passioni e il tuo modo di alleggerire il clima, la tua presenza nel gruppo e come amico singolarmente è qualcosa di speciale e che davvero spero possa rimanere per tutta la vita. Grazie per le corse, le pedalate, le sciate e le grandi bevute insieme. Sei uno di quegli amici rari da trovare e noi ci siamo proprio trovati.

Grazie a Gigi, un'altra di quelle persone entrate troppo tardi nella mia vita, ma con cui è scattata subito quell'intesa. Grazie per il tuo modo di fare, per la serenità con cui affronti le cose e per essere stata quella voce di conforto che nello stesso tempo ti fa ridere e ti riporta alla realtà.

Grazie a Macca per tutte le cazzate sparate insieme, per quella conversazione a Mentone su Lacoste e il senso del Poli e per la serenità con cui hai vissuto tutte le cose che abbiamo condiviso in questi anni.

Grazie a Bobo per le serate e i momenti di studio serio passati insieme, per i progetti e le cene a casa tua.

Grazie a Chiara per i momenti in aula studio, le serate a casa tua, per l'attenzione in più che hai sempre portato nel gruppo e per le innumerevoli giornate al Comala.

Grazie a Mattia, che sei diventato qualcosa di speciale in questa magistrale: sei stato il compagno di banco di cazzate e di studio, ma davvero quello speciale, quello che, quando entri in aula, cerchi con lo sguardo per sederti vicino. Sei davvero una bellissima persona, grazie per l'aiuto nello studio, per i pranzi a casa tua e tutti i momenti passati a studiare e cazzeggiare insieme. Sei stato davvero tra le persone più importanti in questi due anni di magistrale, grazie.

Grazie ad Andre, grazie a Flavio, grazie a Lollo, grazie a Giulio, grazie a Davide, grazie a Gio, grazie ad Annamaria per tutti i momenti di studio e di festa condivisi insieme, per i progetti, le cene di Natale, i caffè al Mixto, per l'esempio umano che siete per me. Grazie.

In tutti questi anni di Poli ci sono state poi le passioni che mi hanno permesso di condividere momenti bellissimi con amici che hanno alleggerito e allietato questo percorso.

Grazie allora a Marco, Ale, Luca, Emi e tutto il gruppo dell'Escape per le serate a scalare, le gite, le sciate e queste passioni forti condivise.

Grazie al gruppo del Bisa per l'ultimo anno passato insieme, per i martedì sera appuntamento fisso e per le pizze da Angelo.

Grazie super speciale a Corinna, quella che ora posso finalmente rivelare al mondo essere il famoso "mio contatto" che tutto il corso di Rinnovabili del mio anno conosce, grazie per l'attenzione con cui mi hai sempre trattato, per gli appunti e l'aiuto con gli esami, grazie per la persona che sei, per l'energia che trasmetti e per i valori che hai. Sei stata quell'esempio poco più grande che fa un percorso simile, di cui tutti avremmo bisogno e che per me è stato davvero una guida da seguire su molte cose, un passetto alla volta.

Grazie a tutto il gruppo degli Alpolizzati per essere stati quegli amici con cui ci si può sempre divertire, per avermi insegnato la bellezza rara di avere amici di tutte le parti d'Italia come voi, per tutte le serate insieme, per i Comala e i calcetti, per la semplicità e la profondità contemporanee con cui vivete.

Grazie quindi uno a uno a Lucilla, a Pietro, a Federica, a Pen, a Luca e a tutti gli altri.

Infine, vorrei ringraziare le persone che sono state parte di quest'ultimo e incredibile anno, che ha coronato molto bene il mio percorso al Poli.

Il primo è uno dei grazie più importanti.



Grazie a Chiara, per essere stata la persona di cui avevo bisogno, per aver fatto questo incredibile lungo viaggio a Barcellona insieme, per essere stata carica e gasata come me dal primo all'ultimo giorno, per essere stata quella spalla emotiva e pratica che ha reso tutto possibile. Grazie per le mille avventure e per le chiacchierate alla scrivania, per le serate e i viaggi: sei stata una parte centrale del mio Erasmus.

Grazie a Fabienne per essere stata quella sorpresa che non ti aspetti di incontrare, per avermi insegnato per la prima volta che la lingua non è un ostacolo nelle relazioni umane. Ricorderò per tutta la vita quella birra. Sei una persona splendida, umanamente la tua capacità di interessarti all'altra persona e curarti dell'altro è una qualità bellissima e unica. Grazie per le deep conversations, i pranzi e le cene insieme, le risate e le giornate al mare, grazie per avermi insegnato davvero che siamo tutti europei. La tua storia di vita e il tuo carattere sono un grande esempio per me.

Grazie a Emma per essere stata un'amica vera in un caos come Barcellona, per i caffè condivisi e per avermi insegnato che l'amicizia non ha confini di lingua o nazione, ma che, se si è persone simili, la cultura non esiste.

Grazie a Hagen per essere stato il "bro" di cui avevo bisogno, per gli allenamenti, le serate e i viaggi passati insieme, per le conversazioni e per, insieme a tutti gli altri, aver aperto il mio punto di vista sull'Europa e sul mondo

Grazie a Pietro, Elena, Roberta, Adelina, Javi, Alessandro, Marta, Moritz, Leo, Delfina, a Lucas e Luna, ai ragazzi del Beach Volley per essere stati la mia Erasmus. Siete persone splendide, super interessanti, e le vostre storie sono tutte per me incredibili e di esempio. Siete stati voi davvero il senso di questa avventura.

Grazie a Giorgia e Ludovica per essere state quelle amiche che ti fanno sentire a casa anche lontano da casa, per le cene insieme, per il corso di vela, per le serate e le chiacchierate, per avermi fatto sentire accolto ed essere state un po' delle guide nel percorso all'estero.

Gli ultimi grazie vanno alle persone che hanno concretamente reso possibile tutto questo.

Un enorme grazie va a Lorenzo, grazie per averci accolto e trattato come si fa con degli amici prima che con dei colleghi. Sei una persona splendida, sei per me un grande esempio professionale e umano, sei stato molto più di un supervisor, sei stato un amico. Mi ritengo fortunatissimo ad averti incontrato nel mio percorso. Sei stato una guida e un esempio in questi mesi a Barcellona e un grande supporto per la tesi. Grazie davvero.

Un grazie conclusivo va alla professoressa Gandiglio che ha reso tutto questo possibile, per la professionalità e la cura con cui ha seguito tutto il processo, anche se da distante, per l'attenzione alla persona e alla riuscita del progetto.

È stato un percorso faticoso e bello, ricco di ostacoli e grandi soddisfazioni. A livello professionale, ad ora è la soddisfazione più grande che abbia mai raggiunto, ma come in tutte le cose il senso io l'ho trovato negli incontri con le persone e nelle relazioni umane.

Grazie.



111 Bibliography

Bibliography

[1] S. Shiva Kumar and V. Himabindu, "Hydrogen production by pem water electrolysis – a review," *Materials Science for Energy Technologies*, vol. 2, no. 3, pp. 442–454, 2019.

- [2] U.S. Department of Energy, "Hydrogen production: Thermochemical water splitting," 2025.
- [3] L. S. Frowijn and W. G. van Sark, "Analysis of photon-driven solar-to-hydrogen production methods in the netherlands," Sustainable Energy Technologies and Assessments, vol. 48, p. 101631, 2021.
- [4] S. Shiva Kumar and H. Lim, "An overview of water electrolysis technologies for green hydrogen production," *Energy Reports*, vol. 8, pp. 13793–13813, 2022.
- [5] H. V. Ghadim, R. Canessa, J. Haas, and R. Peer, "Electrolyzer cost projections compared to actual market costs: A critical analysis," in 2023 IEEE PES Innovative Smart Grid Technologies - Asia (ISGT Asia), pp. 1–5, 2023.
- [6] R. Bernat, J. Milewski, O. Dybinski, A. Martsinchyk, and P. Shuhayeu, "Review of aem electrolysis research from the perspective of developing a reliable model," *Energies*, vol. 17, no. 20, 2024.
- [7] G. H. A. Wijaya, K. S. Im, and S. Y. Nam, "Advancements in commercial anion exchange membranes: A review of membrane properties in water electrolysis applications," *Desalination and Water Treatment*, vol. 320, p. 100605, 2024.
- [8] Enapter, "Aem multicore™ brochure," 2021.
- [9] M. J. Palys and P. Daoutidis, "Power-to-x: A review and perspective," Computers & Chemical Engineering, vol. 165, p. 107948, 2022.
- [10] I. R. E. Agency, "Green hydrogen cost reduction: The potential of green hydrogen to reduce costs and accelerate the energy transition," tech. rep., International Renewable Energy Agency (IRENA), 2020.
- [11] X. Wei, S. Sharma, A. Waeber, D. Wen, S. N. Sampathkumar, M. Margni, F. Maréchal, and J. Van herle, "Comparative life cycle analysis of electrolyzer technologies for hydrogen production: Manufacturing and operations," *Joule*, vol. 8, no. 12, pp. 3347–3372, 2024.
- [12] J. Abe, A. Popoola, E. Ajenifuja, and O. Popoola, "Hydrogen energy, economy and storage: Review and recommendation," *International Journal of Hydrogen Energy*, vol. 44, no. 29, pp. 15072–15086, 2019.
- [13] N. Klopčič, I. Grimmer, F. Winkler, M. Sartory, and A. Trattner, "A review on metal hydride materials for hydrogen storage," *Journal of Energy Storage*, vol. 72, p. 108456, 2023.
- [14] A. B. Santisteban, "Modeling and analysis of an electrolyser for power to gas applications," master's thesis, Escola Tècnica Superior d'Enginyeria Industrial de Barcelona, Universitat Politècnica de Catalunya, Barcelona, Spain, July 2022. Supervisors: Oriol Gomis-Bellmunt, Saman Dadjo Tavakoli.



```
System_parameters.py
import numpy as np
import math
```

```
# -----
# CLASSE: SystemParameters
# Gestisce tutte le costanti fisiche e i parametri dell'impianto e dello storage.
# -----
class SystemParameters:
   def __init__(self):
       # Costanti Fisiche
       self.F = 96485 # Costante di Faraday (C/mol)
       self.R = 8.314 \# Costante dei gas ideali (J/(mol·K))
       self.T = 333.15 # Temperatura di riferimento (K)
       self.deltaG = 236480 # Energia libera di Gibbs standard (J/mol)
       self.z = 2 # Numero di elettroni trasferiti
       self.E0 = self.deltaG / (self.z * self.F) # Potenziale standard di cella (V)
       # Parametri Impianto Elettrolizzatore
       self.n_cells = 215  # Numero di celle nello stack
       self.cell_area_cm2 = 85 * 85 # Area di una singola cella (cm^2)
       self.cell_area_m2 = self.cell_area_cm2 / 1e4 # Area di una singola cella (m^2)
       self.alpha_ca = 0.5  # Coefficiente di trasferimento di carica catodico
       self.alpha_an = 2  # Coefficiente di trasferimento di carica anodico
       self.iO_an = 2e-7 # Densità di corrente di scambio anodica (A/cm^2)
       self.i0_ca = 2e-3 # Densità di corrente di scambio catodica (A/cm^2)
       # PARAMETRI AGGIUSTATI PER COERENZA CON IL GRAFICO DI RIFERIMENTO
       self.t_me_cm = 0.010  # Spessore della membrana elettrolitica (cm) - Modificato da 0.025
       self.lambda_m = 16  # Conduttività protonica (S/cm) - Modificato da 14
       self.t_me_m = self.t_me_cm / 100 # Spessore della membrana elettrolitica (m)
       # Calcolo conduttività e resistenza della membrana
       # La conduttività dipende dalla temperatura (T)
       sigma_m_cm_calc = (0.005139 * self.lambda_m - 0.00326) * np.exp(1268 * (1 / 303 - 1 / self.T))
       self.sigma_m_cm = max(sigma_m_cm_calc, 1e-6) # Assicura un valore minimo
       self.sigma_m = self.sigma_m_cm * 1e2 # Conversione a S/m
       self.R_ohm = self.t_me_m / self.sigma_m # Resistenza ohmica della membrana (ohm·m^2)
       # Potere calorifico dell'idrogeno
       self.LHV_H2 = 119900000 # Potere calorifico inferiore dell'idrogeno (J/kg)
       self.HHV_H2 = 141600000 # Potere calorifico superiore dell'idrogeno (J/kg)
       # Pressioni (costanti nel tempo)
       self.P_H2Oan = 101325 # Pressione dell'acqua all'anodo (Pa)
       self.P_H2Oca = 101325 # Pressione dell'acqua al catodo (Pa)
       self.P_H2 = 30e5 # Pressione dell'idrogeno in uscita (Pa, 30 bar)
       self.P_02 = 30e5 # Pressione dell'ossigeno in uscita (Pa, 30 bar)
       # Parametri Storage
       self.M_H2 = 2.016 \# Massa molare H2 (g/mol)
       self.R_gas = 8.314  # Costante dei gas ideali (J/(mol·K)) - duplicato con R, ma per chiarezza
       self.elementi = {  # Proprietà degli elementi per l'idruro metallico
           'Ti': {'densita': 4.5, 'peso_atomico': 47.87, 'cp': 523},
           'Fe': {'densita': 7.87, 'peso_atomico': 55.85, 'cp': 449},
```



```
'Mn': {'densita': 7.2, 'peso_atomico': 54.94, 'cp': 479}
       self.composizione = {'Ti': 1, 'Fe': 0.85, 'Mn': 0.05} # Composizione dell'idruro metallico
       self.porosita = 0.3 # Porosità del letto di idruro metallico
       self.wt_percent_H2 = 0.0184 # Percentuale in peso di H2 assorbito
       self.mass_H2_max_kg = 200  # Capacità massima di stoccaggio H2 (kg)
       # Calcolo proprietà idruro metallico
       self.M_molare = sum(self.elementi[e]['peso_atomico'] * self.composizione[e] for e in self.composizion
       self.V_molare = sum(
           (self.elementi[e]['peso_atomico'] * self.composizione[e]) / self.elementi[e]['densita'] for e in
           self.composizione)
       self.densita_teorica = self.M_molare / self.V_molare # Densità teorica (g/cm^3)
       self.densita_effettiva = self.densita_teorica * 1000 * (1 - self.porosita) # Densità effettiva (kg/r
       self.cp_ponderato = sum(self.elementi[e]['cp'] * self.composizione[e] for e in self.composizione) / s
           self.composizione[e] for e in self.composizione) # Calore specifico ponderato (J/kgK)
       self.mass_MH_kg = (self.mass_H2_max_kg * 1000) / (
                   self.wt_percent_H2 * 1000) # Massa totale idruro metallico (kg)
       self.volume_tank_m3 = self.mass_MH_kg / self.densita_effettiva # Volume del serbatoio (m^3)
       self.DeltaH_ref = 32500  # Entalpia di reazione di riferimento (J/mol) - Desorbimento (endotermico)
       self.T_ref = 298.15 # Temperatura di riferimento per DeltaH_ref (K)
       self.DeltaCp_rxn = 0 # Differenza di calore specifico per la reazione (J/molK)
       self.DeltaS = 100  # Entropia di reazione (J/molK) - Aggiunto per P_equilibrio
       self.m_dot_acqua = 5  # Portata massica dell'acqua per lo scambio termico (kg/s)
       self.cp_acqua = 4180 # Calore specifico dell'acqua (J/kgK)
       # Temperature di ingresso del fluido termovettore (modificate per un migliore controllo)
       self.T_in_cold = 25+273.15 # Temperatura ingresso acqua fredda (K) - 40°C
       self.T_in_hot = 80+273.15 # Temperatura ingresso acqua calda (K) -
       # Parametri JMA per la cinetica di assorbimento/desorbimento
       self.m_jma = 0.55  # Esponente JMA per H2 puro
       self.A_preexp = 7.3e4 # Prefattore di Arrhenius [h^(m)]
       self.Ea = 22000 # Energia di attivazione [J/mol]
Photovoltaic_system.py
import numpy as np
import math
from system_parameters import SystemParameters
# -----
# CLASSE: PhotovoltaicSystem
# Modella il comportamento del sistema fotovoltaico.
# -----
class PhotovoltaicSystem:
   def __init__(self, params: SystemParameters, time_s: np.ndarray):
       self.params = params
       self.time_s = time_s
       # Parametri PV specifici
       self.AreaPV=20000
       self.etaPV=0.22
       self.G_STC = 1000
       self.P_PV_rated = self.AreaPV * self.etaPV * self.G_STC # Potenza nominale del campo FV (W)
       self.f_PV = 0.9
                                 # Fattore di derating FV
       self.alpha_P = -0.004
                                 # Coefficiente di temperatura della potenza FV (1/K)
       self.T_c_STC = 25
                                 # Temperatura di cella alle condizioni di test standard (°C)
```



```
self.Preale = 2.5e6
                                 # Potenza nominale massima accettata dall'elettrolizzatore (W)
       self.eta_aux = 0.9
                                  # Efficienza dei sistemi ausiliari FV
   def calculate_irradiance_profile_sine(self, G_peak):
       """Calcola il profilo di irradianza sinusoidale."""
       t_hr = self.time_s / 3600
       return G_peak * np.maximum(0, np.sin(np.pi * (t_hr - 6) / 12))
   def update_pv_power(self, G_t, T_amb):
       Calcola la potenza FV disponibile e la divide tra elettrolizzatore e rete.
       Restituisce P_fv_to_electrolyzer, P_fv_to_grid e P_fvteorico.
       # Temperatura del modulo FV (modello semplice: lineare con T_amb)
       T_c = T_amb + 0.03 * G_t
       # Potenza FV aggiornata
       P_fvteorico = self.f_PV * self.P_PV_rated * \
                     (G_t / self.G_STC) * \
                     (1 + self.alpha_P * (T_c - self.T_c_STC))
       # Potenza disponibile considerando perdite dei sistemi ausiliari
       P_fv = self.eta_aux * P_fvteorico
       # Potenza effettiva FV all'elettrolizzatore (non oltre Preale)
       P_fv_to_electrolyzer = np.minimum(P_fv, self.Preale)
       # Surplus FV immesso in rete (se c'è)
       P_fv_to_grid = np.maximum(P_fv - self.Preale, 0)
       # Restituisce P_fv_to_electrolyzer, P_fv_to_grid e P_fvteorico
       return P_fv_to_electrolyzer, P_fv_to_grid, P_fvteorico
Electrolyzer.py
import numpy as np
from system_parameters import SystemParameters
# -----
# CLASSE: Electrolyzer
# Modella il comportamento dell'elettrolizzatore.
class Electrolyzer:
   def __init__(self, params: SystemParameters, time_s: np.ndarray):
       self.params = params
       self.time_s = time_s
       # Preallocazione vettori di output
       self.V_cell_t = np.zeros_like(time_s, dtype=float)
       self.V_stack_t = np.zeros_like(time_s, dtype=float)
       self.P_stack = np.zeros_like(time_s, dtype=float)
       self.I_t = np.zeros_like(time_s, dtype=float)
       self.m_H2 = np.zeros_like(time_s, dtype=float)
       self.E_n_t = np.zeros_like(time_s, dtype=float)
       self.V_an_t = np.zeros_like(time_s, dtype=float)
       self.V_ca_t = np.zeros_like(time_s, dtype=float)
       self.V_ohm_t = np.zeros_like(time_s, dtype=float)
       self.eff_vec = np.zeros_like(time_s, dtype=float) # Efficienza istantanea
       # Inizializzazione valori per il primo passo (o per i primi 10, come nell'originale)
       # Questi valori verranno sovrascritti nel loop di simulazione
```



```
self.V_cell_t[0] = 2.23
   self.I_t[0] = 6239.76
   self.m_H2[0] = 11
def simulate_step(self, k, P_fv_electrolyzer_k, V_prev):
   Simula un singolo passo dell'elettrolizzatore.
   Aggiorna gli stati interni e restituisce il flusso di H2 prodotto.
   # Calcolo corrente e densità di corrente
   if P_fv_electrolyzer_k <= 0 or self.params.n_cells * V_prev <= 0:</pre>
       I = 0.0
   else:
       I = P_fv_electrolyzer_k / (self.params.n_cells * V_prev)
   i = I / self.params.cell_area_m2
   i_cm2 = i / 1e4
   self.I_t[k] = I
   # Se la densità di corrente è troppo bassa, non c'è produzione
   if i < 0.0001:
       self.V_cell_t[k] = V_prev
       self.V_stack_t[k] = V_prev * self.params.n_cells
       self.P_stack[k] = V_prev * self.params.n_cells * I
       self.m_H2[k] = 0
       self.eff_vec[k] = 0 # Efficienza zero se non c'è produzione
       self.E_n_t[k] = 0.0 # Inizializza per evitare NaN
       self.V_an_t[k] = 0.0
       self.V_ca_t[k] = 0.0
       self.V_ohm_t[k] = 0.0
       return 0.0 # Ritorna flusso H2 nullo
   # Calcolo efficienza di Faraday
   i_{loss} = 0.01 * i_{cm2}
   eta_F = 1 - i_{loss} / i_{cm2}
   # Sovratensioni anodica e catodica (Butler-Volmer semplificata)
   V_an = (self.params.R * self.params.T) / (2 * self.params.alpha_an * = =self.params.F)
   * np.arcsinh(i_cm2 / (2 * self.params.i0_an))
   V_ca = (self.params.R * self.params.T) / (2 * self.params.alpha_ca * = =self.params.F)
   * np.arcsinh(i_cm2 / (2 * self.params.i0_ca))
   # Potenziale di Nernst
   E_n = self.params.E0 + (self.params.R * self.params.T) / (2 * self.params.F) * np.log((self.params.P
   # Tensione di cella e di stack
   V_cell = E_n + V_an + V_ca + i * self.params.R_ohm
   V_stack = V_cell * self.params.n_cells
   # Aggiornamento vettori di output
   self.V_cell_t[k] = V_cell
   self.V_stack_t[k] = V_stack
   self.P_stack[k] = V_stack * I
   # Produzione di H2 (kg/s)
   N_H2gen = self.params.n_cells * I / (2 * self.params.F) * eta_F
   mH2 = N_H2gen * (self.params.M_H2 / 1000) # Converti g/mol a kg/mol
   self.m_H2[k] = mH2
```



```
# Salvataggio contributi di tensione
       self.E_n_t[k] = E_n
       self.V_an_t[k] = V_an
       self.V_ca_t[k] = V_ca
       self.V_ohm_t[k] = i * self.params.R_ohm
       # Calcolo efficienza istantanea
       potenza_H2 = mH2 * self.params.LHV_H2
       potenza_PV = P_fv_electrolyzer_k if P_fv_electrolyzer_k > 0 else np.nan
       if np.isfinite(potenza_PV) and potenza_PV > 0:
           self.eff_vec[k] = (potenza_H2 / potenza_PV) * 100
           self.eff_vec[k] = np.nan
       return mH2 # Ritorna il flusso di H2 prodotto
hydrogen_storage.py
import numpy as np
from system_parameters import SystemParameters
# -----
# CLASSE: HydrogenStorage
# Modella il comportamento del sistema di stoccaggio dell'idrogeno a idruri metallici.
# -----
class HydrogenStorage:
   def __init__(self, params: SystemParameters, time_s: np.ndarray):
       self.params = params
       self.time_s = time_s
       self.T_amb = 298.15 # Temperatura ambiente iniziale (K)
       # Inizializzazione della temperatura del serbatoio alla temperatura ambiente
       self.T_tank = self.T_amb # Temperatura iniziale del serbatoio (K)
       self.H2_stored = 0.0 # Idrogeno inizialmente immagazzinato (kg)
       # Preallocazione vettori di output
       self.soc_vec = np.zeros_like(time_s, dtype=float)
       self.H2_vec = np.zeros_like(time_s, dtype=float)
       self.Q_termico_vec = np.zeros_like(time_s, dtype=float)
       self.T_tank_vec = np.zeros_like(time_s, dtype=float)
       self.flusso_assorbito_vec = np.zeros_like(time_s, dtype=float)
       self.flusso_rilasciato_vec = np.zeros_like(time_s, dtype=float)
       # Inizializzazione temperatura serbatoio in Celsius per output
       self.T_tank_vec[:] = self.T_tank - 273.15 # Converti la temperatura iniziale in Celsius
       # Variabili per la gestione della scarica dinamica
       self.H2_stored_at_discharge_start = 0.0
       self.discharge_target_rate = 0.0
       self.discharge_phase_active = False  # Flag per indicare l'inizio della fase di scarica
   def deltaH_rxn(self, T):
       """Calcola l'entalpia di reazione in funzione della temperatura (entalpia di desorbimento)."""
       # self.params.DeltaH_ref è positivo per il desorbimento (endotermico)
       return self.params.DeltaH_ref + self.params.DeltaCp_rxn * (T - self.params.T_ref)
   def P_equilibrio(self, T):
```



```
"""Calcola la pressione di equilibrio (Van't Hoff)."""
    # Assicurati che T sia sempre positivo per evitare logaritmi di numeri negativi o zero
   T_safe = max(T, 1e-6)
   return np.exp(
    (-self.params.DeltaH_ref / (self.params.R_gas * T_safe)) + (self.params.DeltaS / self.params.R_gas))
def k_Sieverts(self, T):
    """Calcola la costante di Sieverts."""
   return np.sqrt(self.P_equilibrio(T))
def simulate_step(self, k, flusso_in_PEM, dt_sec):
    Simula un singolo passo del sistema di stoccaggio.
    Aggiorna gli stati interni (H2_stored, T_tank) e restituisce i valori.
    # Flusso di H2 che tenta di entrare nello storage (metà del flusso PEM)
   flusso_in_storage_from_pem = 0.5 * flusso_in_PEM
    # CINETICA BASATA SU MODELLO JMA
    # Temperatura attuale del serbatoio (in K)
   T_eff = self.T_tank_vec[k - 1] + 273.15
   T_{eff} = max(T_{eff}, 273.15) # Assicurati che la temperatura sia almeno 0°C (273.15 K)
    # Calcolo di k(T) con legge di Arrhenius
   k_jma = self.params.A_preexp * np.exp(-self.params.Ea / (self.params.R_gas * T_eff))
    # Tempo cumulativo in ore (tempo dall'inizio della simulazione)
    time_h = self.time_s[k] / 3600
    time_h_safe = max(time_h, 1e-9) # Assicurati che time_h non sia zero
    # Stato di carica attuale (alpha)
    alpha_attuale = self.H2_stored / self.params.mass_H2_max_kg
    alpha_attuale = np.clip(alpha_attuale, 1e-6, 0.9999) # Evita log(0) o log(negativo)
    # Derivata d(alpha)/dt secondo JMA
    ln_term = -np.log(1 - alpha_attuale)
    if ln_term < 1e-9: # Gestione caso limite per evitare valori indefiniti
       dalpha_dt = 0.0
    else:
       dalpha_dt = k_jma * self.params.m_jma * (time_h_safe ** (self.params.m_jma - 1)) * (
                   1 - alpha_attuale) * ln_term
    # Tasso di assorbimento/desorbimento massimo (kg/s) basato sulla cinetica
    flusso_jma_kinetic = (dalpha_dt * self.params.mass_H2_max_kg) / 3600
   hour = (self.time_s[k] / 3600) \% 24
   flusso_assorbito = 0.0
   flusso_rilasciato = 0.0
    # Logica di carica/scarica basata sul profilo solare e cinetica
    if 6 <= hour < 18: # Ore diurne: priorità all'assorbimento
       if flusso_in_storage_from_pem > 0: # C'è H2 disponibile dall'elettrolizzatore
           flusso_assorbito = min(flusso_in_storage_from_pem, flusso_jma_kinetic)
       else:
           flusso_assorbito = 0.0
       self.discharge_phase_active = False # Reset flag per la scarica
```



```
self.discharge_target_rate = 0.0 # Reset target rate
else: # Ore notturne: priorità alla scarica (18:00 - 06:00)
    # Attiva la fase di scarica e calcola il tasso target solo all'inizio della fase
    # e solo se c'è idrogeno da scaricare.
    if not self.discharge_phase_active and self.H2_stored > 0:
        self.H2_stored_at_discharge_start = self.H2_stored
        # Calcola il tasso costante necessario per scaricare questa quantità in 12 ore
        # Se H2_stored_at_discharge_start è 0, il tasso sarà 0, evitando divisione per 0.
        self.discharge_target_rate = self.H2_stored_at_discharge_start / (12 * 3600)
        self.discharge_phase_active = True
    flusso_target_rilascio_notturno = self.discharge_target_rate
    # Se il target rate non è stato impostato (es. no H2 stored at 18h), o è molto piccolo
    if flusso_target_rilascio_notturno <= 1e-9: # Usa un valore minimo per evitare
    scariche nulle se il target è quasi zero
        flusso_target_rilascio_notturno = 0.0 # Se non c'è H2 o
        il target è nullo, non scaricare
    # Rilascia il minimo tra il target uniforme (dinamico), il tasso cinetico JMA
    e l'H2 disponibile
    if flusso_target_rilascio_notturno > 0: # Solo se c'è un target di scarica
        flusso_rilasciato = min(flusso_target_rilascio_notturno,
        flusso_jma_kinetic, self.H2_stored / dt_sec)
        flusso_rilasciato = 0.0
    flusso_assorbito = 0.0
# Aggiorna quantità H2 immagazzinata
self.H2_stored += (flusso_assorbito - flusso_rilasciato) * dt_sec
self.H2_stored = max(0.0, min(self.H2_stored, self.params.mass_H2_max_kg))
# Aggiorna vettori di flusso
self.flusso_assorbito_vec[k] = flusso_assorbito
self.flusso_rilasciato_vec[k] = flusso_rilasciato
# BILANCIO ENERGETICO SERBATOIO
delta_H2_mass = (flusso_assorbito - flusso_rilasciato) * dt_sec
moles_H2_change = (delta_H2_mass * 1000) / self.params.M_H2 # Variazione moli H2
# Q_reaction_to_tank: calore trasferito dalla reazione al tank (positivo se tank
riceve calore, negativo se tank cede calore)
# self.deltaH_rxn(T) è l'entalpia di desorbimento (positiva, endotermica)
Q_reaction_to_tank = 0.0
if delta_H2_mass > 0: # Assorbimento (esotermico: rilascia calore al tank)
    # Calore rilasciato dalla reazione esotermica è positivo per il tank
    Q_reaction_to_tank = abs(moles_H2_change) * self.deltaH_rxn(self.T_tank)
elif delta_H2_mass < 0: # Desorbimento (endotermico: assorbe calore dal tank)
    # Calore assorbito dalla reazione endotermica è negativo per il tank
    Q_reaction_to_tank = -abs(moles_H2_change) * self.deltaH_rxn(self.T_tank)
# Calore scambiato con l'acqua (Q_HX_to_tank: positivo se tank riceve calore,
negativo se tank cede calore)
Q_HX_{to_tank} = 0.0
if delta_H2_mass > 0: # Fase di carica (assorbimento) - Il tank dovrebbe tendere a T_in_cold
    # Se T_tank > T_in_cold, il tank cede calore all'acqua (Q_HX_to_tank negativo)
    # Se T_tank < T_in_cold, l'acqua cede calore al tank (Q_HX_to_tank positivo)
```



```
Q_HX_to_tank = self.params.m_dot_acqua * self.params.cp_acqua * (
                      self.params.T_in_cold - self.T_tank) * dt_sec
       elif delta_H2_mass < 0: # Fase di scarica (desorbimento) - Il tank dovrebbe tendere a T_in_hot
           # Se T_tank < T_in_hot, 1'acqua cede calore al tank (Q_HX_to_tank positivo)
           # Se T_tank > T_in_hot, il tank cede calore all'acqua (Q_HX_to_tank negativo)
           Q_HX_to_tank = self.params.m_dot_acqua * self.params.cp_acqua * (
                      self.params.T_in_hot - self.T_tank) * dt_sec
       # Bilancio energetico: variazione energia interna del tank = calore dalla reazione + calore dal HX
       deltaE = Q_reaction_to_tank + Q_HX_to_tank
       deltaT_tank = deltaE / (self.params.mass_MH_kg * self.params.cp_ponderato)
       if self.params.mass_MH_kg > 0 else 0
       self.T_tank += deltaT_tank
       # Assicurati che la temperatura non scenda troppo o salga troppo
       self.T_tank = np.clip(self.T_tank, 250, 450) # Min -23°C, max 177°C (LIMITI ALLENTATI)
       # Energia immagazzinata chimicamente (LHV)
       energy_stored_H2_chemical = self.H2_stored * self.params.LHV_H2
       # === alla fine del ciclo, salvataggio ===
       self.soc_vec[k] = self.H2_stored / self.params.mass_H2_max_kg * 100
       self.H2_vec[k] = self.H2_stored
       self.Q_termico_vec[k] = energy_stored_H2_chemical / 1e6 # Converti J a MJ
       self.T_tank_vec[k] = self.T_tank - 273.15 # Converti K a °C
plotting.py
import numpy as np
import pandas as pd
import matplotlib.pyplot as plt
import matplotlib.cm as cm
from mpl_toolkits.mplot3d import Axes3D
from system_parameters import SystemParameters
# -----
# CLASS: Plotting
# Manages the generation of all simulation plots.
class Plotting:
   def __init__(self, df: pd.DataFrame, params: SystemParameters, time_s: np.ndarray):
       self.df = df
       self.params = params
       self.time_s = time_s
   def _customize_xticks(self):
       """Helper function to customize X-axis labels."""
       tick_locs = np.arange(6, 31, 6)
       tick_labels = [str(int(t)) for t in tick_locs]
       for i, loc in enumerate(tick_locs):
           if loc == 24:
               tick_labels[i] = '24'
           elif loc == 30:
               tick_labels[i] = '6'
       plt.xticks(tick_locs, tick_labels)
   def plot_pv_power(self, P_fvteorico: np.ndarray):
       """PLOT PV Power."""
       plt.figure(figsize=(10, 5))
```



```
plt.plot(self.df["Time_h"], P_fvteorico / 1e6, label="PV Power")
   plt.xlabel("Time [h]")
   plt.ylabel("PV Power [MW]")
   plt.title("Photovoltaic Power over time")
   plt.grid(True)
   plt.legend()
   plt.tight_layout()
   plt.xlim(6, 30)
   self._customize_xticks()
def plot_current(self):
    """Electric Current - Solar Profile."""
   plt.figure(figsize=(10, 5))
    plt.plot(self.df["Time_h"], self.df["I_A"])
   plt.title("Electric Current - Solar Profile")
   plt.xlabel("Time [h]")
   plt.ylabel("Current [A]")
   plt.ylim(0, 10000)
   plt.yticks(np.arange(0, 10001, 2000))
   plt.grid()
   plt.tight_layout()
   plt.xlim(6, 30)
   self._customize_xticks()
def plot_h2_instantaneous_production(self):
    """Instantaneous H Production [g/s]."""
   plt.figure(figsize=(10, 5))
   plt.plot(self.df["Time_h"], self.df["H2_flow_g_s"])
   plt.title("Instantaneous H Production")
   plt.xlabel("Time [h]")
   {\tt plt.ylabel("H\ Flow\ [g/s]")}
   plt.ylim(0, 20)
   plt.yticks(np.arange(0, 21, 2))
   plt.grid()
   plt.tight_layout()
   plt.xlim(6, 30)
    self._customize_xticks()
def plot_h2_cumulative_production(self):
    """Cumulative H Production [kg]."""
   plt.figure(figsize=(10, 5))
   plt.plot(self.df["Time_h"], self.df["H2_total_kg"])
   plt.title("Cumulative H Production")
   plt.xlabel("Time [h]")
   plt.ylabel("Cumulative H Mass [kg]")
   plt.grid()
   plt.tight_layout()
   plt.xlim(6, 30)
   self._customize_xticks()
def plot_electrical_energy_cumulative(self):
    """Cumulative Electrical Energy [MWh]."""
   plt.figure(figsize=(10, 5))
   plt.plot(self.df["Time_h"], self.df["Energy_el_MWh"], label="Electrical Energy Consumed")
   plt.title("Cumulative Electrical Energy Consumed")
   plt.xlabel("Time [h]")
   plt.ylabel("Cumulative Electrical Energy [MWh]")
   plt.grid(True)
   plt.tight_layout()
   plt.xlim(6, 30)
```



```
self._customize_xticks()
def plot_electrolyzer_efficiency(self):
    """Electrical Efficiency [%] ( 100 %), excluding NaN and zeros."""
    plt.figure(figsize=(10, 5))
    df_clean = self.df[(self.df["Efficiency_percent"].notna()) & (self.df["Efficiency_percent"] > 0)]
    plt.plot(df_clean["Time_h"], df_clean["Efficiency_percent"], label="Efficiency")
    plt.axhline(100, color='gray', linestyle='--', label="100 %")
   plt.ylim(0, 100)
   plt.title("Electrolyzer Efficiency over time")
   plt.xlabel("Time [h]")
   plt.ylabel("Efficiency [%]")
    plt.legend()
    plt.grid()
    plt.tight_layout()
    plt.xlim(6, 30)
    self._customize_xticks()
def plot_pem_cell_voltage(self):
    """PEM Cell Voltage (production only)."""
   plt.figure(figsize=(10, 5))
   mask = self.df["I_A"] > 1e-6
   plt.plot(self.df["Time_h"][mask], self.df["V_cell_V"][mask], label="V_cell")
   plt.title("PEM Cell Voltage (production only)")
   plt.xlabel("Time [h]")
   plt.ylabel("Cell Voltage [V]")
   plt.ylim(1, 3)
    plt.yticks(np.arange(1, 3, 0.2))
    plt.legend()
   plt.grid()
   plt.tight_layout()
    plt.xlim(6, 30)
    self._customize_xticks()
def plot_polarization_curve(self):
    """Polarization Curve: Nominal vs Real."""
    i_range = np.linspace(0.01, 2.0, 200)
    # === Common Parameters ===
   T_{nom} = 25 + 273.15
   T_real = self.params.T
    lambda_m = self.params.lambda_m
    t_me_cm = self.params.t_me_cm
   R_gas = self.params.R_gas
    F = self.params.F
    alpha_an = self.params.alpha_an
    alpha_ca = self.params.alpha_ca
    i0_an = self.params.i0_an
    i0_ca = self.params.i0_ca
   E0 = self.params.E0
    # === Pressures ===
    P_{std} = 101325
    P_H2_real = self.params.P_H2
    P_02_real = self.params.P_02
   P_H20 = self.params.P_H20an
    # === Curve at Nominal Conditions (1 atm, 25°C) ===
    sigma_nom = (0.005139 * lambda_m - 0.00326) * np.exp(1268 * (1 / 303 - 1 / T_nom))
    R_ohm_nom_calc = t_me_cm / sigma_nom
```



```
E_n_m = E0 + (R_gas * T_nom) / (2 * F) * np.log((P_std * np.sqrt(P_std)) / P_std)
   V_an_nom = (R_gas * T_nom) / (2 * alpha_an * F) * np.arcsinh(i_range / (2 * i0_an))
   V_ca_nom = (R_gas * T_nom) / (2 * alpha_ca * F) * np.arcsinh(i_range / (2 * i0_ca))
   V_ohm_nom = i_range * R_ohm_nom_calc
   V_cell_nom = E_n_nom + V_an_nom + V_ca_nom + V_ohm_nom
   # === Curve at Real Conditions (30 bar, 60°C) ===
   sigma_real = (0.005139 * lambda_m - 0.00326) * np.exp(1268 * (1 / 303 - 1 / T_real))
   R_ohm_real_calc = t_me_cm / sigma_real
   V_an_real = (R_gas * T_real) / (2 * alpha_an * F) * np.arcsinh(i_range / (2 * i0_an))
   V_ca_real = (R_gas * T_real) / (2 * alpha_ca * F) * np.arcsinh(i_range / (2 * i0_ca))
   V_ohm_real = i_range * R_ohm_real_calc
   V_cell_real = E_n_real + V_an_real + V_ca_real + V_ohm_real
   # === Plot ===
   plt.figure(figsize=(10, 5))
   plt.plot(i_range, V_cell_nom, label="Nominal Conditions (1 atm, 25°C)")
   plt.plot(i_range, V_cell_real, label="Operating Conditions (30 bar, 60°C)")
   plt.title("Polarization Curve: Nominal vs Real")
   plt.xlabel("Current Density [A/cm2]")
   plt.ylabel("Cell Voltage [V]")
   plt.grid()
   plt.legend()
   plt.tight_layout()
   plt.xlim(i_range.min(), i_range.max())
def plot_energy_comparison(self):
    """Comparison of Electrical and H Energy [MWh]."""
   plt.figure(figsize=(10, 5))
   plt.plot(self.df["Time_h"], self.df["Energy_el_MWh"], label="Electrical Energy Consumed")
   {\tt plt.plot(self.df["Time\_h"], self.df["Energy\_H2\_LHV\_MWh"], label="H (LHV)")}
   plt.plot(self.df["Time_h"], self.df["Energy_H2_HHV_MWh"], label="H (HHV)")
   plt.title("Cumulative Energy Comparison")
   plt.xlabel("Time [h]")
   plt.ylabel("Cumulative Energy [MWh]")
   plt.legend()
   plt.grid()
   plt.tight_layout()
   plt.xlim(6, 30)
   self._customize_xticks()
def plot_stack_temperature(self):
    """Stack Temperature [°C]."""
   plt.figure(figsize=(10, 5))
   plt.plot(self.df["Time_h"], self.df["T_stack_K"] - 273.15, 'r-')
   plt.title("Stack Temperature over time")
   plt.xlabel("Time [h]")
   plt.ylabel("Temperature [°C]")
   plt.grid()
   plt.tight_layout()
   plt.xlim(6, 30)
   self._customize_xticks()
def plot_polarization_curves_3d(self):
    """3D Polarization Curves during the day."""
   i_range = np.linspace(0.01, 2.0, 100)
   time_vals_continuous = self.time_s / 3600
   mask_time = (time_vals_continuous >= 6) & (time_vals_continuous <= 30)
   time_vals_plot = time_vals_continuous[mask_time]
```



```
V_curves = []
    start_idx = np.where(time_vals_continuous >= 6)[0][0]
    end_idx = np.where(time_vals_continuous <= 30)[0][-1] + 1</pre>
    num_points_3d = 100
    step_3d = max(1, int((end_idx - start_idx) / num_points_3d))
    selected_indices = np.arange(start_idx, end_idx, step_3d)
    for idx in selected_indices:
        T = self.df["T_stack_K"].iloc[idx]
        sigma = (0.005139 * self.params.lambda_m - 0.00326) * np.exp(1268 * (1 / 303 - 1 / T))
        R_ohm_calc = self.params.t_me_cm / sigma
        V_act_an = (self.params.R * T) / (2 * self.params.alpha_an * self.params.F) =
        =* np.arcsinh(i_range / (2 * self.params.i0_an))
        V_act_ca = (self.params.R * T) / (2 * self.params.alpha_ca * self.params.F) =
        =* np.arcsinh(i_range / (2 * self.params.i0_ca))
        V_ohm = i_range * R_ohm_calc
        E_n = self.params.E0 + (self.params.R * T) / (2 * self.params.F) =
        = * np.log((self.params.P_H2 * np.sqrt(self.params.P_O2)) / self.params.P_H2Oan)
        V_curves.append(E_n + V_act_an + V_act_ca + V_ohm)
   n_curves = len(V_curves)
    colors = cm.viridis(np.linspace(0, 1, n_curves))
    fig = plt.figure(figsize=(10, 8))
    ax = fig.add_subplot(111, projection='3d')
    ax.set_xlabel("Current Density [A/cm2]")
    ax.set_ylabel("Time [h]")
    ax.set_zlabel("Cell Voltage [V]")
    ax.set_title("Polarization Curves during the day")
    ax.set_xlim(i_range.min(), i_range.max())
    ax.set_ylim(time_vals_continuous[selected_indices].min(), time_vals_continuous[selected_indices].max
    ax.set_zlim(
        min(curve.min() for curve in V_curves),
        max(curve.max() for curve in V_curves)
    )
    for j, curve in enumerate(V_curves):
        t = time_vals_continuous[selected_indices[j]]
        y = np.full_like(i_range, t)
        ax.plot(i_range, y, curve, color=colors[j], linewidth=1)
    sm = cm.ScalarMappable(cmap="viridis",
                           norm=plt.Normalize(vmin=time_vals_continuous[selected_indices].min(),
                                              vmax=time_vals_continuous[selected_indices].max()))
    sm.set_array([])
    cbar = fig.colorbar(sm, ax=ax, pad=0.1, aspect=10)
    cbar.set_label("Time")
   plt.tight_layout()
def plot_h2_stored(self):
    """H2 stored [kg]."""
    plt.figure(figsize=(10, 5))
    plt.plot(self.df["Time_h"], self.df["H2_Stored_kg"])
    plt.title("H2 stored")
    plt.xlabel("Time [h]")
    plt.ylabel("H2 stored [kg]")
    plt.grid(True)
    plt.tight_layout()
    plt.xlim(6, 30)
    self._customize_xticks()
```



```
def plot_soc_storage(self):
    """H2 Storage SoC Trend."""
   plt.figure(figsize=(10, 5))
   plt.plot(self.df["Time_h"], self.df["SoC_percent"], label="SoC (%)")
   plt.xlabel("Time [h]")
   plt.ylabel("State of Charge (%)")
   plt.title("H2 Storage State of Charge Trend")
   plt.grid(True)
   plt.legend()
   plt.tight_layout()
   plt.xlim(6, 30)
   self._customize_xticks()
def plot_tank_temperature(self):
    """Tank Temperature over Time."""
   plt.figure(figsize=(10, 5))
    plt.plot(self.df["Time_h"], self.df["T_tank_C"], label="Tank Temperature (°C)", color='orange')
   plt.xlabel("Time [h]")
   plt.ylabel("Temperature (°C)")
   plt.title("Tank Temperature over Time")
   plt.grid(True)
   plt.legend()
   plt.tight_layout()
   plt.xlim(6, 30)
    self._customize_xticks()
def plot_kinetic_constant_k(self):
    """Kinetic constant k(T) over time."""
   T_k_array = self.df["T_tank_C"].values + 273.15
   T_k_array = np.maximum(T_k_array, 1e-6)
   k_jma_vec = self.params.A_preexp * np.exp(-self.params.Ea / (self.params.R_gas * T_k_array))
   plt.figure(figsize=(10, 5))
   plt.plot(self.df["Time_h"], k_jma_vec, label="k(T) [h$^{-m}$]")
   plt.xlabel("Time [h]")
   plt.ylabel("k [h$^{-m}$]")
   plt.title("Kinetic constant k(T) over time")
   plt.grid(True)
   plt.legend()
   plt.tight_layout()
   plt.xlim(6, 30)
   self._customize_xticks()
def plot_soc_hydrode(self):
    """Hydride State of Charge."""
   plt.figure(figsize=(10, 5))
   plt.plot(self.df["Time_h"], self.df["SoC_percent"], label="State of Charge [%]")
   plt.xlabel("Time [h]")
   plt.ylabel("SoC [%]")
   plt.title("Hydride State of Charge")
   plt.grid(True)
   plt.legend()
   plt.tight_layout()
   plt.xlim(6, 30)
    self._customize_xticks()
def plot_tank_temperature_hydrode(self):
    """Tank Temperature Trend."""
    plt.figure(figsize=(10, 5))
```



```
plt.plot(self.df["Time_h"], self.df["T_tank_C"], label="Tank Temp. [°C]")
       plt.xlabel("Time [h]")
       plt.ylabel("Temperature [°C]")
       plt.title("Tank Temperature Trend")
       plt.grid(True)
       plt.legend()
       plt.tight_layout()
       plt.xlim(6, 30)
       self._customize_xticks()
   def plot_thermal_energy_stored(self):
       """Energy stored in the storage system."""
       plt.figure(figsize=(10, 5))
       plt.plot(self.df["Time_h"], self.df["Q_termico_MJ"], label="Thermal Energy [MJ]")
       plt.xlabel("Time [h]")
       plt.ylabel("Thermal Energy [MJ]")
       plt.title("Energy stored in the storage system")
       plt.grid(True)
       plt.legend()
       plt.tight_layout()
       plt.xlim(6, 30)
       self._customize_xticks()
   def show_all_plots(self):
       """Shows all generated plots."""
       plt.show()
Main.py
import numpy as np
import pandas as pd
import matplotlib.pyplot as plt
import math
# Importa le classi dai rispettivi file
from system_parameters import SystemParameters
from photovoltaic_system import PhotovoltaicSystem
from electrolyzer import Electrolyzer
from hydrogen_storage import HydrogenStorage
from plotting import Plotting # Importa la nuova classe Plotting
# ------
# FUNZIONE MAIN
# Orchesta la simulazione, inizializza le classi e gestisce il loop temporale.
# ------
def main():
   # 1. Inizializzazione Parametri di Sistema
   params = SystemParameters()
   # Parametri Tempo
   dt_sec = 60 # Intervallo di tempo (secondi)
   # Modifica qui: la simulazione inizia alle 6 del mattino e dura 24 ore (fino alle 6 del giorno successivo
   time_start_sec = 6 * 3600 # Inizia alle 6 del mattino in secondi
   time_end_sec = (6 + 24) * 3600 # Termina alle 6 del mattino del giorno successivo in secondi
   time_s = np.arange(time_start_sec, time_end_sec, dt_sec) # Array del tempo per 24 ore
   # Parametri Ambientali
   T_amb = 23.8 # Temperatura ambiente (°C)
   # Input Irradianza
```



```
irradianza_mensile_mj = 655.505 \# MJ/m^2/mese
giorni_mese = 30
ore_sole = 12
fattore_seno = (math.pi / 4) * ore_sole
mj_giorno = irradianza_mensile_mj / giorni_mese
kwh_giorno = mj_giorno * 0.27778
G_peak = kwh_giorno / fattore_seno * 1000 # Potenza di picco (W/m^2)
print(f"Irradianza di picco calcolata (G_peak): {G_peak:.2f} W/m2")
# 2. Inizializzazione Classi di Modello
pv_system = PhotovoltaicSystem(params, time_s)
electrolyzer = Electrolyzer(params, time_s)
storage = HydrogenStorage(params, time_s)
# Calcolo profilo di irradianza
# --- Invece di calcolare un profilo sinusoidale, usa l'irradianza fissa ---
fixed_irradiance_W_m2 = 1000
#G_t = np.full_like(time_s, fixed_irradiance_W_m2, dtype=float)
# --- FINE MODIFICA ---
G_t = pv_system.calculate_irradiance_profile_sine(G_peak)
# Calcolo potenza FV per ogni istante di tempo
P_fv_to_electrolyzer, P_fv_to_grid, P_fvteorico = pv_system.update_pv_power(G_t, T_amb)
# Inizializzazione per il loop
V_prev = electrolyzer.V_cell_t[0] # Usa il valore iniziale preallocato
# 3. Loop di Simulazione
for k in range(1, len(time_s)):
    # Simula l'elettrolizzatore
    # V_prev è la tensione di cella del passo precedente
    flusso_in_PEM = electrolyzer.simulate_step(k, P_fv_to_electrolyzer[k], V_prev)
    V_prev = electrolyzer.V_cell_t[k] # Aggiorna V_prev per il prossimo passo
    # Simula lo storage
    storage.simulate_step(k, flusso_in_PEM, dt_sec)
# Fissa i primi 10 valori iniziali uguali al valore all'undicesima iterazione (index 10)
# Questo è un workaround per allinearsi al comportamento del codice originale.
# In una simulazione più robusta, i primi valori dovrebbero essere calcolati o
# inizializzati correttamente.
for k in range(10):
    electrolyzer.I_t[k] = electrolyzer.I_t[10]
    electrolyzer.P_stack[k] = electrolyzer.P_stack[10]
    electrolyzer.V_cell_t[k] = electrolyzer.V_cell_t[10]
    electrolyzer.V_stack_t[k] = electrolyzer.V_stack_t[10]
    electrolyzer.m_H2[k] = electrolyzer.m_H2[10]
    electrolyzer.eff_vec[k] = electrolyzer.eff_vec[10]
    storage.soc_vec[k] = storage.soc_vec[10]
    storage.H2_vec[k] = storage.H2_vec[10]
    storage.Q_termico_vec[k] = storage.Q_termico_vec[10]
    storage.T_tank_vec[k] = storage.T_tank_vec[10]
    storage.flusso_assorbito_vec[k] = storage.flusso_assorbito_vec[10]
    storage.flusso_rilasciato_vec[k] = storage.flusso_rilasciato_vec[10]
# 4. Elaborazione e Salvataggio Risultati Finali
m_H2_cum = np.cumsum(electrolyzer.m_H2 * dt_sec)
E_stack = np.cumsum(electrolyzer.P_stack * dt_sec)
```



```
T_nom_arr = np.full_like(time_s, params.T) # Temperatura nominale (costante)
df = pd.DataFrame({
    # Calcola Time_h in modo continuo per il plotting
    "Time_h": time_s / 3600,
    "I_A": electrolyzer.I_t,
    "V_cell_V": electrolyzer.V_cell_t,
    "V_stack_V": electrolyzer.V_stack_t,
    "T_stack_K": T_nom_arr,
    "H2_flow_kg_s": electrolyzer.m_H2,
    "H2_flow_g_s": electrolyzer.m_H2 * 1000,
    "H2_total_kg": m_H2_cum,
    "Energy_H2_LHV_MWh": (m_H2_cum * params.LHV_H2) / 3.6e9,
    "Energy_H2_HHV_MWh": (m_H2_cum * params.HHV_H2) / 3.6e9,
    "Energy_el_MWh": E_stack / 3.6e9,
    "Efficiency_percent": electrolyzer.eff_vec,
    "H2_Stored_kg": storage.H2_vec,
    "SoC_percent": storage.soc_vec,
    "Q_termico_MJ": storage.Q_termico_vec,
    "T_tank_C": storage.T_tank_vec,
    "E_n_V": electrolyzer.E_n_t,
    "V_an_V": electrolyzer.V_an_t,
    "V_ca_V": electrolyzer.V_ca_t,
    "V_ohm_V": electrolyzer.V_ohm_t,
    "P_stack_W": electrolyzer.P_stack,
    "H2_cum_kg": m_H2_cum,
    "H2_abs_kg_s": storage.flusso_assorbito_vec,
    "H2_rel_kg_s": storage.flusso_rilasciato_vec,
    "P_H2_bar": params.P_H2 / 1e5 # Converti Pa a bar
})
print("\nSimulazione completata. Prime 5 righe del DataFrame dei risultati:")
print(df.head())
# 5. Visualizzazione (Esempio) - Ora gestita dalla classe Plotting
plotter = Plotting(df, params, time_s) # Passiamo time_s originale per la cinetica JMA se necessario
plotter.plot_pv_power(P_fvteorico)
plotter.plot_current()
plotter.plot_h2_instantaneous_production()
plotter.plot_h2_cumulative_production()
plotter.plot_electrical_energy_cumulative()
plotter.plot_electrolyzer_efficiency()
plotter.plot_pem_cell_voltage()
plotter.plot_polarization_curve()
plotter.plot_energy_comparison()
plotter.plot_stack_temperature()
plotter.plot_polarization_curves_3d()
plotter.plot_h2_stored()
plotter.plot_soc_storage()
plotter.plot_tank_temperature()
plotter.plot_kinetic_constant_k()
plotter.plot_soc_hydrode()
plotter.plot_tank_temperature_hydrode()
plotter.plot_thermal_energy_stored()
# Chiamata singola a plt.show() per visualizzare tutti i grafici
plotter.show_all_plots()
# DEBUG PRODUZIONE H2 E STACK - Rimangono qui in main
```



```
print("\n--- DEBUG PRODUZIONE H2 E STACK ---")
   print(f"Corrente media stack [A]:
                                            {np.mean(electrolyzer.I_t):.2f}")
   print(f"Densita di corrente [A/cm2]:
                                               {np.mean(electrolyzer.I_t) / params.cell_area_cm2:.2f}")
                                            {np.mean(electrolyzer.V_cell_t):.4f}")
   print(f"Tensione media cella [V]:
                          {params.E0:.4f}") # E0 è costante, non ha senso mediare
   print(f"E0 [V]:
   print(f"V_an [V]:
                            {np.mean(electrolyzer.V_an_t):.4f}")
   print(f"V_ca [V]:
                            {np.mean(electrolyzer.V_ca_t):.4f}")
    print(f"Tensione media stack [V]:
                                            {np.mean(electrolyzer.V_stack_t):.2f}")
                                            {np.mean(electrolyzer.P_stack) / 1e6:.3f}")
    print(f"Potenza media assorbita [MW]:
                                            {np.sum(electrolyzer.m_H2) * dt_sec :.2f}")
    print(f"Produzione totale H2 [kg/g]:
   print(f"Efficienza media [%]:
                                            {np.nanmean(electrolyzer.eff_vec):.2f}")
if __name__ == "__main__":
    main()
Idrogeno 2023.py
import numpy as np
import matplotlib.pyplot as plt
import math
from system_parameters import SystemParameters
from photovoltaic_system import PhotovoltaicSystem
from electrolyzer import Electrolyzer
from hydrogen_storage import HydrogenStorage
def simulate_yearly_production():
    # Monthly data: average temperature (°C) and global irradiance (MJ/m²/month)
    T_{media_C} = [6.2, 5.5, 10.1, 11.9, 18.2, 22.6, 24.4, 23.8, 21.3, 16.9, 8.5, 5.8]
    irradianza_mensile_MJ = [144.571, 245.137, 403.169, 529.804, 596.424, 771.272,
                             795.202, 655.505, 537.152, 317.604, 215.314, 141.824]
    giorni_mese = [31, 28, 31, 30, 31, 30, 31, 30, 31, 30, 31]
    mesi = ["Jan", "Feb", "Mar", "Apr", "May", "Jun", "Jul", "Aug", "Sep", "Oct", "Nov", "Dec"]
    # Time parameters and constants
    dt_sec = 60
    time_start_sec = 6 * 3600
    time_end_sec = (6 + 24) * 3600
    time_s = np.arange(time_start_sec, time_end_sec, dt_sec)
    ore_sole = 12
    params = SystemParameters()
   produzione_mensile_kg = []
    for mese_idx in range(12):
        T_amb = T_media_C[mese_idx]
        irradianza_mj = irradianza_mensile_MJ[mese_idx]
        giorni = giorni_mese[mese_idx]
        # Calculate G_peak
        fattore_seno = (math.pi / 4) * ore_sole
        mj_giorno = irradianza_mj / giorni
        kwh_giorno = mj_giorno * 0.27778
        G_peak = kwh_giorno / fattore_seno * 1000
        # Initialize components
        pv_system = PhotovoltaicSystem(params, time_s)
        electrolyzer = Electrolyzer(params, time_s)
        storage = HydrogenStorage(params, time_s)
```



```
# Irradiance and PV power
        G_t = pv_system.calculate_irradiance_profile_sine(G_peak)
        P_fv_to_electrolyzer, _, _ = pv_system.update_pv_power(G_t, T_amb)
        # Daily simulation
        V_prev = electrolyzer.V_cell_t[0]
        for k in range(1, len(time_s)):
            flusso_in_PEM = electrolyzer.simulate_step(k, P_fv_to_electrolyzer[k], V_prev)
            V_prev = electrolyzer.V_cell_t[k]
            storage.simulate_step(k, flusso_in_PEM, dt_sec)
        # Align initial values (workaround)
        for k in range(10):
            electrolyzer.I_t[k] = electrolyzer.I_t[10]
            electrolyzer.P_stack[k] = electrolyzer.P_stack[10]
            electrolyzer.V_cell_t[k] = electrolyzer.V_cell_t[10]
            electrolyzer.V_stack_t[k] = electrolyzer.V_stack_t[10]
            electrolyzer.m_H2[k] = electrolyzer.m_H2[10]
            electrolyzer.eff_vec[k] = electrolyzer.eff_vec[10]
            storage.soc_vec[k] = storage.soc_vec[10]
            storage.H2_vec[k] = storage.H2_vec[10]
            storage.Q_termico_vec[k] = storage.Q_termico_vec[10]
            storage.T_tank_vec[k] = storage.T_tank_vec[10]
            storage.flusso_assorbito_vec[k] = storage.flusso_assorbito_vec[10]
            storage.flusso_rilasciato_vec[k] = storage.flusso_rilasciato_vec[10]
        produzione_giornaliera_kg = np.sum(electrolyzer.m_H2) * dt_sec
        produzione_mese = produzione_giornaliera_kg * giorni
        produzione_mensile_kg.append(produzione_mese)
        print(f"{mesi[mese_idx]}: {produzione_mese:.2f} kg H2")
    produzione_annua = sum(produzione_mensile_kg)
    print(f"\nTotal annual hydrogen production: {produzione_annua:.2f} kg")
    # Monthly chart
    plt.figure()
    plt.bar(mesi, produzione_mensile_kg) # Use 'mesi' (months) for x-axis labels
    plt.ylabel("Monthly H production [kg]")
    plt.title("Monthly hydrogen production (daily simulation multiplied)")
    plt.grid(True)
    plt.tight_layout()
    plt.show()
if __name__ == "__main__":
    simulate_yearly_production()
CO2 e Methane reduction.py
import matplotlib.pyplot as plt
import pandas as pd
# === Energy constants ===
PCS_CH4 = 10.7 \# kWh/Sm3 of methane
PCS_H2 = 33.33 # kWh/kg of hydrogen
CO2_EMISSION_FACTOR_CH4 = 2.024 # kg CO2/Sm3 of methane
# === Annual methane consumption ===
annual_methane_consumption_m3 = 84543271 # m3/year
# === Annual usable hydrogen data (in kg) ===
```



```
hydrogen_data = {
    1999: 86448.00, 2000: 89031.41, 2001: 88248.87, 2002: 84655.52, 2003: 95330.74,
    2004: 87515.27, 2005: 90784.62, 2006: 90670.98, 2007: 86031.65, 2008: 80481.18,
    2009: 86001.51, 2010: 82565.70, 2011: 90774.72, 2012: 90623.63, 2013: 84628.54,
    2014: 83264.19, 2015: 87259.07, 2016: 82839.69, 2017: 87362.69, 2018: 82771.75,
    2019: 85675.20, 2020: 92257.90, 2021: 92154.50, 2022: 94091.86, 2023: 92663.52
# === Calculation of results for each year ===
results = []
for year, h2_kg in hydrogen_data.items():
   h2_energy_kwh = h2_kg * PCS_H2
   methane_saved_m3 = h2_energy_kwh / PCS_CH4
    co2_avoided_tonnes = (methane_saved_m3 * CO2_EMISSION_FACTOR_CH4) / 1000
   results.append({
        "Year": year,
        "H2_kg": h2_kg,
        "Methane_Saved_m3": methane_saved_m3,
        "CO2_Avoided_tonnes": co2_avoided_tonnes
    })
# === DataFrame creation ===
df = pd.DataFrame(results)
# === Totals over 25 years ===
total_methane_saved = df["Methane_Saved_m3"].sum()
total_co2_avoided = df["CO2_Avoided_tonnes"].sum()
print(f"Total methane saved: {total_methane_saved:,.0f} m3")
print(f"Total CO avoided: {total_co2_avoided:,.0f} tonnes")
# === Plot: Methane saved ===
plt.figure(figsize=(12, 6))
plt.bar(df["Year"], df["Methane_Saved_m3"], color='orange')
plt.xlabel("Year")
plt.ylabel("Methane saved (m3)")
plt.title("Annual reduction in methane consumption due to H substitution")
plt.grid(True)
plt.tight_layout()
plt.show()
# === Plot: CO2 avoided ===
plt.figure(figsize=(12, 6))
plt.bar(df["Year"], df["CO2_Avoided_tonnes"], color='green')
plt.xlabel("Year")
plt.ylabel("CO avoided (tonnes)")
plt.title("CO emissions avoided annually due to H substitution")
plt.grid(True)
plt.tight_layout()
plt.show()
Cost Analysis.py
import numpy as np
import matplotlib.pyplot as plt
# MODIFIABLE ECONOMIC PARAMETERS
# Modify these values to change scenarios and prices
```



```
# Plant power (kW)
PV_kW = 4400 # Peak power of the photovoltaic system in kW
PEM_kW = 2500 # Nominal power of the PEM electrolyzer in kW
# Market prices
price\_CH4 = 2 \# €/m^3 - Price of saved methane
price_H2_market = 4 # €/kg H2 - Selling price of hydrogen on the market
# Discount rate
discount_rate = 0.049 # Real discount rate
# --- Scenario 2025 Parameters ---
capex_PV_2025_per_kW = 1200 # €/kW
capex_PEM_2025_per_kW = 1500 # €/kW
opex_PV_2025_per_kW_per_year = 24 # €/kW/year
opex_PEM_2025_perc_capex = 0.03 # % of CAPEX_PEM
replacement_PEM_2025_perc_capex = 0 # Replacement cost of the PEM electrolyzer
# --- Scenario 2030 Parameters ---
capex_PV_2030_per_kW = 1000 # €/kW (reduced compared to 2025)
capex_PEM_2030_per_kW = 1000 # €/kW
opex_PV_2030_per_kW_per_year = 24 # €/kW/year
opex_PEM_2030_perc_capex = 0.03 # % of CAPEX_PEM
replacement_PEM_2030_perc_capex = 0
# --- Scenario 2050 Parameters (Added) ---
# Hypothetical values based on the reduction trend
capex_PV_2050_per_kW = 600 # €/kW
capex_PEM_2050_per_kW = 800 # €/kW
opex_PV_2050_per_kW_per_year = 24 # €/kW/year (assuming further reduction)
opex_PEM_2050_perc_capex = 0.02 # % of CAPEX_PEM (assuming further reduction)
replacement_PEM_2050_perc_capex = 0 # No replacement cost
# -----
# END OF MODIFIABLE PARAMETERS
# ------
def calculate_LCOE_LCOH(
   avg_annual_energy_kWh,
   total_H2_kg,
   capex_PV,
   capex_PEM,
   opex_PV,
   opex_PEM,
   replacement_PEM,
   years=25,
   discount_rate=0.049
):
   Calculates the LCOE, LCOH, and NPC for a given scenario.
   CAPEX = capex_PV + capex_PEM
   year_array = np.arange(1, years + 1)
   annual_OPEX = opex_PV + opex_PEM
   discounted_OPEX = annual_OPEX / (1 + discount_rate) ** year_array
   discounted_RC = np.zeros(years)
   if replacement_PEM > 0 and years > 5:
```



```
discounted_RC[4] = replacement_PEM / (1 + discount_rate) ** 5
   NPC = CAPEX + np.sum(discounted_OPEX + discounted_RC)
   discounted_energy = (avg_annual_energy_kWh/1000) / (1 + discount_rate) ** year_array
   total_discounted_energy = np.sum(discounted_energy)
   LCOE = NPC / total_discounted_energy
   LCOH = NPC / total_H2_kg
   return LCOE, LCOH, NPC, discounted_energy, discounted_OPEX + discounted_RC, CAPEX
# Production data (does not vary between scenarios)
avg_annual_energy_kWh = 3972933.82 # Average annual PV production (kWh)
total_H2_kg = 2194132.725 # Total H2 production over 25 years (kg)
# Years for economic analysis
years_for_economic_analysis = np.arange(1, 26)
# Saved methane data
metano_risparmiato_m3 = [
   270000, 280000, 265000, 275000, 295000,
   285000, 278000, 268000, 250000, 260000,
   288000, 276000, 270000, 265000, 258000,
   260000, 275000, 268000, 262000, 255000,
   285000, 289000, 290000, 292000, 288000
1
guadagni_metano_risparmiato = np.array(metano_risparmiato_m3) * price_CH4 # &/year
# Function to calculate Payback Period
def calculate_payback_npv(capex, opex, revenues_per_year, years, discount_rate):
   npv_series = np.zeros(len(years) + 1)
   npv_series[0] = -capex # Initial cost (CAPEX) at year 0
   for i in range(len(years)):
       year_idx = i + 1
       discount_factor = (1 + discount_rate) ** year_idx
       net_flow = (revenues_per_year[i] - opex) / discount_factor
       npv_series[year_idx] = npv_series[year_idx-1] + net_flow
   return npv_series[1:]
# Function to find the break-even year
def find_break_even_year(npv_array):
   for i, val in enumerate(npv_array):
       if val >= 0:
           return i + 1
   return None
# CALCULATIONS FOR ALL SCENARIOS
# -----
# Scenario 2025 Calculations
capex_PV_2025 = capex_PV_2025_per_kW * PV_kW
capex_PEM_2025 = capex_PEM_2025_per_kW * PEM_kW
opex_PV_2025 = opex_PV_2025_per_kW_per_year * PV_kW
opex_PEM_2025 = opex_PEM_2025_perc_capex * capex_PEM_2025
opex_tot_2025 = opex_PV_2025 + opex_PEM_2025
replacement_PEM_2025 = replacement_PEM_2025_perc_capex * capex_PEM_2025
```



```
# LCOE Calculation for PV ONLY
LCOE_25, _, NPC_25, energy_disc_25, cost_ann_25, capex_2025 = calculate_LCOE_LCOH(
    avg_annual_energy_kWh, total_H2_kg,
    capex_PV_2025, 0, opex_PV_2025, 0, 0
# LCOH Calculation for PEM (can be used for comparison only, not in the LCOE chart)
_, LCOH_25_val, *_ = calculate_LCOE_LCOH(
    avg_annual_energy_kWh, total_H2_kg,
    {\tt capex\_PV\_2025,\ capex\_PEM\_2025,\ opex\_PV\_2025,\ opex\_PEM\_2025,\ replacement\_PEM\_2025}
payback_2025 = calculate_payback_npv(capex_2025, opex_tot_2025, guadagni_metano_risparmiato,
years_for_economic_analysis, discount_rate)
break_even_2025_year = find_break_even_year(payback_2025)
# Scenario 2030 Calculations
capex_PV_2030 = capex_PV_2030_per_kW * PV_kW
capex_PEM_2030 = capex_PEM_2030_per_kW * PEM_kW
opex_PV_2030 = opex_PV_2030_per_kW_per_year * PV_kW
opex_PEM_2030 = opex_PEM_2030_perc_capex * capex_PEM_2030
opex_tot_2030 = opex_PV_2030 + opex_PEM_2030
replacement_PEM_2030 = replacement_PEM_2030_perc_capex * capex_PEM_2030
# LCOE for PV only
LCOE_30, _, NPC_30, energy_disc_30, cost_ann_30, capex_2030 = calculate_LCOE_LCOH(
    avg_annual_energy_kWh, total_H2_kg,
    capex_PV_2030, 0, opex_PV_2030, 0, 0
)
# LCOH for PV + PEM
_, LCOH_30_val, *_ = calculate_LCOE_LCOH(
    avg_annual_energy_kWh, total_H2_kg,
    capex_PV_2030, capex_PEM_2030,
    opex_PV_2030, opex_PEM_2030,
    replacement_PEM_2030
payback_2030 = calculate_payback_npv(capex_2030, opex_tot_2030, guadagni_metano_risparmiato,
years_for_economic_analysis, discount_rate)
break_even_2030_year = find_break_even_year(payback_2030)
# Scenario 2050 Calculations (ADDED)
capex_PV_2050 = capex_PV_2050_per_kW * PV_kW
capex_PEM_2050 = capex_PEM_2050_per_kW * PEM_kW
opex_PV_2050 = opex_PV_2050_per_kW_per_year * PV_kW
opex_PEM_2050 = opex_PEM_2050_perc_capex * capex_PEM_2050
opex_tot_2050 = opex_PV_2050 + opex_PEM_2050
replacement_PEM_2050 = replacement_PEM_2050_perc_capex * capex_PEM_2050
# LCOE for PV only
LCOE_50, _, NPC_50, energy_disc_50, cost_ann_50, capex_2050 = calculate_LCOE_LCOH(
    avg_annual_energy_kWh, total_H2_kg,
    capex_PV_2050, 0, opex_PV_2050, 0, 0
# LCOH for PV + PEM
_, LCOH_50_val, *_ = calculate_LCOE_LCOH(
    avg_annual_energy_kWh, total_H2_kg,
    capex_PV_2050, capex_PEM_2050,
    opex_PV_2050, opex_PEM_2050,
    replacement_PEM_2050
```



```
payback_2050 = calculate_payback_npv(capex_2050, opex_tot_2050, guadagni_metano_risparmiato,
years_for_economic_analysis, discount_rate)
break_even_2050_year = find_break_even_year(payback_2050)
# H2 sales calculations
annual_H2_production_kg_avg = total_H2_kg / 25
annual_revenue_H2_undiscounted = np.full(len(years_for_economic_analysis),
annual_H2_production_kg_avg * price_H2_market)
payback_H2_market_2025_costs = calculate_payback_npv(capex_2025, opex_tot_2025,
annual_revenue_H2_undiscounted, years_for_economic_analysis, discount_rate)
payback_H2_market_2030_costs = calculate_payback_npv(capex_2030, opex_tot_2030,
annual_revenue_H2_undiscounted, years_for_economic_analysis, discount_rate)
payback_H2_market_2050_costs = calculate_payback_npv(capex_2050, opex_tot_2050,
annual_revenue_H2_undiscounted, years_for_economic_analysis, discount_rate)
break_even_H2_market_2025_costs_year = find_break_even_year(payback_H2_market_2025_costs)
break_even_H2_market_2030_costs_year = find_break_even_year(payback_H2_market_2030_costs)
break_even_H2_market_2050_costs_year = find_break_even_year(payback_H2_market_2050_costs)
# Plot 1: Discounted Energy per Year
plt.figure(figsize=(10, 5))
plt.plot(years_for_economic_analysis, energy_disc_25 / 1e6, label='2025', marker='o')
plt.plot(years_for_economic_analysis, energy_disc_30 / 1e6, label='2030', marker='s')
plt.plot(years_for_economic_analysis, energy_disc_50 / 1e6, label='2050', marker='^')
plt.title("Discounted Annual PV Electricity Production")
plt.xlabel("Year")
plt.ylabel("Energy [MWh]")
plt.grid(True)
plt.legend()
plt.tight_layout()
plt.show()
# Plot 2: Discounted OPEX + Replacement
plt.figure(figsize=(10, 5))
bar_width = 0.25
r1 = np.arange(len(years_for_economic_analysis))
r2 = [x + bar\_width for x in r1]
r3 = [x + bar_width for x in r2]
plt.bar(r1, cost_ann_25 / 1e6, width=bar_width, label='2025')
plt.bar(r2, cost_ann_30 / 1e6, width=bar_width, label='2030')
plt.bar(r3, cost_ann_50 / 1e6, width=bar_width, label='2050')
plt.title("Discounted Annual OPEX + Replacement Costs")
plt.xlabel("Year")
plt.ylabel("Cost [Million €]")
plt.xticks([r + bar_width for r in range(len(years_for_economic_analysis))],
years_for_economic_analysis)
plt.grid(axis='y')
plt.legend()
plt.tight_layout()
plt.show()
# Plot 3a: LCOE Comparison
labels = ['2025', '2030', '2050']
LCOE_values = [LCOE_25 , LCOE_30, LCOE_50 ] # €/MWh
```



```
plt.figure(figsize=(8, 5))
plt.bar(labels, LCOE_values, color=['skyblue', 'lightgreen', 'darkblue'])
plt.title("LCOE Comparison")
plt.xlabel("Scenario")
plt.ylabel("LCOE [€/MWh]")
plt.grid(axis='y')
plt.tight_layout()
plt.show()
# Plot 3b: LCOH Comparison
LCOH_values = [LCOH_25_val, LCOH_30_val, LCOH_50_val] # €/kg H2
plt.figure(figsize=(8, 5))
plt.bar(labels, LCOH_values, color=['salmon', 'gold', 'firebrick'])
plt.title("LCOH Comparison")
plt.xlabel("Scenario")
plt.ylabel("LCOH [€/kg H2]")
plt.grid(axis='y')
plt.tight_layout()
plt.show()
# Plot 4: NPV Comparison - Saved Methane
plt.figure(figsize=(10, 6))
plt.title(f"Discounted Cash Flow - Saved Methane (Cost: {price_CH4} €/m³)")
plt.plot(years_for_economic_analysis, payback_2025 / 1e6, label="Scenario 2025", color='blue')
plt.plot(years_for_economic_analysis, payback_2030 / 1e6, label="Scenario 2030", color='green')
plt.plot(years_for_economic_analysis, payback_2050 / 1e6, label="Scenario 2050", color='orange')
plt.axhline(0, color='black', linestyle='--', linewidth=0.8)
# Break-even point annotations
if break_even_2025_year is not None:
    plt.axvline(break_even_2025_year, color='blue', linestyle=':', linewidth=0.8)
    plt.text(break_even_2025_year + 0.2, payback_2025[-1] / 1e6 * 0.7, f'{break_even_2025_year}',
    color='blue')
if break_even_2030_year is not None:
    plt.axvline(break_even_2030_year, color='green', linestyle=':', linewidth=0.8)
    plt.text(break_even_2030_year + 0.2, payback_2030[-1] / 1e6 * 0.7, f'{break_even_2030_year}',
    color='green')
if break_even_2050_year is not None:
    plt.axvline(break_even_2050_year, color='orange', linestyle=':', linewidth=0.8)
    plt.text(break_even_2050_year + 0.2, payback_2050[-1] / 1e6 * 0.7, f'{break_even_2050_year}',
    color='orange')
plt.title("Discounted Cash Flow - Saved Methane")
plt.title(f"Discounted Cash Flow - (price: {price_CH4} €/m³)")
plt.xlabel("Year")
plt.ylabel("Net Present Value [Million €]")
plt.grid(True)
plt.legend()
plt.tight_layout()
plt.show()
# Plot 5: NPV Comparison - H2 Sales
plt.figure(figsize=(10, 6))
plt.plot(years_for_economic_analysis, payback_H2_market_2025_costs / 1e6, label=f"2025 Costs",
color='purple')
plt.plot(years_for_economic_analysis, payback_H2_market_2030_costs / 1e6, label=f"2030 Costs",
color='darkorange')
plt.plot(years_for_economic_analysis, payback_H2_market_2050_costs / 1e6, label=f"2050 Costs",
```



```
color='cvan')
plt.axhline(0, color='black', linestyle='--', linewidth=0.8)
if break_even_H2_market_2025_costs_year is not None:
   plt.axvline(break_even_H2_market_2025_costs_year, color='purple', linestyle=':', =
    = linewidth=0.8)
    plt.text(break_even_H2_market_2025_costs_year + 0.2, payback_H2_market_2025_costs[-1] /
    1e6 * 0.7, f'{break_even_H2_market_2025_costs_year}', color='purple')
if break_even_H2_market_2030_costs_year is not None:
    plt.axvline(break_even_H2_market_2030_costs_year, color='darkorange', linestyle=':', =
    = linewidth=0.8)
    plt.text(break_even_H2_market_2030_costs_year + 0.2, payback_H2_market_2030_costs[-1] /
    1e6 * 0.7, f'{break_even_H2_market_2030_costs_year}', color='darkorange')
if break_even_H2_market_2050_costs_year is not None:
    plt.axvline(break_even_H2_market_2050_costs_year, color='cyan', linestyle=':', =
    = linewidth=0.8)
    plt.text(break_even_H2_market_2050_costs_year + 0.2, payback_H2_market_2050_costs[-1] / 1e6 * 0.7,
    f'{break_even_H2_market_2050_costs_year}', color='cyan')
plt.title(f"Discounted Cash Flow - H2 Sales at {price_H2_market} &/kg")
plt.xlabel("Year")
plt.ylabel("Net Present Value [Million €]")
plt.grid(True)
plt.legend()
plt.tight_layout()
plt.show()
# ====== FINAL UPDATED OUTPUT =======
print("===== ECONOMIC ANALYSIS SUMMARY =====")
print("\n===== SCENARIO: 2025 (Saved Methane) =====")
print(f"Total NPC: {NPC_25:,.2f} €")
print(f"LCOE: {LCOE_25:.2f} €/MWh")
print(f"LCOH: {LCOH_25_val:.2f} €/kg H2")
print(f"Payback Period: Year {break_even_2025_year}" if break_even_2025_year is not None else
"Payback Period: Not reached within 25 years")
print("\n===== SCENARIO: 2030 (Saved Methane) =====")
print(f"Total NPC: {NPC_30:,.2f} €")
print(f"LCOE: {LCOE_30:.2f} €/MWh")
print(f"LCOH: {LCOH_30_val:.2f} €/kg H2")
print(f"Payback Period: Year {break_even_2030_year}" if break_even_2030_year is not None else
"Payback Period: Not reached within 25 years")
print("\n===== SCENARIO: 2050 (Saved Methane) =====")
print(f"Total NPC: {NPC_50:,.2f} €")
print(f"LCOE: {LCOE_50:.2f} €/MWh")
print(f"LCOH: {LCOH_50_val:.2f} €/kg H2")
print(f"Payback Period: Year {break_even_2050_year}" if break_even_2050_year is not None else
"Payback Period: Not reached within 25 years")
\label{local_print}  \text{print}(\texttt{f"} = \texttt{SCENARIO}: \ \texttt{H2 Sales at \{price\_H2\_market\}} \ \texttt{\textit{$\mathfrak{C}$/kg =====""}}) 
print(f"Annual H2 revenue (average): {annual_revenue_H2_undiscounted[0]:,.2f} €")
print("\n--- With 2025 Costs ---")
print(f"Payback Period: Year {break_even_H2_market_2025_costs_year}"
if break_even_H2_market_2025_costs_year is not None else "Payback Period: Not reached within 25 years")
print("\n--- With 2030 Costs ---")
```



```
print(f"Payback Period: Year {break_even_H2_market_2030_costs_year}"
if break_even_H2_market_2030_costs_year is not None else "Payback Period: Not reached within 25 years")
print("\n--- With 2050 Costs ---")
print(f"Payback Period: Year {break_even_H2_market_2050_costs_year}"
if break_even_H2_market_2050_costs_year is not None else "Payback Period: Not reached within 25 years")
Life time analisys.py
import numpy as np
import matplotlib.pyplot as plt
import math
from system_parameters import SystemParameters
from photovoltaic_system import PhotovoltaicSystem
from electrolyzer import Electrolyzer
from hydrogen_storage import HydrogenStorage
def simulate_h2_production():
    years = list(range(1999, 2024))
    months = ["Jan", "Feb", "Mar", "Apr", "May", "Jun", "Jul", "Aug", "Sep", "Oct", "Nov", "Dec"]
    days_in_month = [31, 28, 31, 30, 31, 30, 31, 30, 31, 30, 31]
    dt_sec = 60
    time_start_sec = 6 * 3600
    time_end_sec = (6 + 24) * 3600
    time_s = np.arange(time_start_sec, time_end_sec, dt_sec)
    sun_hours = 12
    params = SystemParameters()
    \# Monthly temperature data (°C) and monthly irradiance (MJ/m²)
    T mensili = [
        [2.9, 2.6, 8.6, 12.8, 18.4, 21, 23.1, 22.5, 19.7, 13.8, 6.6, 2.5],
        [0.6, 4.3, 8.1, 14.1, 18.5, 22.2, 21, 23.2, 18.4, 14.5, 10, 6.3],
        [5.5, 5.6, 10, 11.8, 19.4, 19.9, 22.7, 23.9, 15.8, 15.9, 6.5, 1],
        [1, 5.6, 10.1, 12.5, 17.6, 22.6, 23, 22.2, 17.6, 13.8, 11.2, 5.9]
        [2.7, 2.4, 8.3, 11.7, 19.4, 25.1, 24.5, 26.1, 17.5, 11.3, 9.7, 4.9]
        [2, 2.9, 7.6, 12.6, 15.4, 20.6, 22.7, 22.5, 18.2, 15.3, 8.1, 5.2],
        [1.7, 2.3, 7.4, 11.9, 18, 21.6, 22.9, 20.4, 18.5, 13.3, 7.4, 2.9],
        [1.7, 3.9, 6.8, 12.6, 16.9, 21.9, 25.8, 19.9, 19.7, 15.4, 9, 5.8],
        [5.8, 7.1, 10.3, 16, 18.8, 21.9, 23, 21.7, 16.7, 12.6, 7.4, 3.5],
        [5.3, 4.9, 8.2, 12.3, 18.2, 21.8, 23.3, 23.2, 17.3, 14.1, 8.3, 4.7],
        [3.5, 4.5, 8.2, 14.2, 19.3, 20.6, 23.2, 24.1, 20.1, 13.4, 9.7, 3.8],
        [2.2, 4.8, 7.8, 13.6, 16.9, 21.4, 24.6, 22.3, 17.8, 12.5, 9.9, 3.1],
        [3.1, 5, 8.8, 15.1, 19.3, 21.6, 22.1, 23.8, 21.8, 13, 8.1, 4.9],
        [2.1, 2.1, 11, 12.2, 17.6, 22.7, 24.9, 24.8, 19.9, 14.5, 10.4, 3.3],
        [4.1, 4, 7.4, 13.8, 16.2, 21.3, 24.9, 23.4, 18.7, 14.7, 9.8, 5.4],
        [7.1, 8, 10.9, 14.7, 17.2, 21.7, 21.6, 20.9, 18, 15.5, 11.7, 5.8],
        [4.2, 5.5, 9.2, 12.4, 18, 21.9, 26, 24.1, 18.9, 13.6, 8.1, 4.3],
        [2.7, 7.1, 9.4, 13.6, 16.6, 21.4, 24.5, 22.9, 20.9, 13.1, 9.2, 3.6],
        [0.9, 6.3, 10.9, 13.9, 18.3, 23.1, 24, 24.7, 17.1, 13.6, 8.4, 3.5],
        [5.8, 3.8, 7.4, 16.1, 20.2, 22.8, 24.5, 25, 20.3, 15.6, 10.9, 3.9],
        [2.7, 6.4, 9.8, 13.4, 14.9, 24.8, 24.4, 24.6, 19.1, 15.3, 10.9, 6.3],
        [4.2, 7.1, 9.4, 14.2, 17.9, 20.8, 23.4, 24, 19.9, 13.3, 8.5, 6.2],
        [3.4, 7.1, 8.3, 11.4, 15.5, 23.6, 24.3, 22.9, 19.9, 12.8, 9.5, 4.2],
        [3.3, 6, 7.7, 11.9, 19.8, 24.2, 26.4, 25, 18.7, 16.4, 10.2, 6.4],
        [6.2, 5.5, 10.1, 11.9, 18.2, 22.6, 24.4, 23.8, 21.3, 16.9, 8.5, 5.8]
```



```
irradianza mensile = [
    [161.246, 257.694, 386.764, 491.332, 620.019, 726.91, 715.212, 574.306, 455.855,
    254.82, 171.419, 115.37],
    [202.24, 241.854, 380.783, 471.99, 667.107, 814.722, 750.564, 682.778, 459.168,
    225.335, 129.955, 104.977],
    [111.629, 241.326, 294.339, 552.321, 694.426, 734.912, 711.704, 680.425, 385.352,
    286.161, 187.636, 178.222],
    [164.459, 142.287, 414.967, 491.596, 575.028, 736.813, 732.376, 637.78, 439.468,
    292.952, 127.024, 96.912],
    [161.692, 335.207, 465.764, 510.524, 745.248, 779.916, 784.341, 681.755, 486.211,
    277.293, 154.217, 136.783],
    [153.539, 143.253, 374.676, 459.005, 674.594, 700.162, 791.872, 683.757, 491.803,
    209.775, 180.57, 154.286],
    [173.253, 275.663, 416.593, 507.574, 740.376, 778.818, 770.276, 562.934, 432.377,
    246.504, 154.876, 139.984],
    [179.948, 227.128, 340.454, 468.162, 668.883, 814.578, 819.824, 585.809, 490.73,
    314.729, 176.089, 137.894],
    [109.853, 201.136, 362.652, 607.104, 627.061, 614.766, 746.541, 552.296, 461.698,
    292.858, 186.607, 154.726],
    [111.623, 220.539, 310.462, 431.046, 652.986, 609.739, 710.951, 658.585,
    433.525, 274.319, 134.857, 51.774],
    [65.201, 244.306, 372.082, 467.766, 667.974, 669.618, 761.421, 691.979, 463.944,
    327.922, 101.33, 120.585],
    [138.239, 172.449, 345.876, 560.022, 530.532, 672.147, 744.358, 607.97, 419.097,
    299.684, 117.855, 105.636],
    [113.531, 221.52, 396.108, 594.721, 774.939, 642.48, 702.899, 684.115, 464.628,
    332.763, 191.979, 114.842],
    [177.25, 267.459, 492.442, 429.659, 710.994, 705.396, 790.453, 707.725,
    418.589, 265.03, 141.188, 121.721],
    [116.217, 216.154, 280.965, 498.273, 576.942, 752.189, 788.797, 680.544,
    433.732, 225.358, 159.508, 137.141],
    [85.867, 164.635, 440.824, 479.809, 674.318, 742.914, 650.883, 579.91,
    404.311, 298.399, 138.986, 108.748],
    [152.435, 221.212, 405.165, 567.766, 611.352, 710.041, 764.672, 612.746,
    443.228, 255.165, 152.642, 117.07],
    [134.298, 144.941, 348.161, 495.399, 584.839, 620.685, 720.069, 677.312,
    450.865, 267.836, 138.54, 153.677],
    [192.958, 162.69, 420.6, 521.965, 674.607, 704.631, 755.986, 675.002, 353.33,
    280.231, 154.35, 128.284],
    [125.737, 197.144, 306.083, 496.185, 576.105, 683.618, 706.131, 634.686, 469.253,
    274.923, 149.406, 134.615],
    [170.905, 264.483, 447.763, 429.393, 494.765, 766.178, 727.924, 647.765, 449.067,
    264.955, 121.664, 130.476],
    [189.858, 250.47, 427.011, 640.623, 685.445, 638.652, 782.059, 639.399, 475.586,
    278.973, 210.79, 91.392],
    [138.992, 220.98, 488.991, 537.136, 639.059, 780.135, 709.101, 671.576, 490.931,
    336.928, 158.416, 131.166],
    [196.837, 258.434, 480.394, 546.83, 703.551, 734.422, 814.019, 678.755, 460.668,
    326.275, 173.578, 83.858],
    [144.571, 245.137, 403.169, 529.804, 596.424, 771.272, 795.202, 655.505, 537.152,
    317.604, 215.314, 141.824]
]
annual_production = []
annual_energy = []
production_2023_monthly = []
total_production = 0
for anno_idx, anno in enumerate(years):
    yearly_production = 0
```



```
current_yearly_energy = 0
    for mese_idx in range(12):
        T_amb = T_mensili[anno_idx][mese_idx]
        irradiance = irradianza_mensile[anno_idx] [mese_idx]
        days = days_in_month[mese_idx]
        sine_factor = (math.pi / 4) * sun_hours
        mj_day = irradiance / days
        kwh_day = mj_day * 0.27778
        G_peak = kwh_day / sine_factor * 1000
        pv = PhotovoltaicSystem(params, time_s)
        el = Electrolyzer(params, time_s)
        st = HydrogenStorage(params, time_s)
        G_t = pv.calculate_irradiance_profile_sine(G_peak)
        P_fv_to_electrolyzer, _, _ = pv.update_pv_power(G_t, T_amb)
        # Daily PV energy production (in kWh)
        daily_energy_kWh = np.sum(P_fv_to_electrolyzer) * dt_sec / 3600
        # Monthly energy (kWh)
        monthly_energy_kWh = daily_energy_kWh * days
        # Sum for the year
        current_yearly_energy += monthly_energy_kWh
        V_prev = el.V_cell_t[0]
        for k in range(1, len(time_s)):
            flow = el.simulate_step(k, P_fv_to_electrolyzer[k], V_prev)
            V_prev = el.V_cell_t[k]
            st.simulate_step(k, flow, dt_sec)
        for k in range(10):
            el.m_H2[k] = el.m_H2[10]
        daily_production = np.sum(el.m_H2) * dt_sec
        monthly_production = daily_production * days
        yearly_production += monthly_production
        if anno == 2023:
            production_2023_monthly.append(monthly_production)
    annual_production.append(yearly_production)
    annual_energy.append(current_yearly_energy)
    print(f"{anno}: {yearly_production:.2f} kg H")
    total_production += yearly_production
# PLOT 1: Monthly production for 2023
plt.figure(figsize=(8, 4))
plt.bar(months, production_2023_monthly)
plt.title("Monthly H Production - Year 2023")
plt.ylabel("Production [kg]")
plt.grid(True)
plt.tight_layout()
plt.show()
# PLOT 2: Annual production
plt.figure(figsize=(10, 5))
```



```
plt.plot(years, annual_production, marker='0')
   plt.title("Annual H Production (1999-2023)")
   plt.xlabel("Year")
   plt.ylabel("H Production [kg]")
   plt.grid(True)
   plt.tight_layout()
   plt.ylim(65000, 115000)
   plt.show()
   print(total_production)
    # Convert from Wh to kWh
    annual_energy_kwh = np.array(annual_energy) / 1e3
    average_annual_energy_kwh = np.mean(annual_energy_kwh)
    print(f"Average annual PV production: {average_annual_energy_kwh:.2f} kWh")
    # PLOT: Annual PV electric energy in kWh
    plt.figure(figsize=(10, 5))
    plt.plot(years, annual_energy_kwh, marker='o')
   plt.title("Annual PV Electric Energy Production (1999-2023)")
   plt.xlabel("Year")
   plt.ylabel("PV Energy [kWh]")
   plt.axhline(y=average_annual_energy_kwh, color='r', linestyle='--',
                label=f"Average: {average_annual_energy_kwh:,.0f} kWh")
   plt.grid(True)
   plt.legend()
    plt.tight_layout()
    plt.show()
if __name__ == "__main__":
    simulate_h2_production()
```





